Ice Assessment, Hesselø OWF

Ice Assessment

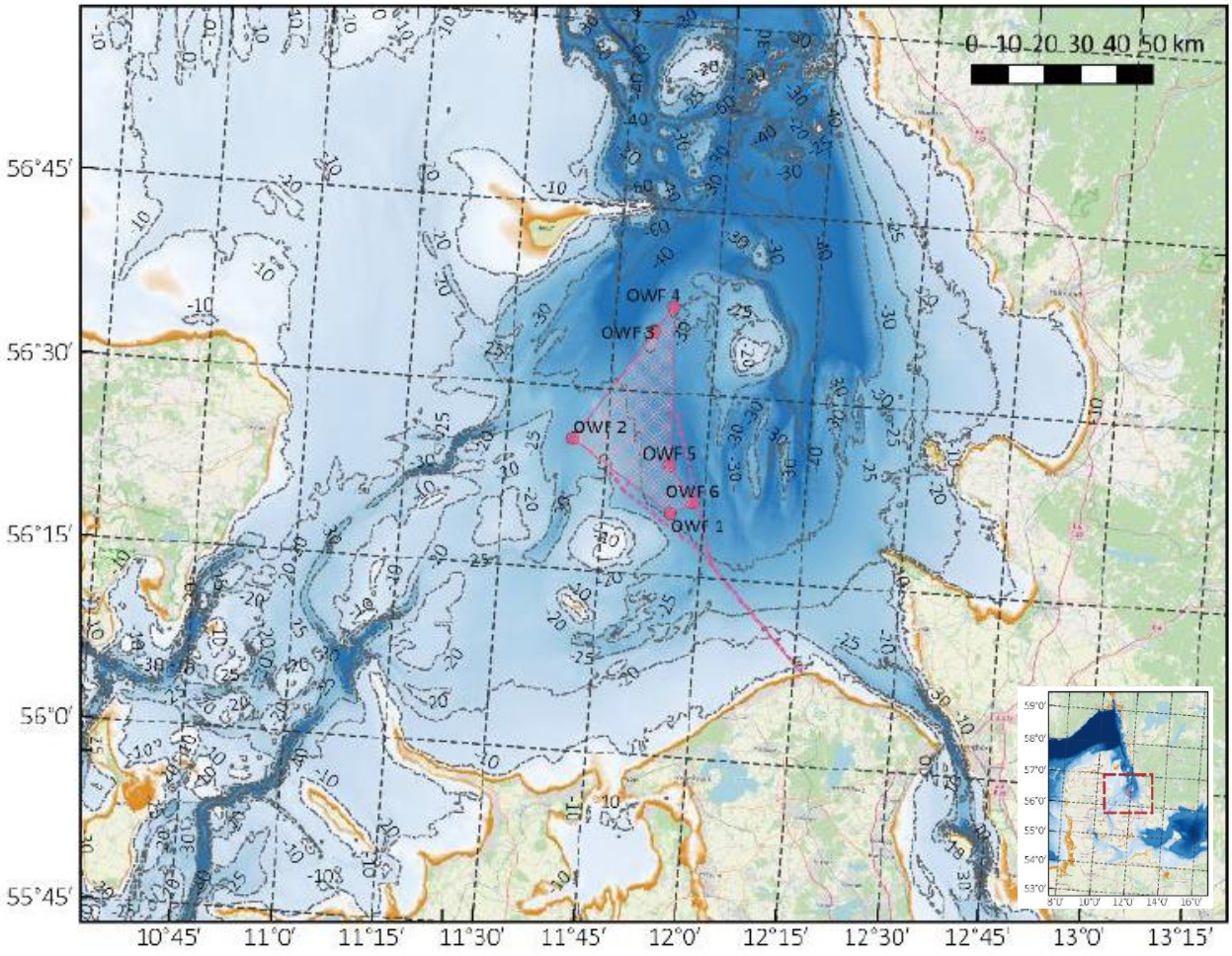

SWECO

Change list

Ver:	Date:	Description of the change	Reviewed	Approved by
00	3/12 2021	Draft	LAJ, HLG, DFX	LAJ
01	21/2 2022	Update based on DNV input	LAJ, HLG	LAJ
02	8/3 2022	Correction of minor typos.	LAJ, HLG	LAJ

Project Name:	Hesselø Ice Assessment
Project Number:	23.1511.01
Client:	Energinet.dk
Ver:	02
Date:	8/3/2022
Author:	Lars Bülow Jørgensen
Controlled by	Helge Gravesen
Approved by	Lars Bülow Jørgensen
Document Reference:	p:\tm\23.1511.01_hesselø_owf,_ice_assessment\04_output\ice assessment hesselø owf ver 02.docx

Table of contents

Sweco Danmark
Ørestads Boulevard 41

DK 2300 København S, Denmark
Telephone +45 72 20 72 07
Fax +45 72 42 89 00
www.sweco.dk

Sweco Danmark A/S
Reg. No.: 48233511
Reg. Office: Ørestad

Member of the Sweco Group

Lars Bülow Jørgensen
Wind Energy Expert
Coastal Engineering
Telephone direct +45 43 48 64 14
Mobile +45 27 23 64 14
larsbulow.jorgensen@sweco.dk

Summary

This Ice Assessment shall be used as a part of the metocean basis for the preliminary design of the offshore wind farm. The intent is to help developers to assess risks and mitigation options related to ice loads on their designs. For the final design it shall be proved that conservative design parameters are used. This applies especially for the ice thickness and the ice crushing strength.

Below in Table 0-1 is a list of the key sea ice design parameters for the Hesselø Offshore Wind Farm (OWF) located in the Danish water Kattegat north east of the island Hesslø with the reference coordinate:

- Latitude / Longitude (degrees) 56° 27'N / 11° 50'E

References to the report sections are given in the last column of Table 0-1. Background documentation are listed in the reference list in section 13.

Parameter	Return period	Design value	Unit	Internal ref.
Frost index 1/5 years	1/5y	91	[deg days]	4.1
Frost index 1/50 years	1/50y	292	[deg days]	4.1
Frost index 1/100 years	1/100y	352	[deg days]	4.1
Ice thickness 1/1 year	1/1y	0	[m]	4.2
Ice thickness 1/5 years	1/5y	0.14	[m]	4.2
Ice thickness 1/50 years	1/50y	0.35	[m]	4.2
Ice thickness 1/100 years	1/100y	0.39	[m]	4.2
Ice floe speed	1hr/1y	0.7	[m/s]	4.5
High water level	1hr/1y	1.50	[mMSL]	5.2.1
Low water level (few data)	1hr/1y	-0.85	[mMSL]	5.2.1
Ice floe size	-	2	[km]	4.4
Ice crushing strength, C_R ice floe	1/y	0.85 -1.0	[MPa]	6.1.1
Ice crushing strength, C_R ice ridge	Average	0.66	[MPa]	6.1.1
Ice bending strength 1/50 years	1/50y	0.43	[MPa]	5.8.3
Ice bending strength 1/100 years	1/100y	0.47	[MPa]	5.8.3
Ice ridge consolidated layer	1/50y	0.56	[m]	10.2
Ice ridge keep depth	1/50y	8.45	[m]	10.2
Ice ridge consolidated layer	1/100y	0.62	[m]	10.2
Ice ridge keel depth	1/100y	8.45	[m]	10.2
Marine icing		0-100	[mm]	11
Atmospheric icing	1/1y	30	[mm]	11

Table 0-1 Overall ice design parameters for Hesselø OWF.

The 1/50y or 1/100y ice thickness event shall be combined with the 1/y crushing strength, a relevant ice floe speed (section 4.5) and water level (section 5.2.1). As the water level has little correlation to the extreme ice floe impact it would be natural to combine the extreme ice to a 1hr/1y water level event. Furthermore, it is reasonable to assume that the 1/50y or 1/100y ice thickness does not coincide with 1hr/50y or 1hr/100y ice floe speed, but rather the 1hr/1y ice floe speed.

The area around Hesselø has experienced ice ridges during the past 40 years according the ice observation records therefor it is found relevant to design for ice ridges. Further it is likely that the wind turbine foundations or nearby wind turbine foundation will generate ice ridges as described in section 10.

Horizontal load due to temperature fluctuation in a fast ice cover (thermal ice pressure) is not expected as an overall load for the Hesselø OWF foundations due to the location in the open waters of Kattegat and assumed distance between foundations (>1km). Further the ice cover estimate predicts less than 80% ice cover. Thermal loads shall be considered for structures adjected to the main structure and for jackup structures.

Horizontal load from a fast ice cover subject to water level fluctuations and arch effect is not expected for the Hesselø OWF foundations due to the location in the open waters in Kattegat (coast distance >40km) on water depth of 30m and with nearby ground water depth of more than 6m. Further the ice cover estimate predicts less than 80% ice cover.

Horizontal load from moving ice is covered by the assessment of ice thickness, frequency, movement and ice strength for Hesselø OWF as described in the report.

Pressure from hummocked ice and ice ridges due to both subduction and ridging processes is covered by the assessment of the magnitude of ice ridges and ice strength.

Vertical force from fast ice covers subject to water level fluctuations is covered by the assessment of water level fluctuations and ice strength.

1 Introduction

The present report contains an ice assessment study for Hesselø offshore wind farm (OWF) project for design of the wind turbines support structures (cylindrical structures), planned for installation in the Kattegat north east of the island Hesselø. The ice assessment is made as a supplement to the “Metocean studies for Hesselø OWF which is expected to be released in the Spring 2022. The ice assessment is based on ice reports, historical data, model data from ERA5, model analysis by MIKE, public available data, literature and standards.

1.1 Codes, Standards and References

Normative standards:

- IEC International Standard, IEC 61400-3 Edition 2019, Wind Turbines – Part 3: Design Requirements for offshore wind turbines
- ISO 19906:2019 Petroleum and natural gas industries - Arctic offshore structures
- DNVGL-ST-0437 Edition 2016-11 (Loads and site conditions for offshore wind turbines)
- DNVGL-RP-0175 Edition 2017-12 (Icing of wind turbines)

A complete list of references can be found in section 13.

1.2 Data set

1.2.1 Model description

The MetOcean parameters used for the Ice assessment, Hesselø OWF are adopted from high-resolution atmospheric and oceanic models. The atmospheric model is provided by ECMWF and the oceanic models are provided partly by a MIKE HD model and partly by ECMWF. The ice assessment should be updated upon finalisation of the MetOcean report for Hesselø OWF if the etimates for current and water level deviate considerably (factor 2) from the conclusions in ths report.

1.2.2 ERA5 model

The atmospheric model used is ERA5 which is the fifth generation ECMWF reanalysis for the global climate ref. Figure 1-1 and weather for the past 4 decades. Data is available from 1979 and onwards. The data set is a reanalysis data set. Reanalysis combines model data with observations from across the world into a globally complete and consistent dataset using the laws of physics.

ERA5 provides hourly estimates for a large number of atmospheric and land-surface quantities.

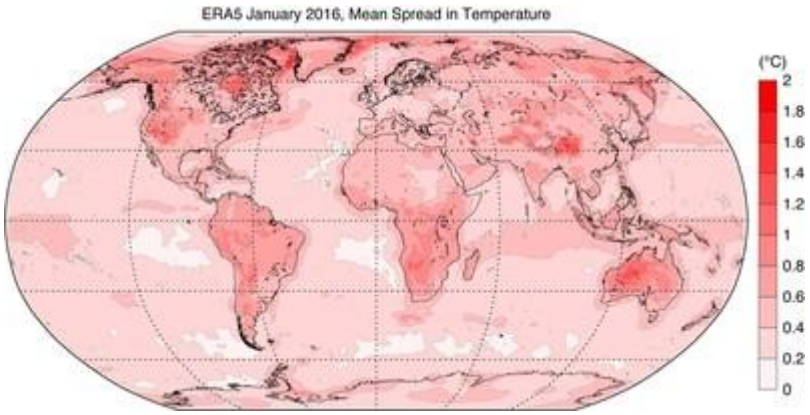

Figure 1-1 ERA5 model data global coverage.

The ERA5 data set has a global resolution of 0.25° x 0.25° for the atmosphere parameters and a 0.5° x 0.5° for ocean parameters. This corresponds to roughly respectively 28 km and 56 km.

1.2.3 MIKE model

The MIKE HD model is a hydrodynamic model in the region around Denmark including the Baltic Sea, Kattegat and the North Sea to UK ref. Figure 1-2. The full model is shown on the left-hand side and a zoom of the area of interest is shown on the right-hand side. The mesh is also shown. The mesh size is between 2-3 km in length and width.

The model is driven by the wind field from ERA5. The model is set up with boundaries far from the area of interest and data is available from 1979 and onwards. The model is calibrated against local water level measurements across the whole region.

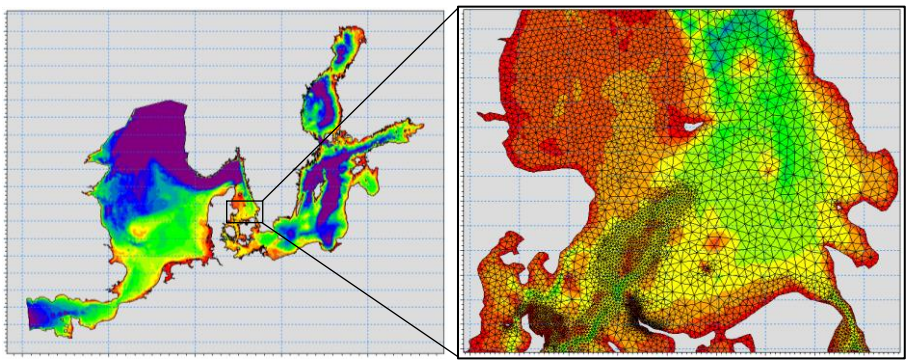

Figure 1-2 MIKE model coverage and grid resulotion - Bathymetry

1.3 Data Basis

In this section the MetOcean data is presented. The parameters of greatest importance are calibrated against local measurement. This is a method to validate the model in the local region, however direct local measurement is not available to calibrate the data directly.

1.3.1 Climate data

The climate data comes from the ERA5 model. These parameters include air temperature, ice temperature, relative humidity. The air temperature is calibrated against DMI measurement gathered in Anholt Havn ref. Figure 1-3. Between 2000 and 2014 the air temperature was logged hourly from August to January. A direct comparison between the 2 datasets is shown below in Figure 1-3 with a cropped period shown ranging from 01/10-2002 to 01/01-2003. The ERA5 model captures the temperature in the region to a satisfying degree and is therefore used as it is.

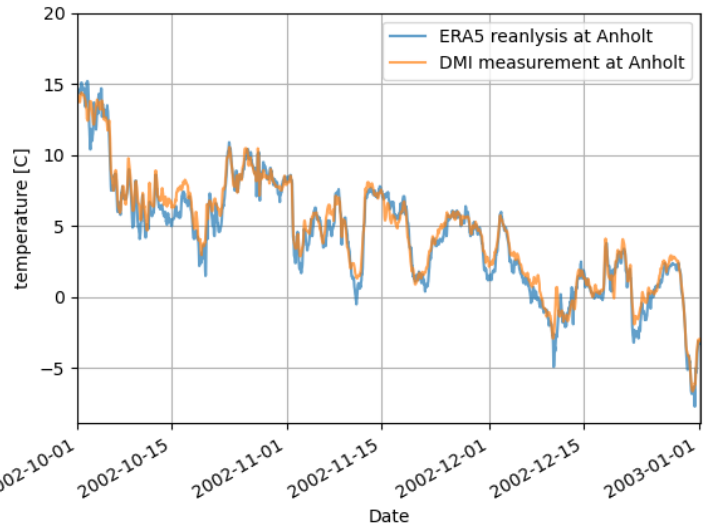

Figure 1-3 Comparison of temperature data at Anholt (ERA5 versus DMI measurements)

1.3.2 Wind data

The wind data comes from the ERA5 model. The output of the model is not validated against measurement directly, but the model includes calibration itself.

1.3.3 Water level and current

The water level and current speed and the associated direction are derived directly from the regional MIKE HD model. The precision on water level is very accurate as the model is optimized and calibrated for water levels. The current speed and direction are not calibrated for this model. Furthermore, the current speed is depth averaged with a depth in the range of -20m to -30m. It is only surface current wich is of interest. A safety factor of 2 have been multiplied to the depth average current, inorder to make a conservative surface current.

1.4 Data availability

For the 40-year period, 1979-2018, the time series of the below model data have been delivered for the position, as hourly values. Individual hours with invalid data are removed from the data set. If a single parameter is invalid within a time-step, all parameters are removed. A total of 4498 time-steps have been removed. This is 1.2% of all data available. The distribution of the removed data is random but is grouped with multiple hours in succession.

From ERA5 the following wind data were delivered:

- Wind Speed at 10m (U10) [m/s] at direction U
- Wind Speed at 10m (V10) [m/s] at direction V

From ERA5 the following climate data were delivered:

- Sea Surface Temperature (SST) [ºC]
- Air Temperature at 2m (t2m) [ºC]
- Dewpoint temperature at 2m (dt2m) [ºC]
- Relative humidity at 2m (RH) [%] (calculated from Dewpoint temperature at 2m (dt2m)
- Surface Pressure (P) [Pa]
- Ice temperature in 4 ranges (it1, it2, it3, it4) [ºC]
- Sea ice cover (SIC) [%]

From the Hydrodynamic model (HD) the following variables were delivered

- Water Level (WL) [m MSL]
- Current Speed (CS) [m/s] (depth-averaged)
- Current Direction (CD) [Deg. N. (going-to)] (depth-averaged)

1.5 Ice observation reports

Ice observation reports are available since year 1861 for the Danish waters [1]. Various Danish organisations have managed the data acquisition and reporting over the years. The present ice reporting organization is the national defence marin department (SOK). The ice coverage, ice thickness, ice structure, hinderance for ship trafic and other parameters are based on subjective visual inspections for each winter.

Ice observations for danish waters are also available from Swedish and German sources. The analysis are supplemented with these data where relevant.

2 Project site

The Hesselø OWF site is located north east of the island Hesselø in the Danish water Kattegat approximately 75 km east of the city Grenå and 50 km north of Sealand in Denmark, as shown in Figure 2-1. The Hesselø site covers approximately 250 km^2 and the water depth range is around -25 - -30 mMSL as shown in Figure 2-1. The project site is located in the easter furrow in Kattegat (water depth max. -43 mMSL) north of the bank Lysegrund and west of the bank Store Middelgrund (water depth on banks is down to -6 mMSL). The metocean data used for the analysis are generated for the coordinate: 56° 27' N, 11° 50' E and is considered to cover the entire Hesselø OWF area.

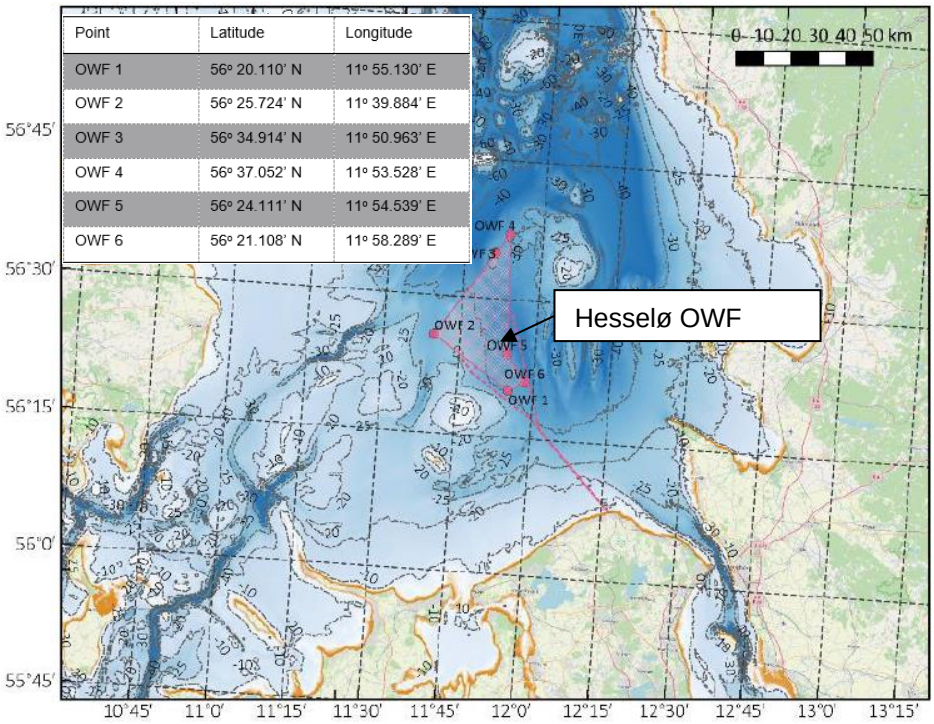

Point	Latitude	Longitude
OWF 1	56° 20.110' N	11° 55.130' E
OWF 2	56° 25.724' N	11° 39.884' E
OWF 3	56° 34.914' N	11° 50.963' E
OWF 4	56° 37.052' N	11° 53.528' E
OWF 5	56° 24.111' N	11° 54.539' E
OWF 6	56° 21.108' N	11° 58.289' E

Figure 2-1 Map and coordinates of Hessleø OWF and cable route.

Wind farms exists and are planned in the sourroding of Hesselø OWF ref. Figure 10-1. These wind farms will interfere with ice movements and rigde generation which will affect Hessselø OWF.

3 Occurrence of Sea Ice

Hesselø OWF site is located 50-100km from the coast toward east, south and west in the eastern furrow in Kattegat. The location and water depth reduces the occurrence and severity of sea ice, as is characteristic for deeper waters located away from the coast.

In ice winters ice will preliminary be generated near the coasts and spread to deeper locations over time depending on the severity and length of the ice period. Ice will also be generated in the open waters but will stay for shorter time due to the water movement.

The Hesselø OWF area is located in a region dominated by the inflow from the North Sea to the Baltic Sea and return depending on wind direction and level of water in the Baltic sea. The in/out flow will affect the flow, temperature and salinity in the region.

Global warming is affecting the ice generation and a clear tendency of reduced ice coverage and frequency is observed in the years from year 1942. It is found sufficiently conservative to base the ice assessment on the period from year 1979 until 2019. The slight reduction in frost days and frequency since year 1979 is not taken into account.

3.1 Historical ice observations

Ice formation and ice navigate observations are made by Danish, Swedish and German authorities for the Danish straights and waters. Observations from Danish sources are available since year 1861 [1]. Very severe winters occurred in the years 1940, 1941, 1942 and 1947 but the tendency is that the severity and frequency of ice winters are reduced in the recent years. In light of the general tendency and the global warming it is evaluated that it will be safe concentrate on the recent 40 years when analyzing the ice conditions for the Hesselø OWF for the coming 30-40 years. Ice analysis as used for references are however made for different periods and output from these will be included as found appropriate.

In Figure 3-1 the Danish country average Frost Index for all stations is given for the period 1918 – 2019 based on the information in Ref. [1].

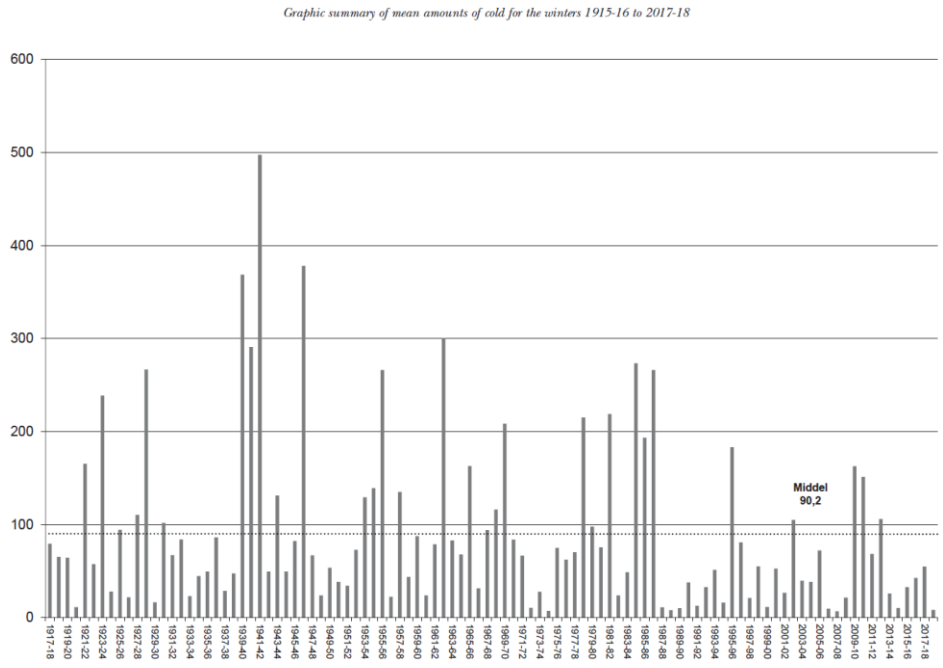

Figure 3-1: Country average Frost Index for Danish waters (1918-2019) for all stations. Ref. [1].

In Figure 3-2 the relative frequency of ice occurrence in the winter period is shown based on German ice opservations from year 1965 to 2005. For the Hesselø OWF central point located at 56° 27'N, 11° 50'E Figure 3-2 shows a large area in Kattegat of ice occurrence with a frequency of 20-30% means average occurrence once per 4 years of winters is expected. The amount of ice during ice winters is described in section 3.

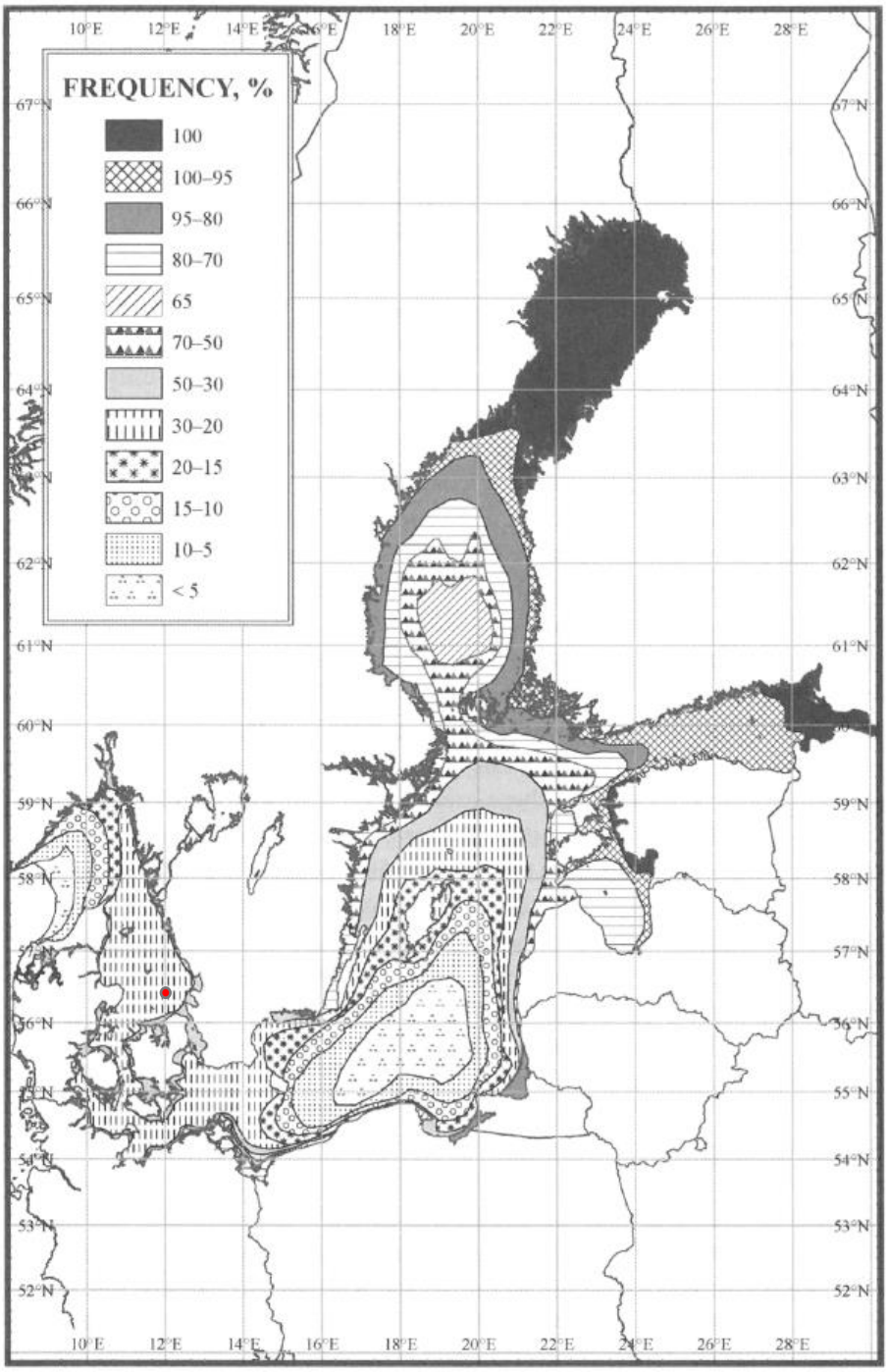

Figure 3-2 Relative frequency of ice occurrence in the Kattegat in the period from year 1956 to 2005. Red dot: Hesselø OWF.

The following plots Figure 3-3, Figure 3-4 and Figure 3-5 show the observed ice occurrence in the years 1985, 1986 and 1987 according Danish observations [1]. Similar observations are made according Swedish observations in Figure 3-6, Figure 3-7 and Figure 3-8.

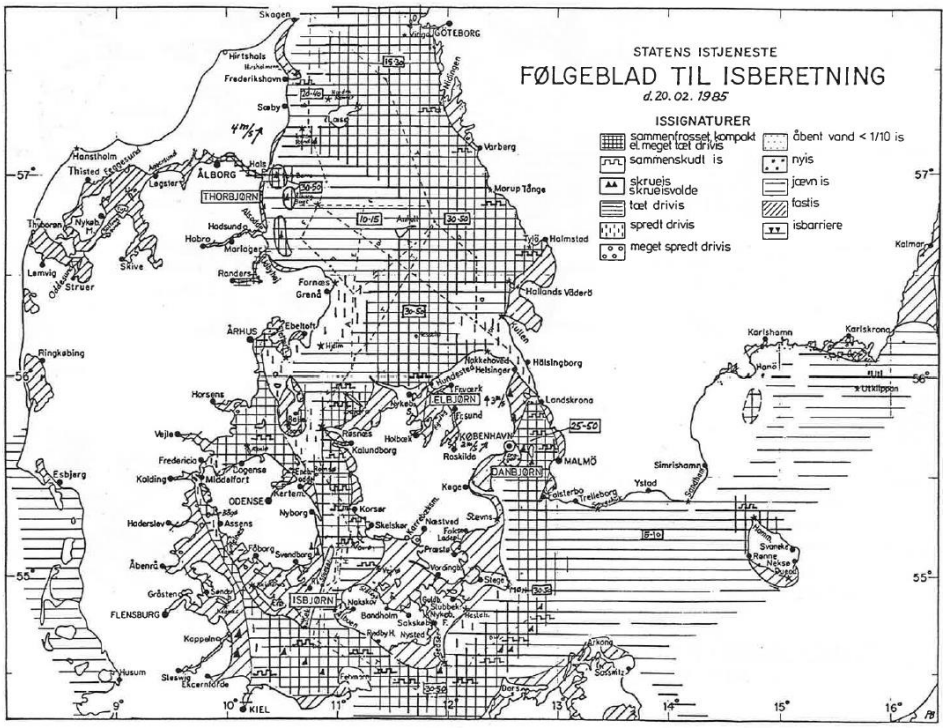

Figure 3-3 Ice observations the 20th February 1985 ref. [1]

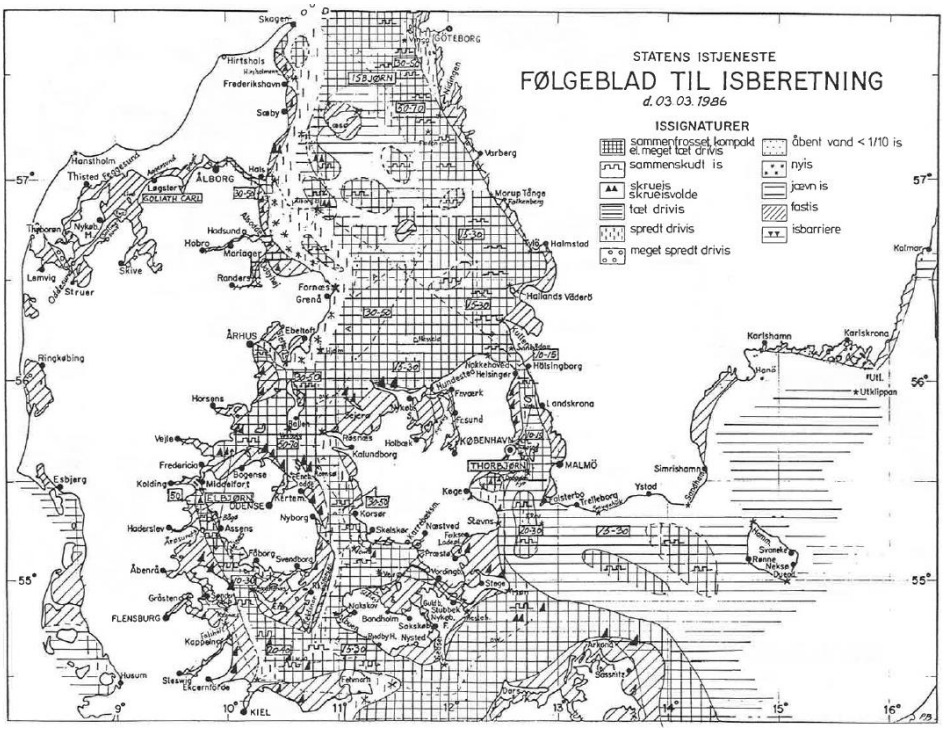

Figure 3-4 Ice observations the 3rd March 1986 ref. [1]

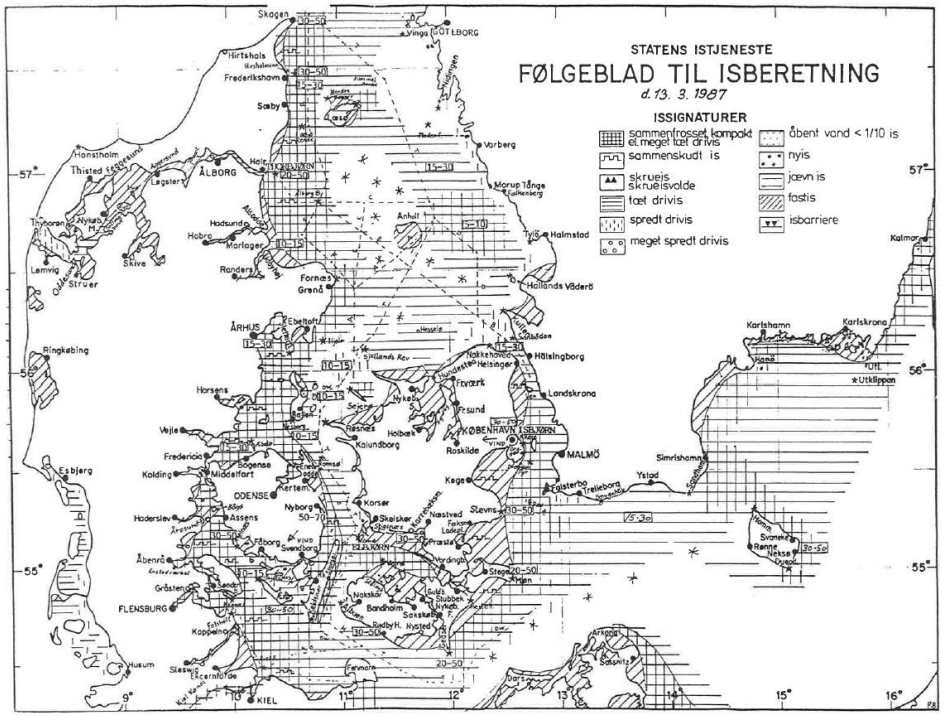

Figure 3-5 Ice observations the 13th March 1987 ref. [1]

The following plots in Figure 3-6, Figure 3-7 and Figure 3-8 show the observations of ice occurrence in the years 1985, 1986 and 1987 according Swedish observations.

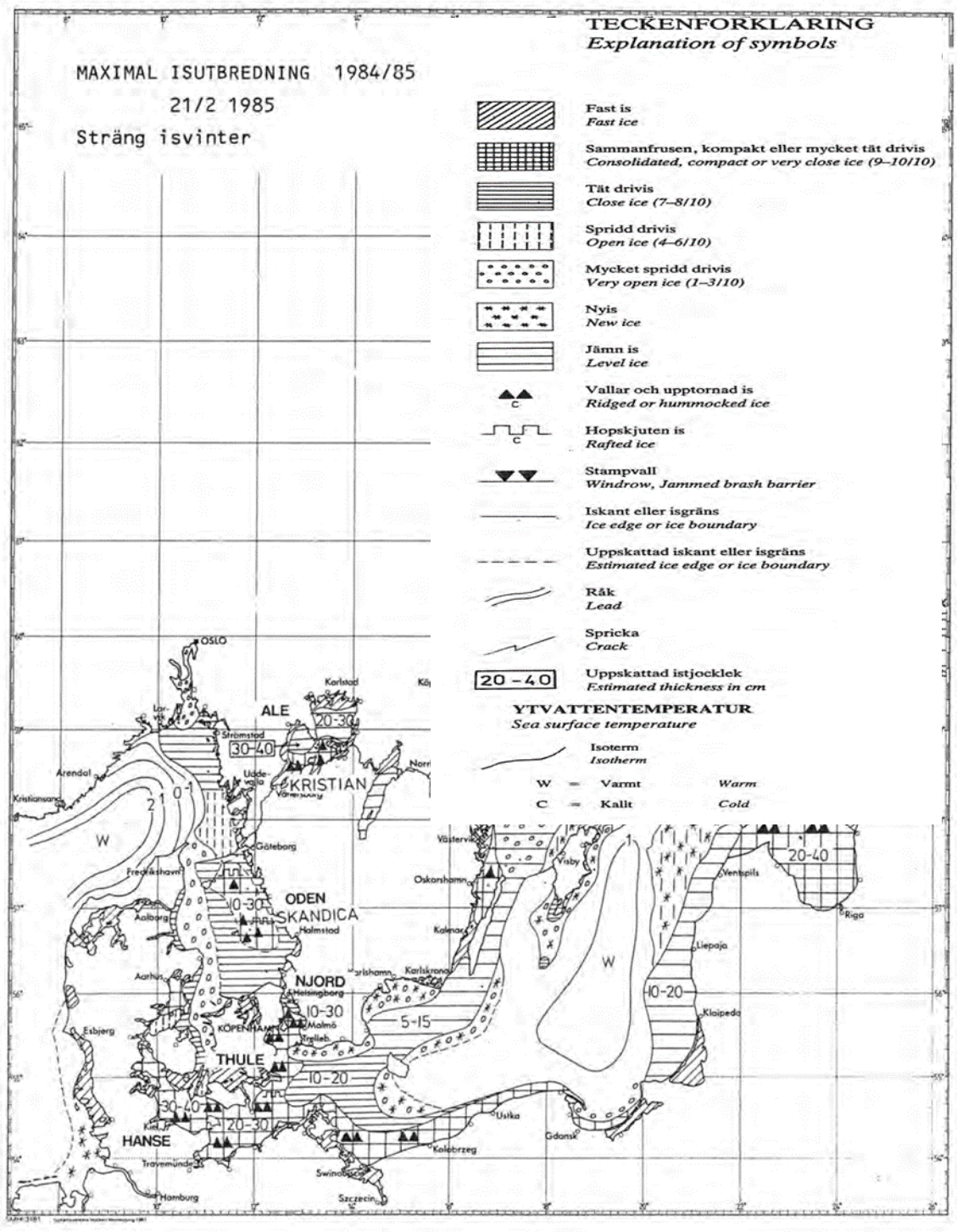

Figure 3-6 Occurrence of dominant ice types, extreme extent, on the 21st February year 1985.

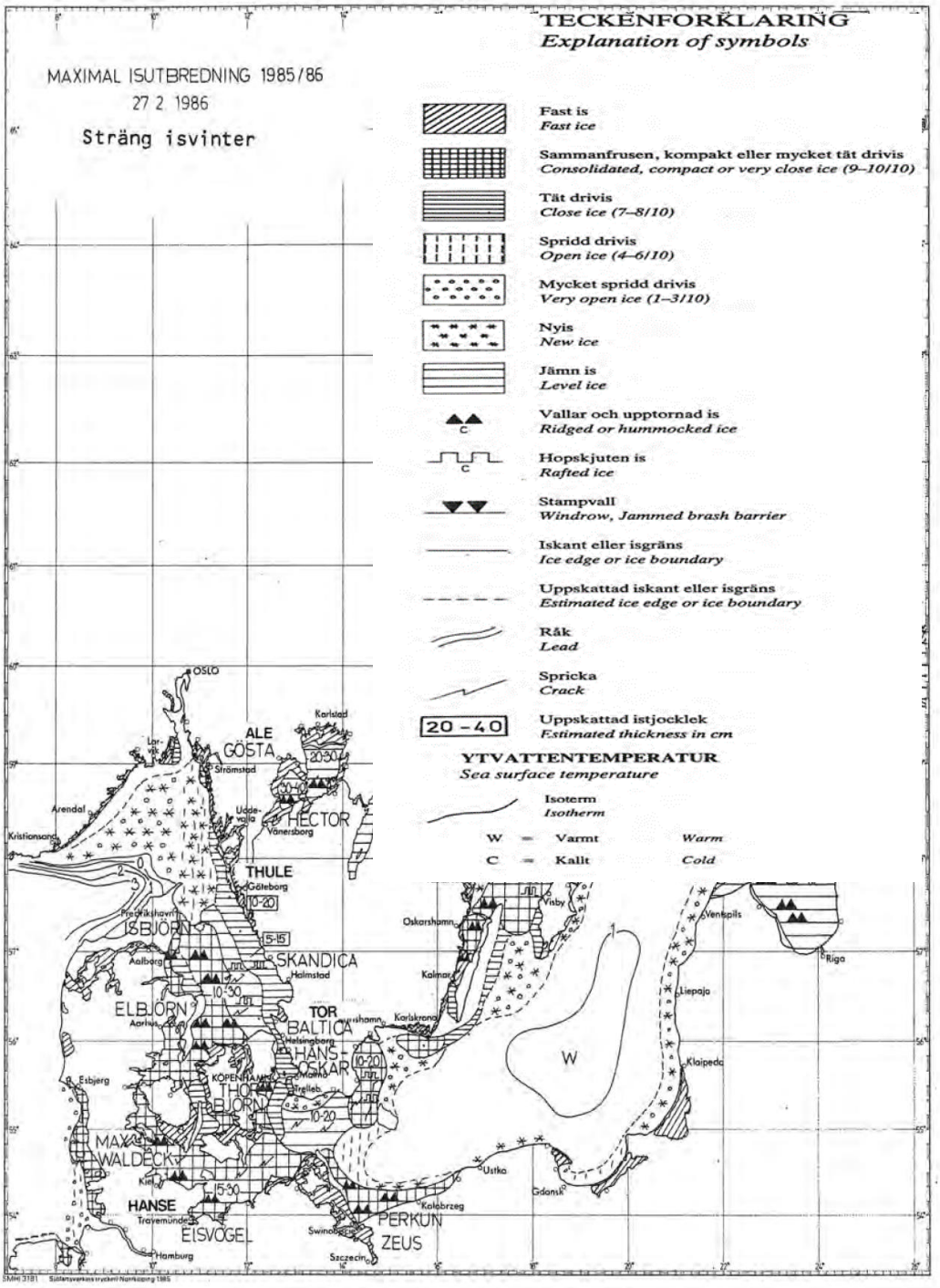

Figure 3-7 Occurrence of dominant ice types, extreme extent, on the 27th February year 1986.

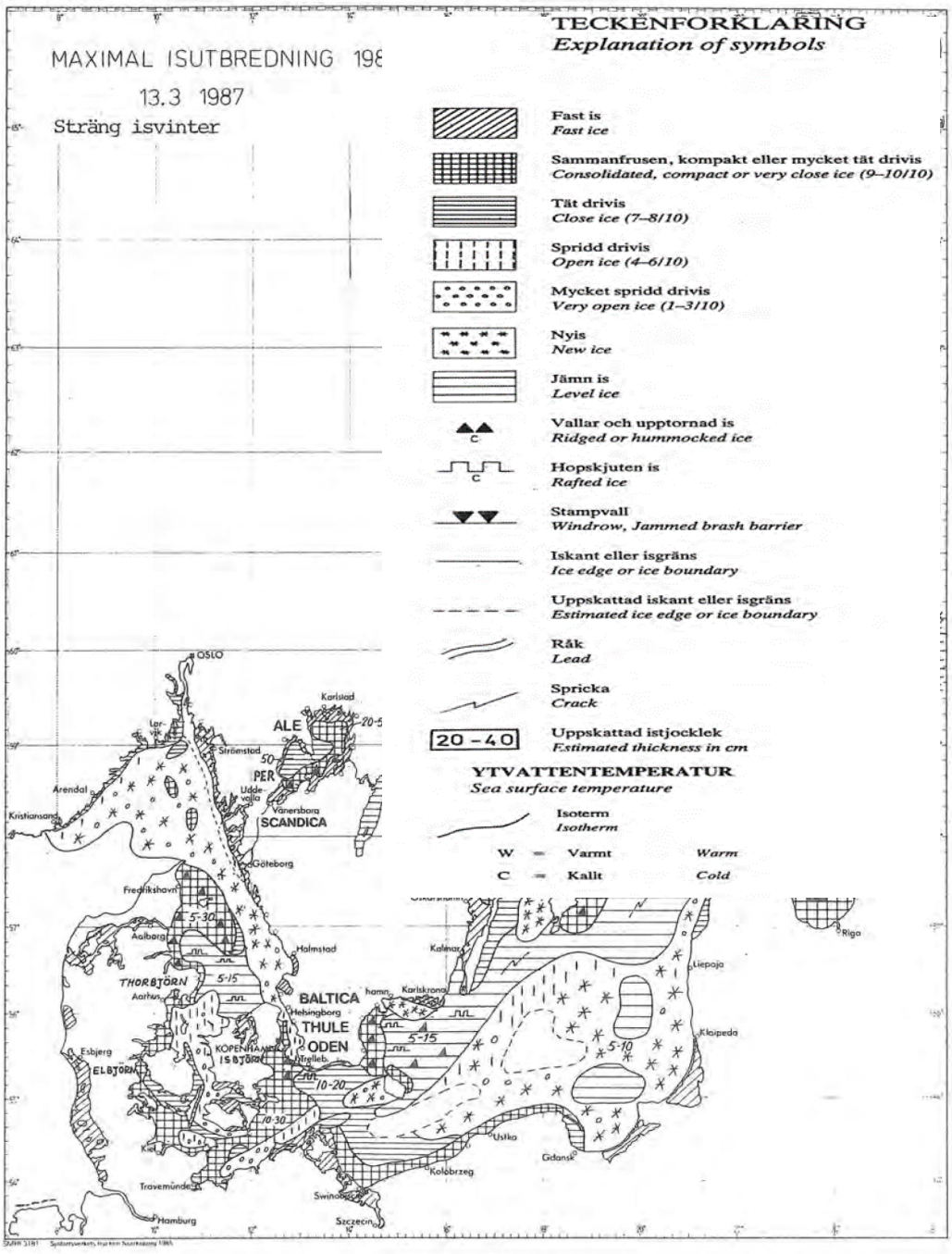

Figure 3-8 Occurrence of dominant ice types, extreme extent, on the 13th March year 1987.

The Danish ice chart Figure 3-3 show an ice thickness of (30-50cm) for 20.02.1985 where the Swedish ice chart Figure 3-6 show and ice thickness of (10-20cm) for 21.02.1985.

The Danish ice chart Figure 3-4 show an ice thickness of (15-30cm) for 03.03.1986 where the Swedish ice chart Figure 3-7 show and ice thickness of (10-30cm) for 27.02.1986

The Danish ice chart Figure 3-5 show an ice thickness of (15-30cm) for 13.03.1987 where the Swedish ice chart Figure 3-8 show and ice thickness of (5-15cm) for 13.03.1987

The comparison of the Danish and Swedish ice charts illustrates the difficulties of estimating the ice thickness over this large area and that the Danish records are more conservative than the Swedish. The concluded 1/50y ice thickness of 35 cm is considered to be realistic based on the three ice winters.

3.2 Local ice observations

Ice observations have been made for the Danish waters at strategic spots each year from year 1861 ref. [1]. The observations points have not been the same for all the years. For the Hesselø OWF following nearby observations spots ref. Figure 3-9 are available for the years 1983 to 2019:

- Læsø Østerby waters,
- Anholt waters toward west
- Anholt lighthouse toward south east
- Fornæs toward east
- Grenå toward east

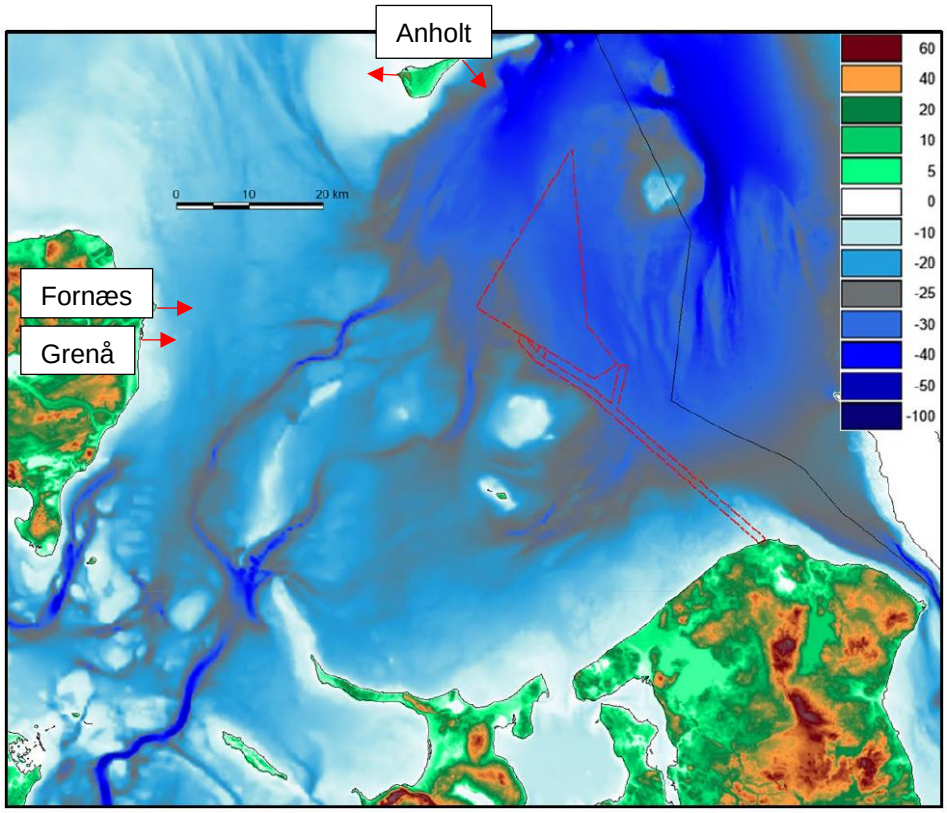

Figure 3-9 Location of ice observation spots near Hesselø OWF. Arrows indicate the direction of the ice observation. Bathymetric map with waterdepths in meters.

The Anholt lighthouse south east observations are considered as the most representative for the Hesselø OWF. Unfortunately data is missing for this observation point for more of the ice winters after year 1983.

The location at Hesselø OWF is categorized as open waters. The main flow direction toward north or south is governed by the in and out flow from the Baltic sea through Øresund and Storebælt.

Ice observations in Ref. [1] uses 2 different systems for reporting the observations. In the period 1929-1983 only simple observations of the concentration of the ice, numbers of days with ice and the maximum measured ice thickness are reported. Thus the system used does not provide information on for example topography of the ice or the stage of the ice development. In year 1983 the general accepted Baltic Sea Ice Code (ASTK) was introduced, see Table 3-1 for a description of the code and the ice observations during ice winters in the periode 1983-2019. The introduction of ASTK has provided more details of the sea ice conditions from 1983 to today. Ice observations in the ice winters since year 1983 are included in Table 3-1.

Table 3-1 Ice observations during ice winters in the period 1983 - 2019 ref. [1]

Ice observations		Frost	Observation point	Number of days										
Year		Index		A: Amount and arrangement of sea ice										
From	To	DK		0	1	2	3	4	5	6	7	8	9	X
2010	2011	151	Læsø, Østerby	2			2				2			
			Anholt, vest											
			Anholt fyr SØ											
			Fornæs fyr, Ø											
			Grenå, farvandet		1			5						
2009	2010	163	Læsø, Østerby	3	6	2	1	1	2	2	4			
			Anholt, vest	3		10				12	3	3		
			Anholt fyr SØ											
			Fornæs fyr, Ø	2		5	4	6						
			Grenå, farvandet	2		1	4	4						
1995	1996	183	Læsø, Østerby	6	8	1	3	1						
			Anholt, vest		5	5	1	1						
			Anholt fyr SØ											
			Fornæs fyr, Ø	6	5	4	1		1					
			Grenå, farvandet	11	4		15	2	1					
1986	1987	266	Læsø, Østerby	32	10		3	3		6	4	9	7	
			Anholt, vest	20	2	4	8	7	6	16				5
			Anholt fyr SØ	25	6	0	8	6	19	6	0	0	0	0
			Fornæs fyr, Ø	21	3	10	5	6	11	3				9
			Grenå, farvandet	35	4	2	1	1		21	1	3	2	3
1985	1986	193	Læsø, Østerby			5	2	1	4	9	2			
			Anholt, vest		2	7	3	3	4	10				
			Anholt fyr SØ											
			Fornæs fyr, Ø		12	3	11	6	2	2	5			
			Grenå, farvandet	1	6	5	2	1	5	16	2		1	3
1984	1985	273	Læsø, Østerby	22	7	8	2	9	14	2				
			Anholt, vest	19	10	6	7	7	3	4				1
			Anholt fyr SØ	12	3	3	2	6	11	0	0	6	0	16
			Fornæs fyr, Ø	3	12	9	7	5		2				
			Grenå, farvandet	37	4	1	7		4	4		1		7
				0 Ice free	1 Open water - concentration less than 1/10	2 Very open drift ice - concentration 1/10 to less than 4/10	3 Open drift ice - concentration 4/10 to 6/10	4 Close drift ice - concentration 7/10 to 8/10	5 Very close drift ice - concentration 9/10 to 9+/10*)	6 Compact drift ice, including consolidated drift ice - concentration 10/10	7 Fast ice with drift ice outside	8 Fast ice	9 Lead in very close or compact drift ice or along the fast ice edge	X Unable to report

Ice observations		Frost	Observation point	Number of days										
Year		Index		S: Stage of ice development										
From	To	DK		0	1	2	3	4	5	6	7	8	9	X
2010	2011	151	Læsø, Østerby	2	2									2
			Anholt, vest											
			Anholt fyr SØ											
			Fornæs fyr, Ø											
			Grenå, farvandet	1	1	4								
2009	2010	163	Læsø, Østerby		4	2					5			10
			Anholt, vest	8	4	15			1					3
			Anholt fyr SØ											
			Fornæs fyr, Ø		11		4							2
			Grenå, farvandet		4	1	4							2
1995	1996	183	Læsø, Østerby	5	1	2	4				2			5
			Anholt, vest	5	4	3					1			
			Anholt fyr SØ											
			Fornæs fyr, Ø	11	5									
			Grenå, farvandet	4		1	3		5					37
1986	1987	266	Læsø, Østerby			12	29	1						32
			Anholt, vest	21	5	29	8							5
			Anholt fyr SØ	5	0	1	32	0	0	0	0	0	0	32
			Fornæs fyr, Ø	1		5	30					2		30
			Grenå, farvandet	4	3	14	14							38
1985	1986	193	Læsø, Østerby				6	3				12	2	
			Anholt, vest	5	6	3	15							
			Anholt fyr SØ											
			Fornæs fyr, Ø	3	8	3	19	8						
			Grenå, farvandet	1	6	7	11				4	10		3
1984	1985	273	Læsø, Østerby	6	2	6	28							22
			Anholt, vest	9	8	18	1							21
			Anholt fyr SØ	5	8	6	12	0	0	0	0	0	0	28
			Fornæs fyr, Ø	3	4	5	23							3
			Grenå, farvandet	1	2	13	5							44
				0 New ice or dark nilas (less than 5 cm thick)	1 Light nilas (5-10 cm thick) or ice rind	2 10-15 cm thick ice	3 15-30 cm thick ice	4 30-50 cm thick ice	5 50-70 cm thick ice	6 70-120 cm thick ice	7 Ice predominantly thinner than 15 cm with some thicker ice	8 Ice predominantly 15-30 cm thick with some ice thicker than 30 cm	9 Ice predominantly thicker than 30 cm with some thinner ice	X No information or unable to report

Ice observations		Frost	Observation point	Number of days										
Year		Index		T: Topography or form of ice										
From	To	DK		0	1	2	3	4	5	6	7	8	9	X
2010	2011	151	Læsø, Østerby	2	1				2					1
			Anholt, vest											
			Anholt fyr SØ											
			Fornæs fyr, Ø											
			Grenå, farvandet	1	1			4						
2009	2010	163	Læsø, Østerby	5	2	2		2	6					4
			Anholt, vest	3	7			18						3
			Anholt fyr SØ											
			Fornæs fyr, Ø	5	6	4								2
			Grenå, farvandet		5	4								2
1995	1996	183	Læsø, Østerby	1	3	4		1	1					9
			Anholt, vest	7	4	1								
			Anholt fyr SØ											
			Fornæs fyr, Ø	8	8					1				
			Grenå, farvandet	4	2	1	1	1	4					11
1986	1987	266	Læsø, Østerby		8	5			29					32
			Anholt, vest	21	4	12	8	14	4					5
			Anholt fyr SØ	7	9	4	13	0	0	12	0	0	0	25
			Fornæs fyr, Ø	10	2	3	1	9	13					30
			Grenå, farvandet	2	3	2	1	14	12	1				38
1985	1986	193	Læsø, Østerby		8	1			14					
			Anholt, vest	5	7	4	3	2	8					
			Anholt fyr SØ											
			Fornæs fyr, Ø	24	4	2			4	6	1			
			Grenå, farvandet	9	8			1	1	20				3
1984	1985	273	Læsø, Østerby	17	8	17								22
			Anholt, vest	9	6	7	6	4	4					21
			Anholt fyr SØ	19	4	2	0	6	0	0	0	0	0	28
			Fornæs fyr, Ø	18	7	3	2	3	2					3
			Grenå, farvandet	4	8	3	1	4	1					44
				0 Pancake ice, ice cakes, brash ice - less than 20 m across	1 Small ice floes - 20-100 m across	2 Medium ice floes - 100-500 m across	3 Big ice floes - 500-2000 m across	4 Vast or giant ice floes - more than 2000 m across - or level ice	5 Rafted ice	6 Compacted slush or shuga, or compacted brash ice	7 Hummocked or ridged ice	8 Thaw holes or many puddles on the ice	9 Rotten ice	X No information or unable to report

Ice observations		Frost	Observation point	Number of days											Ship	Date of ice	
Year		Index		K: Navigation conditions in ice											affected	occurence	
From	To	DK		0	1	2	3	4	5	6	7	8	9	X	Days	First	Last
2010	2011	151	Læsø, Østerby	2	2	2									4	28/12	2/1
			Anholt, vest														
			Anholt fyr SØ														
			Fornæs fyr, Ø														
			Grenå, farvandet	1	4	1									5	28/12	3/1
2009	2010	163	Læsø, Østerby	1	4	7									11	12/1	27/2
			Anholt, vest	6	9	1	15								25	21/1	21/3
			Anholt fyr SØ														
			Fornæs fyr, Ø	7	10										10	14/2	10/3
			Grenå, farvandet	3	8										8	14/2	10/3
1995	1996	183	Læsø, Østerby	10	7	2									9	5/2	24/2
			Anholt, vest	7	5										5	6/2	18/2
			Anholt fyr SØ														
			Fornæs fyr, Ø	12	1	4									5	7/2	25/2
			Grenå, farvandet	15	2	7									9	31/1	24/2
1986	1987	266	Læsø, Østerby	44		9	20	1							30	13/1	27/3
			Anholt, vest	21	28	14								5	47	12/1	20/3
			Anholt fyr SØ	30	5	4	31	0	0	0	0	0	0	0	40	15/1	25/3
			Fornæs fyr, Ø	22	12	25								9	46	12/1	20/3
			Grenå, farvandet	39	7	17	7							3	34	12/1	25/3
1985	1986	193	Læsø, Østerby		1	2	6	14							22	12/2	6/3
			Anholt, vest		9	9	2	9							20	8/2	8/3
			Anholt fyr SØ														
			Fornæs fyr, Ø	9	16	11	5								32	9/2	21/3
			Grenå, farvandet	8	11	12	6	2						3	34	9/2	22/3
1984	1985	273	Læsø, Østerby	22	17	25									42	9/1	13/3
			Anholt, vest	33	12	10								2	24	7/1	19/3
			Anholt fyr SØ	15	12	10	6	0	0	0	0	0	0	16	44	9/1	8/3
			Fornæs fyr, Ø	10	21	5	3								28	10/1	12/3
			Grenå, farvandet	40	12	4	2							7	15	6/1	11/3
				0 Navigation unobstructed	1 Navigation difficult or dangerous for wooden vessels without ice sheating	2 Navigation difficult for unstrengthened or low-powered vessels built of iron	3 Navigation without icebreaker assistance possible only for high-powered vessels	4 Navigation proceeds in lead or broken ice-channel without the assistance of an icebreaker	5 Icebreaker assistance can only be given to vessels suitable for navigation in ice and of	6 Icebreaker assistance can only be given to vessels of special ice class and special size*)	7 Icebreaker assistance can only be given to vessels after special permission	8 Navigation temporarily closed	9 Navigation has ceased	X Unknown	Number of days where the ship trafic is affected of ice	First date of ice observation	Last date of ice observation

It is observed from Table 3-1 that the largest ice thicknesses of 50 - 70 cm are observed at Anholt west and the the waters outside Greneå as listed in Table 3-2. This region is characterize by lower water depth than for the Hesselø OWF and the observed ice thickness are not considered representative for Hesselø

OWF. The observations from the Anholt lighthouse toward south east (and toward the Hessleø OWF area) indicate max. ice thicknesses of 15-30 cm. The observation data from the Anholt lighthouse is missing for more years.

Table 3-2 Largest observed ice thickness in the period 1983 - 2019, Ref. [1].

Observation point	Læsø Østerby	Anholt West	Anholt Light house South east	Fornæs East	Grenå East
Largest measured ice thickness [cm]	30-50	50-70	15-30	30-50	50-70

In Table 3-3 the information of ship traffic affected ice days and the first and last date of observed ice occurrence are generalized for the five observations points. The analyze is affected of the missing data for more years especially for the observation point at Anholt lighthouse toward south east.

Table 3-3 Average of ship traffic affected ice days and dates of first and last ice observations for the five observation points in the period 1983 - 2019, Ref. [1].

Year	Ship trafic affected [Days]	Date of ice observations	
		First day	Last day
1985	35	8/1	13/3
1986	26	9/2	20/3
1987	40	12/1	25/3
1996	7	5/2	24/2
2010	15	15/1	15/3
2011	5	28/12	3/1

3.3 Ice Ridges

From ice observations as presented in Table 3-1 is can be seen that ice types as: Hummocked or ridged, Compacted slush or shuga, or compacted brash ice and Rafted ice are observed more times and for more days for the majority of the included observation stations. Since the ice is moving around it can not be ruled out the ice ridges will occure at Hesselø OWF. Further the ice maps as included in section 3.1 also include signatures for ice ridge obersevations at Hesselø OWF.

Ice ridges due to blocking effects in the wind farm or neighbouring windfarms may also occur as described in Section 10.

3.4 Climate change effects

Climate change effects (increased average global temperature) affect as well the ice occurrence in the Kattegat. A tendency of reduced frost index, ice thickness and ice coverage can be observed in more data sets, e.g. in the Danish ice observation reports [1]. According Figure 3-10 the average frost

index is diminished since year 1979. A considerable scatter is seen in the dataset due to the random nature of ice winters.

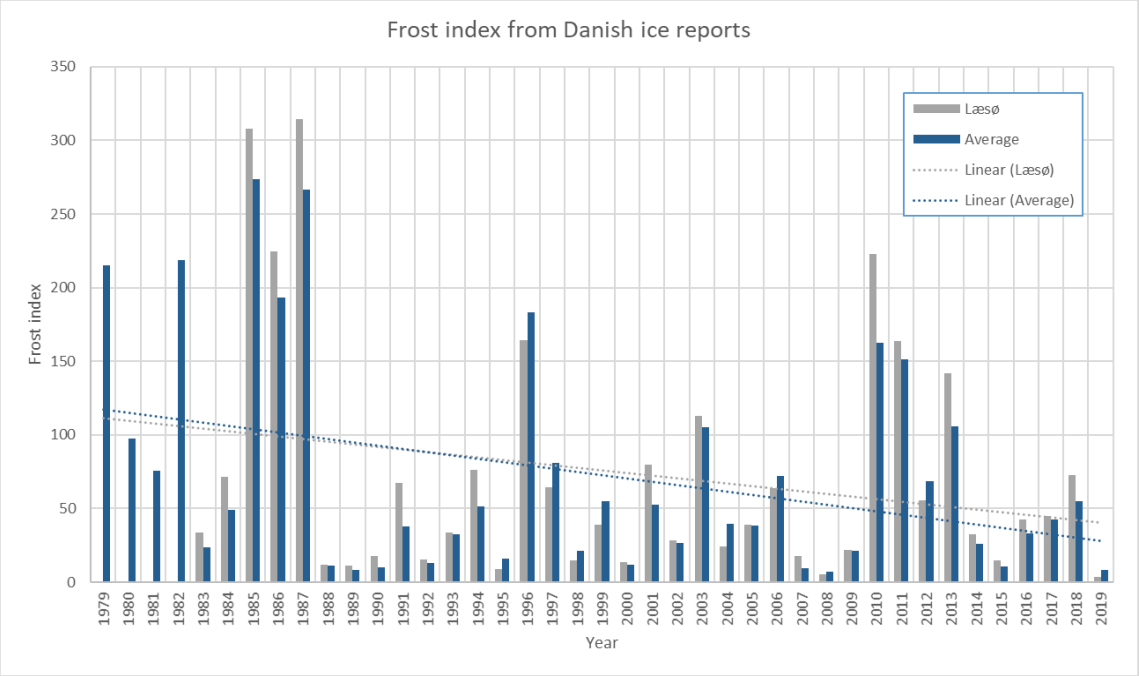

Figure 3-10: Frost index and trend for Denmark average (5 stations) and Læsø for the years 1979-2019, Ref. [1].

According the DMI report concerning climate change effects for Denmark [122] the average temperatures during winters have been analysed since year 1880 until year 2005 and estimated until year 2100 based on the two scenarios RCP2.6 (low) and RCP8.5 (high). Both estimates predict that the winters in average will be warmer than over the past 40 year period.

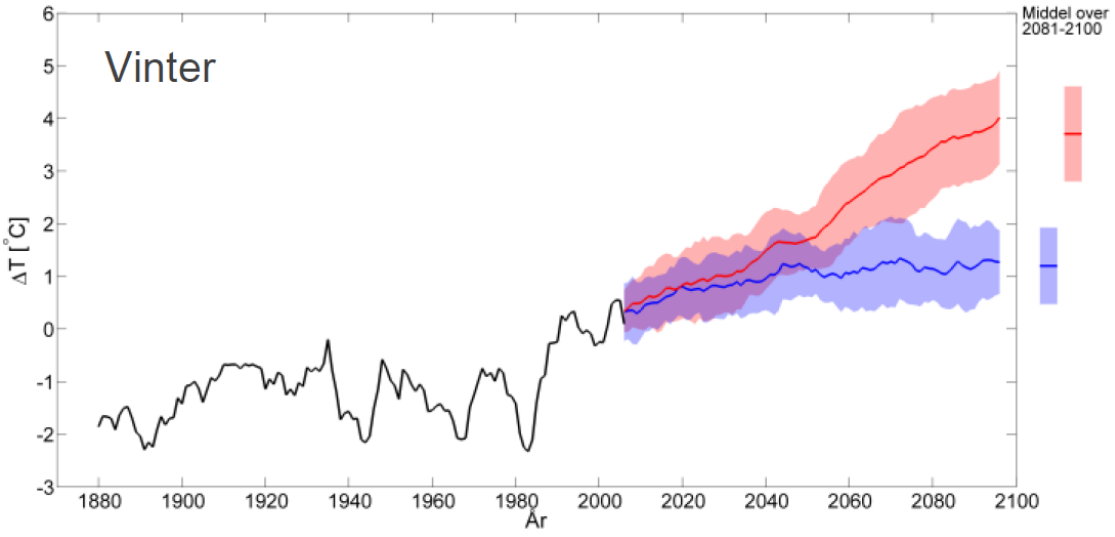

Figure 3-11: Average winter tempertures for the years 1880 to 2010 and estimates (high and low) until year 2100, Ref. [122].

DMI has as well estimated the number of frost days in the period until year 2100 as shown in Table 3-4.

Table 3-4 Estimated number of future frost days for the given year according DMI Ref. [122].

Estimate for year	1990	2050	2100
Frost days [day/year]	85 (+/- 8)	61 (+/- 7)	29 (+/- 5.3)

Due to the scatter of ice winters it is not considered safe to use the tendency of the recent ice winters to predict the future frost index. It is conservatively selected to base the design frost index analysis on the winters since year 1979 for Hesselø OWF.

4 Thickness distribution

4.1 Frost Index

As a basis for the design against ice loads, the frost index K will be used. The frost index is derived from the frost days - defined as the actual accumulated number of days for a winter, where the 24h average air temperature is below the freezing temperature of the water.

$$K = \sum_{days} \left|\tau_{mean^{(day)}}\right|, \tau_{mean < \theta_f} \quad (4.1)$$

Where:

K: Frost index summarized in a winter period

τ_{mean}: Mean air temperature (24h) in a frost period

θ_f: Freezing temperature of the water

The frost index exhibit variability from year to year and may be represented by its probability distribution.

The frost index with return period T_R in units of years is defined as the $(1/T_R)$ quantile in the distribution of the frost index, i.e. it is the frost index which probability of exceedance in one year is $1/T_R$. It is denoted $K(T_R)$ and is expressed as

$$K(T_R) = a * \ln\left(\frac{1}{T_R}\right) + b \quad (4.2)$$

Where:

$K(T_R)$: Frost index for return period T_R

a: Slope of frost index distribution

b: Offset of frost index distribution

As a comparison and reference for the frost index analysis for the Hesselø OWF project, the frost days for Denmark all stations are used. These data are available for 110 years as shown in Figure 4-1. The frost index is based on formulae (4.1)

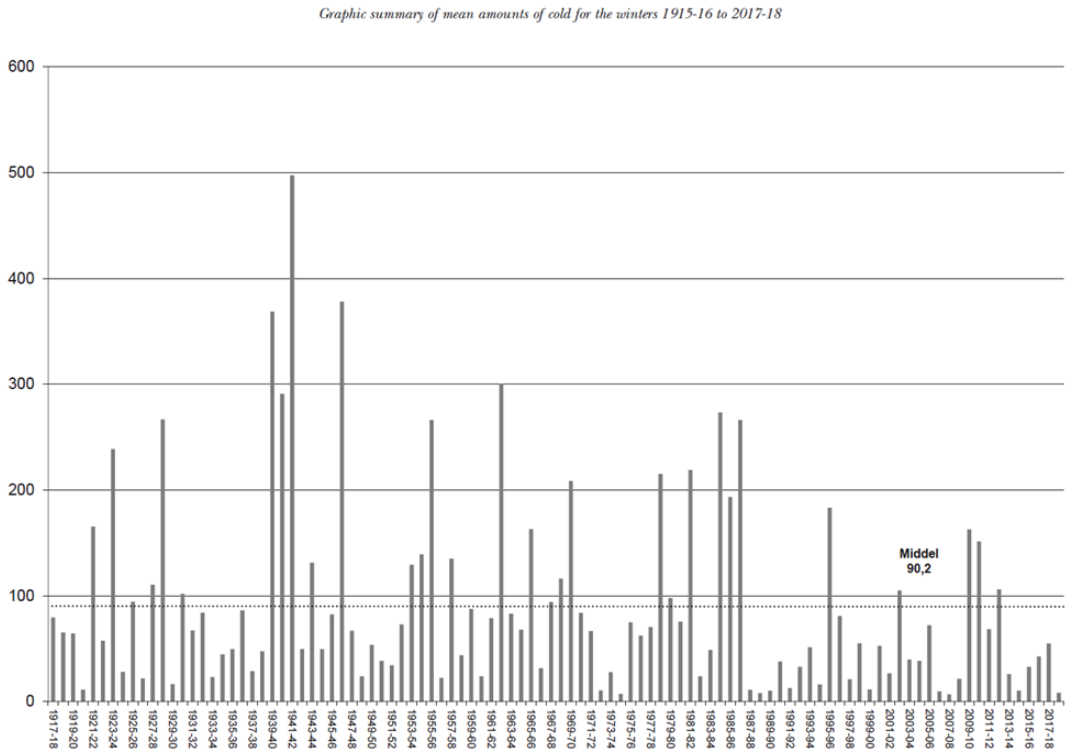

Figure 4-1 Frost days/index (ice freezing temperature: 0ºC) for Denmark year 1917 to 2019 Ref. [1].

For the Hesselø OWF project data for 40+ years are generated from the data set described in section 1.3. The frost index for Hesselø OWF are shown in Figure 4-2 and compared with the average data for Denmark for the same period.

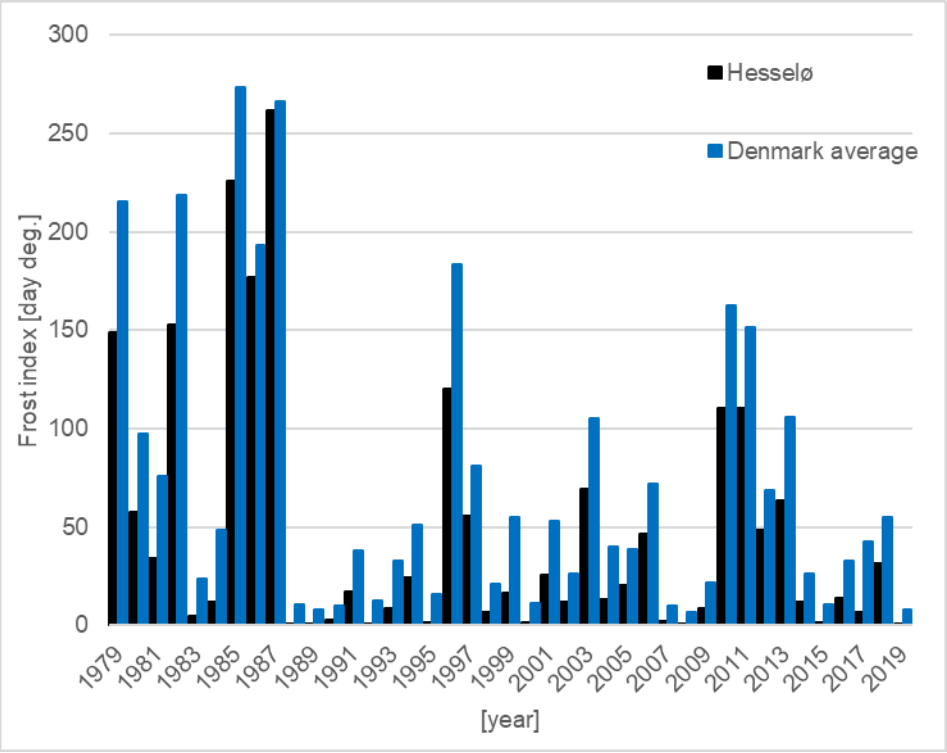

Figure 4-2 Frost index for Hesselø OWF from year 1979 to 2019

Based on the frost index in Figure 4-2 the frost index distribution for Denmark and Hesselø OWF can be found as presented in Figure 4-3. Where the data is arranged according the probability of occurrence according formulae (4.2).

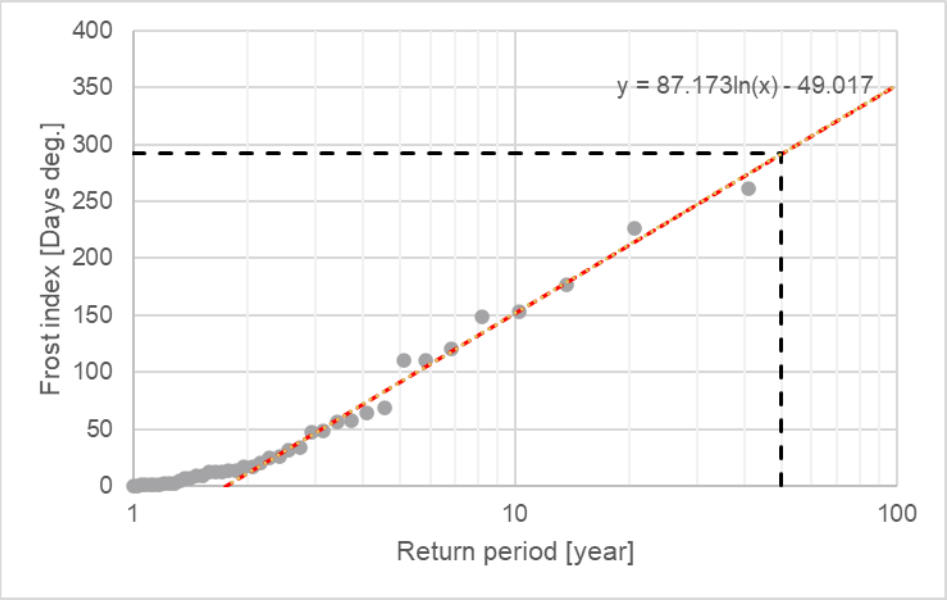

Figure 4-3 Distribution of frost index for Denmark average and the Hesselø OWF project. 1/50 year eq. probability 1/50 = 0.02

According Figure 4-2 and the derived trend lines the following frost indexes are found:

Frost Index (1/50y) for Denmark (1907-2017):	367* Days deg.
Frost Index (1/50y) for Denmark (1979-2019):	321* Days deg.

*) Based on freezing temperature of 0°C

Frost Index (1/5y) for Hesselø OWF:	91** Days deg.
Frost Index (1/50y) for Hesselø OWF:	292** Days deg.
Frost Index (1/100y) for Hesselø OWF:	352** Days deg.

**) Based on freezing temperature of -0.9°C (due to salinity content)

4.2 Ice thickness (50-year return period)

According to ISO 19906 [103] and IEC 61400-3 [102] the ice thickness, t, at the end of a frost period may be estimated by:

$$t = 0.032\sqrt{0.9K - 50} \quad (4.3)$$

Where the ice thickness, t, has a unit of metres and the frost index according formulae (4.2), K, has a unit of days deg. It shall be noted that the formula (4.3) applies for both open and closed waters.

Based on analysis [107] of sea ice occurrence in open waters in Denmark in the winters from year 1941 to 1942, it was found that the formula (4.3) leads to a too conservative design ice thickness for open waters. On this basis it is suggested to modify the formula for ice thickness for open waters in Denmark incl. Kattegat to (ref. [107]) :

$$t_{open} = 0.024\sqrt{0.9K - 50} \quad (4.4)$$

For reference and as an alternative to the above formula (4.4) the sea ice thickness can be calculated according the Lebedev formula (4.5) specified by: "National Snow and Ice Data Center (US)". The Lebedev formula (4.5) derives the sea ice thickness, t, based on the frost index, K ref. formula (4.2), as follows:

$$t = 0.0133 * K^{0.58} \quad (4.5)$$

Based on the above formulas the ice thickness can be calculated for Denmark for reference as shown in Figure 4-1.

Table 4-1 Estimated ice thickness for Denmark.

Denmark	1/50year	
Frost Index (period 1979-2019)	321	*Days deg.*
Ice thickness (open and closed waters), eq. (4.3)	0.51	M
Ice thickness (open waters), eq. (4.4)	0.38	M
Ice thickness (US), eq. (4.5)	0.39	M

The key conclusion of the analysis [107] is shown in Table 4-2.

Table 4-2 Estimated and observed sea ice thickness for Kriegers Flak (west of Bornholm) ref. [107].
h_{ref} is the ice thickness calculated according to equation (4.3) and (4.4).

Winter Year	Frost Index	Calculated ice thickness		Observed max ice thickness	Observed ice thickness of fast ice
	Days deg.	(4.3) m	(4.4) m	m	m
1941-42	495	0.64	0.48	-	0.48 but 0.40 in semi-open waters
1978-79	220	0.39	0.29	0.40	0.21-0.30
1984-85	275	0.45	0.34	0.15-0.50	0.15-0.30
1985-86	190	0.35	0.26	0.20-0.30	0.15-0.30
1986-87	265	0.44	0.33	0.30-0.50	0.15-0.30 (Danish source) 0.10-0.20 (Swedish source)

It is found that the modified equation (4.4) for open waters (factor 0.024) and the US estimate ref. equation (4.5) of the sea ice thickness compare better to the observed sea ice thickness for open waters than equation (4.3).

For Hesselø OWF the same analysis leads to the sea ice thickness as shown in Table 4-3.

Table 4-3 Estimated ice thickness for Hesselø OWF.

Hesselø OWF	1/5 years	1/50 years	1/100 years	Return period
Frost Index	91	292	352	Days deg.
Ice thickness (closed and open waters), eq. (4.3)	0.18	0.47	0.52	m
Ice thickness (open waters), eq. (4.4)	0.14	0.35	0.39	m
Ice thickness (US), eq. (4.5)	0.18	0.36	0.40	m

The ice thickness with one-year return period is considered as zero.

Based on the historical temperatures, the frost index on a daily basis and formulae (4.4) the ice thickness for the ice winters since year 1979 is found as shown in Table 4-4. Formula (4.1) is used on a daily basis to estimate the ice thickness. The dates are given as the first and last frost date for ice generation. The period of ice occurens will be shorter than the frost period.

Table 4-4 Frost index and estimated ice thickness for Hesselø OWF. Dates are given for the first and last frost date.

Frost Index		Ice Thickness		Frost	Date	
Year	Max	Max	Ave	Days	First	Last
1979	149	0.14	0.02	79	01/01/1979	21/03/1979
1980	58					
1981	34					
1982	153	0.16	0.01	82	07/12/1982	27/02/1983
1983	5					
1984	12					
1985	226	0.24	0.03	75	01/01/1985	17/03/1985
1986	177	0.22	0.02	61	02/01/1986	04/03/1986
1987	262	0.26	0.04	93	20/12/1986	23/03/1987
1988	1					
1989	1					
1990	3					
1991	17					
1992	1					
1993	9					
1994	24					
1995	2					
1996	120	0.11	0.00	102	15/12/1995	26/03/1996
1997	56					
1998	7					
1999	16					
2000	1					
2001	26					
2002	12					
2003	69					
2004	13					
2005	21					
2006	47					
2007	2					
2008	0					
2009	8					
2010	111	0.12	0.01	71	29/12/2009	10/03/2010
2011	111	0.04	0.00	98	25/11/2010	03/03/2011
2012	49					
2013	64					
2014	12					
2015	1					
2016	14					
2017	7					
2018	32					
2019	0					
Maximum	262	0.26	0.04	102		
Average	48	0.16	0.02	83		

SMHI has during a 17 years period from year 1963 -1979 made detatiled ice observations for a location (Pos 17) north east of Anholt ref. Annex A. The

location and overall findings are included in Annex A. In the period 1963-1979 the ice conditions was sligthtly more severe than in the resent years but comparable with the winters up to and inclusive year 1987. The conclusion of ice distribution for Pos 17 will in the following section be used for Hesselø OWF. To illustrate the similarity of ice conditions - the temperature, estimated ice thickness and ice coverage for the two locations can be compared in Figure 4-4 and Figure 4-5 for the ice winters 1985, 1986 and 1987.

Below in Figure 4-4 and Figure 4-5 are the air temperature and ice coverage data from the ECMWF database (ref. section 1.2) used to estimate the ice thickness during the ice winters 1985-1987 for Pos 17 and Hesselø OWF by using the frost idex on a daily basis and formula (4.4).

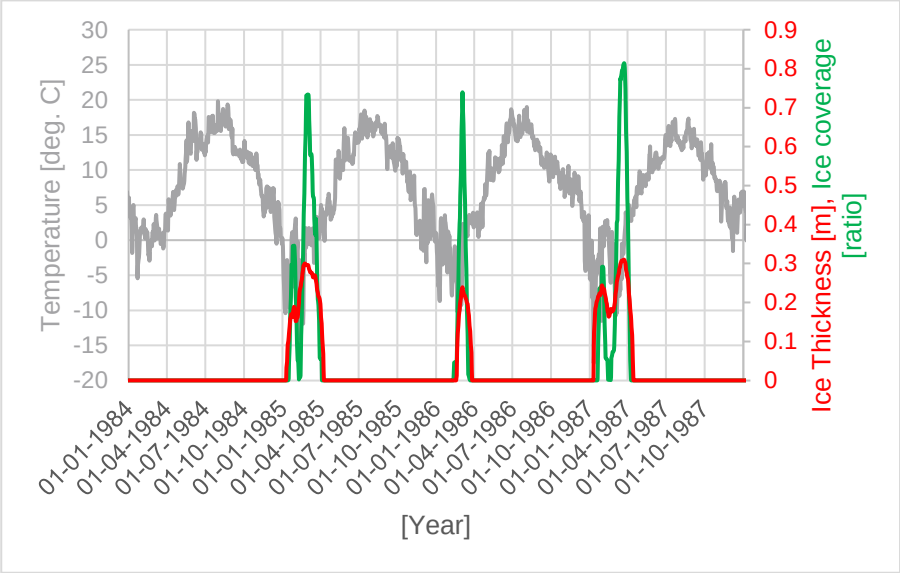

Figure 4-4 Pos 17 Air temperature, ice coverage and ice thickness for the winter periods in 1985-1987 (Data: ECMWF)

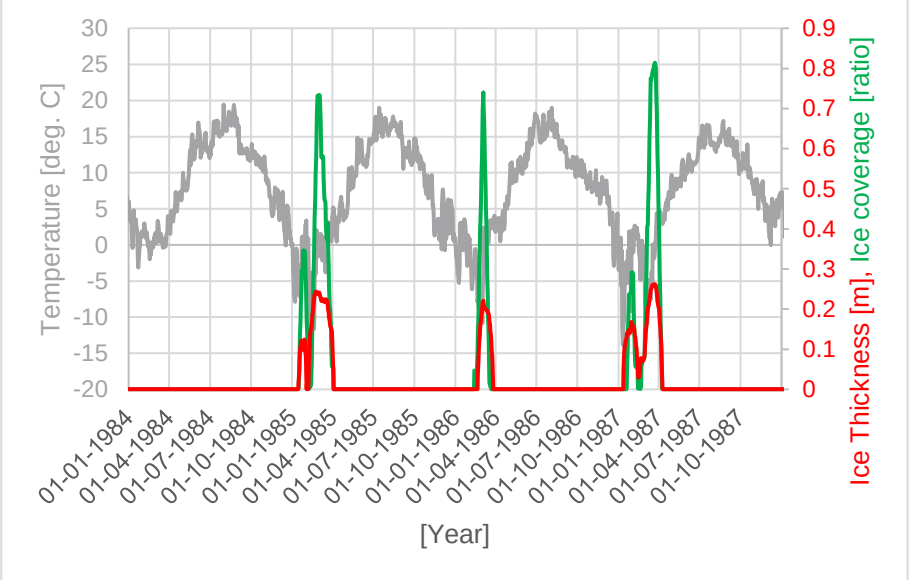

Figure 4-5 Hesselø OWF Air temperature, ice coverage 14 days rolling mean and ice thickness for the winter periods in 1985-1987 (Data: ECMWF)

It can be concluded that the temperature conditions for ice generation are quite similar and that Pos 17 (ref. Annex A) ice conditions might be slightly more severe than for Hesselø OWF.

4.3 Ice occurrence distribution

Observation of ice occurrence have been made carefully by SMHI for the period 1963 to 1979 ref. [2]. The observations summarize and generalize the ice conditions over 17 years for stratetic locations in the Swedish waters. These data have previously been used as a basis for the ice distribution analysis e.g. for Pos 16 (ref. Annex A) near Kriegers Flak in the western part of the Baltic Sea. The observations compares well to similar Danish and German observations for similar nearby locations. The observation point Pos 17 (ref. Annex A) is located North East of Anholt i.e close to the Hesselø OWF with quite identical conditions for ice generation. The ice occurrence is considered identical to Area 17 based on the ice thickness and coverage analysis as shown in Figure 4-4 and Figure 4-5. The map of Swedish observations points and the generalized ice data from ref. [2] are included in Annex A.

Based on the ice thickness distribution on Area 17 [2] the following ice thickness and ice speed distribution ref. Table 4-5 are estimated for the Hesselø OWF area. The ice speed distribution is based on Figure 4-9 with data for the 3 ice winters 1985-1987. The ice bending strength in Table 4-5 is based on input from section 5.8.3.

It is noted that the ice thickness of 35 cm with a recurrence of 0.1 days/25 years in Table 4-5 is conservative considering this is similar to the 50-year ice recurrence.

The bending strength is conservatively set to a minimum of 0.3 MPa for all ice thicknesses below 25 cm ref. section 5.8.3.

Table 4-5 Ice thickness and speed distribution for Hesselø OWF for 25 years.

Hesselø OWF	Ice thickness	[cm]	4	9	16	25	35	
	Ice bending strength	[MPa]	0.30	0.30	0.30	0.30	0.40	Sum [Hours]
	Occurence	days/25 y	73	74	28	10	0.10	185
	Occurence	hours/25 y	1749	1776	663	240	3.0	4431
Distribution Exceedance	Ice floe velocity [m/s]	Part of time	[Hours]	[Hours]	[Hours]	[Hours]	[Hours]	Sum [Hours]
0.96	0.04	0.042	73	75	28	10	0.1	186
0.92	0.06	0.042	73	75	28	10	0.1	186
0.87	0.08	0.042	73	75	28	10	0.1	186
0.83	0.10	0.042	73	75	28	10	0.1	186
0.8	0.11	0.032	56	57	21	8	0.1	142
0.7	0.14	0.1	175	178	66	24	0.3	443
0.6	0.17	0.1	175	178	66	24	0.3	443
0.5	0.20	0.1	175	178	66	24	0.3	443
0.4	0.23	0.1	175	178	66	24	0.3	443
0.3	0.27	0.1	175	178	66	24	0.3	443
0.2	0.31	0.1	175	178	66	24	0.3	443
0.16	0.33	0.04	70	71	27	10	0.1	177
0.12	0.35	0.04	70	71	27	10	0.1	177
0.08	0.39	0.04	70	71	27	10	0.1	177
0.04	0.44	0.04	70	71	27	10	0.1	177
0.01	0.53	0.029	51	52	19	7	0.1	128
0.005	0.58	0.006	10	11	4	1	0.0	27
0.001	0.67	0.004	7	7	3	1	0.0	18
0.0001	0.75	0.001	2	2	1	0	0.0	4
	Total	**1**	**1749**	**1776**	**663**	**240**	**3.0**	**4431**

The ice thickness and velocity distribution according Table 4-5 shall for the detailed design simulations of combined wind and ice load be split in the wind turbine operational modes: idling, strong misalignment and power production depending on wind turbine related criterias as listed below:

- Idling (or strong misalignment) (usual damping estimate say 2 % for 1 mode)
- Uwind < 4 m/s (No production)
- Downtime power production (failures) (Typically assumed to 2 % of time but to be updated for detailed design based on WTG design and grid connection).
- Downtime power production (U wind > 25 m/s) (not actual, se later)
- Downtime power production (icing turbine). This could be estimated to 2-4 % of situations with significant ice
- Strong misalignment (say > 45^0)
- Power production (usual damping estimate say 7% for 1 mode)

4.4 Ice floe size

It is a common practice to use a 2 km diameter ice floe size in open Danish waters including the southern Kattegat. According the ice observations as listed in Table 3-1 ice floes of this size or bigger has been observed in ice winters. The observations points are located on land and may not represent the open water location at Hesselø OWF correctly. To follow the normal Danish practice the ice floe size for Hesselø OWF area is specified to: 2 km in diameter.

4.5 Ice floe speed

Sea ice movement and speed in Kattegat is mainly driven by wind forces from wind blowing over the ice supplemented by the current in the upper water layers. As an estimation of the ice floe speed the following relation to 2.5% of the wind speed, U_{10m}, 10m above the water (see [102]) and the current speed, U_c, may be used by a vectorial summation:

$$\overrightarrow{V_{ice}} = \vec{U_c} + 0.025\overrightarrow{U_{10m}} \quad (4.6)$$

The ice floe speed of the actual thickness <30 cm is not considered to be affected by the thickness of the ice.

The depth average current speed from the data set ref. section 1.3 is multiplied by (2) two to get the surface current speed.

The ice floe movement analysis is based on the 4 winter months of January to April as this is where sea ice is expected in the area.

The data period 1979-2019 has been compared with the three ice winters 1985-1987 and it is found that the wind and current distribution deviate for ice winters ref. Figure 4-7 compared to the overall period ref. Figure 4-6 . This is as expected since ice winters are likely to occure when cold air is arriving from northly toward eastly directions. In the following analysis of the ice movements and misalignment to the wind direction the data for the three ice winters 1985-1987 will be used. 8691 data point are available for the period which is considered sufficient for the data analysis.

In the following pages illustrations of the estimated ice floe probability and floe movement pattern are presented. Following can be concluded for the 3 ice winters 1985-1987:

- The prime wind direction is from north, north-east to east (cold air). The secondary wind direction is from west (tempered air).
- The prime current direction is toward north-west and reverse. This is as expected based on the in and out flow from the Baltic Sea through Øresund.
- The ice movements is dominated by the wind forces.
- The prime ice floe direction is toward north-west and a secondary direction is toward east.
- When the wind speed increases the ice floe direction gets clearly governed by the wind direction. At low wind speed the ice floe direction is also affected by the sea current direction.

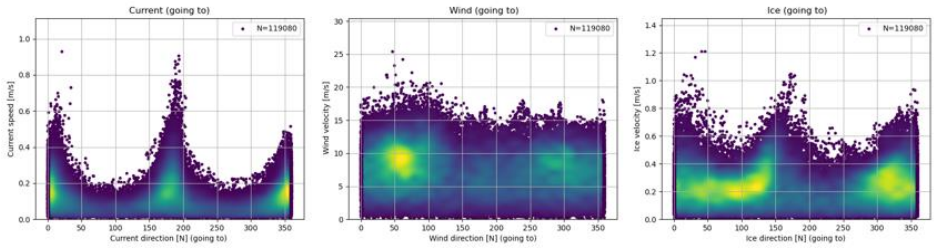

Figure 4-6 Directional distribution of current, wind and ice movements (all toward directions) for the 4 winter rmonths (Januar-April) in the period 1979-2019. OBS: Surface current speed is found as two times the depth current speed. Colours indicate the number of observations: Yellow=high, Dark blue= low.

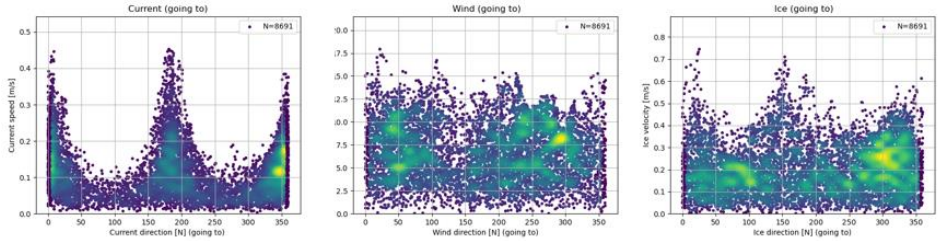

Figure 4-7 Directional distribution of current, wind and ice movements (all toward directions) for the 4 winter rmonths (Januar-April) for the 3 winter months 1985-1987. OBS: Surface current speed is found as two times the depth current speed. Colours indicate the number of observations: Yellow=high, Dark blue= low.

Figure 4-8 illustrate the correlation of ice movements and the direction of current and wind. It can be found that the ice movement is dominated by the wind load input.

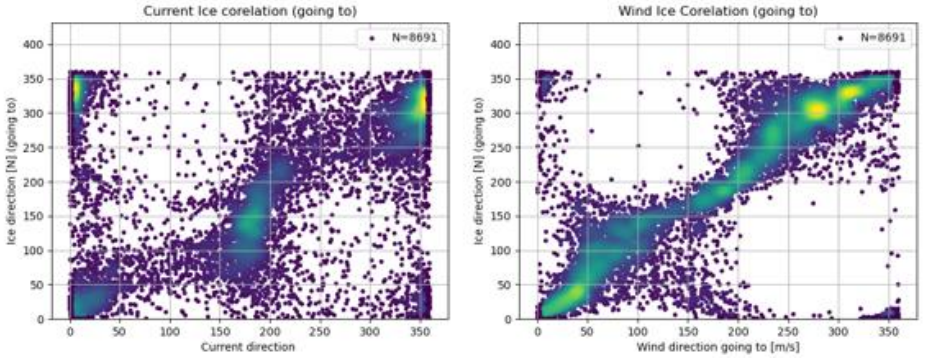

Figure 4-8 Correlation of ice movement vs. current and wind directions (all toward directions) for the 4 winter rmonths (Januar-April) for the 3 winter months 1985-1987. Colours indicate the number of observations: Yellow=high, Dark blue= low.

In Figure 4-9 the probability of ice speed for the 3 winter months January-March is shown for the 3 ice winters 1985-1987.

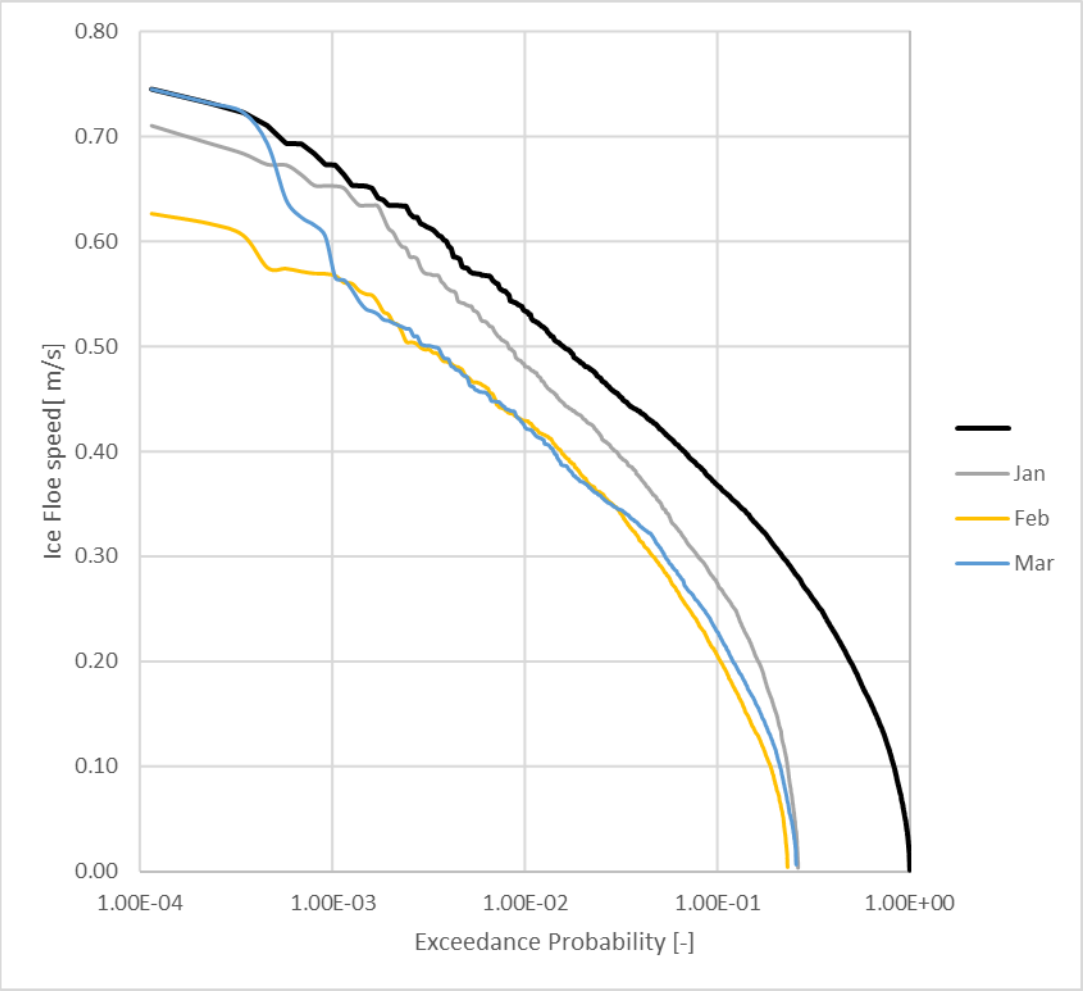

Figure 4-9 Probabilty of ice floe speed for the ice winters 1985-1987 (January-March). 1h/1y = 1/(3*30*24) = $4.6*10^{-4}$

In Table 4-6 and Table 4-7 the current directions and magnitude for the overall period 1979-2019 can be compared with the ice winters 1985-1987. It can be found that the directional distribution is similar but the magnitude of current speed is much less - about half.

Table 4-6 Current speed vs. current directions based on hourly data 1979 - 2019 (January-April).

Current speed[m/s]/ Current direction[Deg. N]	Interval	0.00	0.10	0.20	0.30	0.40	0.50	0.60	0.70	0.80	0.90	Total [%]	Total number events
Interval	Interval	0.10	0.20	0.30	0.40	0.50	0.60	0.70	0.80	0.90	1.00	-	-
345.00	15.00	5.66	12.51	6.53	1.48	0.22	0.03	0.01	0.00	0.00	0.00	26.43	31467
15.00	45.00	4.03	4.03	1.01	0.21	0.05	0.02	0.01	0.00	0.00	0.00	9.35	11131
45.00	75.00	2.64	0.76	0.04	0.00	0.00	0.00	0.00	0.00	0.00	0.00	3.44	4096
75.00	105.00	2.20	0.34	0.00	0.00	0.00	0.00	0.00	0.00	0.00	0.00	2.54	3027
105.00	135.00	2.57	0.53	0.01	0.00	0.00	0.00	0.00	0.00	0.00	0.00	3.12	3713
135.00	165.00	3.71	2.98	0.51	0.06	0.01	0.00	0.00	0.00	0.00	0.00	7.26	8644
165.00	195.00	4.29	8.65	5.35	1.96	0.61	0.18	0.04	0.02	0.01	0.00	21.10	25128
195.00	225.00	3.69	2.66	0.61	0.18	0.04	0.02	0.01	0.00	0.00	0.00	7.20	8572
225.00	255.00	2.69	0.61	0.04	0.00	0.00	0.00	0.00	0.00	0.00	0.00	3.33	3969
255.00	285.00	2.49	0.29	0.01	0.00	0.00	0.00	0.00	0.00	0.00	0.00	2.79	3318
285.00	315.00	3.04	0.62	0.02	0.00	0.00	0.00	0.00	0.00	0.00	0.00	3.69	4390
315.00	345.00	4.94	4.24	0.51	0.08	0.00	0.00	0.00	0.00	0.00	0.00	9.76	11625
Total Procentages [%]	-	41.94	38.21	14.63	3.97	0.92	0.25	0.06	0.02	0.01	0.00	100.00	-
Total Number of events	-	49939	45496	17418	4725	1100	296	71	26	7	2	-	119080

Table 4-7 Current speed vs. current directions based on hourly data 1985 - 1987 (January-April).

Current speed[m/s]/ Current direction[Deg. N]	Interval	0.00	0.10	0.20	0.30	Total [%]	Total number events
Interval	Interval	0.10	0.20	0.30	0.40	-	-
345.00	15.00	6.67	14.83	5.87	1.16	28.54	2480
15.00	45.00	3.97	3.48	0.61	0.10	8.16	709
45.00	75.00	2.27	0.39	0.00	0.00	2.66	231
75.00	105.00	1.88	0.06	0.00	0.00	1.93	168
105.00	135.00	2.18	0.21	0.00	0.00	2.38	207
135.00	165.00	3.43	1.61	0.31	0.01	5.36	466
165.00	195.00	4.44	7.69	3.82	1.28	17.22	1497
195.00	225.00	4.78	3.90	0.86	0.17	9.71	844
225.00	255.00	3.59	0.78	0.00	0.00	4.37	380
255.00	285.00	3.04	0.31	0.00	0.00	3.35	291
285.00	315.00	3.64	0.63	0.00	0.00	4.27	371
315.00	345.00	6.25	5.11	0.27	0.00	11.62	1010
Total Procentages [%]	-	46.12	39.00	11.74	2.73	99.57	-
Total Number of events	-	4008	3389	1020	237	-	8654

In Table 4-8 and Table 4-9 the wind speed and misalignment between wind direction and current directions for the overall period 1979-2019 can be compared with the ice winters 1985-1987. It can be found that the correlation between wind and current does not change much for the ice winter periods.

Table 4-8 Wind speed vs. misalignment to current direction based on hourly data 1979 - 2019 (January-April).

Wind_speed[m/s]/ Miss_aligment_current[Deg. N]	Interval	0.00	2.00	4.00	6.00	8.00	10.00	12.00	14.00	16.00	18.00	20.00	22.00	24.00	Total [%]	Total number events
Interval	Interval	2.00	4.00	6.00	8.00	10.00	12.00	14.00	16.00	18.00	20.00	22.00	24.00	26.00	-	-
-180.00	-150.00	0.01	0.11	0.36	0.42	0.33	0.15	0.09	0.02	0.00	0.00	0.00	0.00	0.00	1.49	1775
-150.00	-120.00	0.01	0.17	0.41	0.45	0.28	0.17	0.06	0.01	0.00	0.00	0.00	0.00	0.00	1.56	1857
-120.00	-90.00	0.03	0.25	0.53	0.63	0.40	0.17	0.06	0.01	0.00	0.00	0.00	0.00	0.00	2.07	2466
-90.00	-60.00	0.06	0.47	0.93	0.92	0.60	0.21	0.07	0.02	0.00	0.00	0.00	0.00	0.00	3.29	3912
-60.00	-30.00	0.20	1.20	1.74	1.72	1.25	0.53	0.19	0.06	0.01	0.00	0.00	0.00	0.00	6.92	8237
-30.00	0.00	1.30	2.55	3.09	3.27	2.87	1.90	0.67	0.19	0.05	0.02	0.01	0.00	0.00	15.92	18956
0.00	30.00	1.54	3.56	4.39	5.11	5.28	3.38	1.43	0.40	0.07	0.01	0.00	0.00	0.00	25.16	29961
30.00	60.00	0.21	1.64	3.75	5.28	5.94	3.90	1.67	0.58	0.13	0.02	0.00	0.00	0.00	23.13	27539
60.00	90.00	0.06	0.62	1.57	2.38	3.02	2.22	0.99	0.33	0.06	0.01	0.00	0.00	0.00	11.27	13420
90.00	120.00	0.02	0.29	0.73	1.05	1.30	0.90	0.41	0.12	0.02	0.00	0.00	0.00	0.00	4.83	5753
120.00	150.00	0.01	0.20	0.51	0.62	0.61	0.46	0.13	0.03	0.00	0.00	0.00	0.00	0.00	2.58	3070
150.00	180.00	0.01	0.14	0.37	0.49	0.43	0.21	0.10	0.02	0.00	0.00	0.00	0.00	0.00	1.79	2134
Total Procentages [%]	-	3.46	11.20	18.36	22.35	22.33	14.19	5.87	1.81	0.36	0.07	0.02	0.00	0.00	100.00	-
Total Number of events	-	4115	13334	21866	26611	26585	16899	6981	2158	426	78	23	2	2	-	119080

Table 4-9 Wind speed vs. misalignment to current direction based on hourly data 1985 - 1987 (January-April).

Wind_speed[m/s]/ Miss_aligment_current[Deg. N]	Interval	0.00	1.00	2.00	3.00	4.00	5.00	6.00	7.00	8.00	9.00	10.00	11.00	12.00	13.00	14.00	15.00	16.00	17.00	18.00	Total [%]	Total number events
Interval	Interval	1.00	2.00	3.00	4.00	5.00	6.00	7.00	8.00	9.00	10.00	11.00	12.00	13.00	14.00	15.00	16.00	17.00	18.00	19.00	-	-
-180.00	-150.00	0.00	0.02	0.05	0.23	0.18	0.15	0.23	0.23	0.16	0.14	0.12	0.06	0.08	0.08	0.02	0.02	0.00	0.00	0.00	1.77	154
-150.00	-120.00	0.00	0.06	0.07	0.17	0.20	0.15	0.35	0.24	0.21	0.15	0.16	0.10	0.01	0.05	0.00	0.00	0.00	0.00	0.00	1.91	166
-120.00	-90.00	0.00	0.02	0.18	0.24	0.21	0.33	0.33	0.31	0.21	0.21	0.07	0.05	0.04	0.01	0.02	0.00	0.00	0.00	0.00	2.23	194
-90.00	-60.00	0.02	0.13	0.24	0.46	0.39	0.58	0.51	0.25	0.18	0.25	0.06	0.00	0.00	0.00	0.00	0.00	0.00	0.00	0.00	3.07	267
-60.00	-30.00	0.04	0.35	0.64	0.87	1.11	0.79	0.64	0.61	0.43	0.17	0.18	0.14	0.04	0.02	0.02	0.00	0.00	0.00	0.00	6.05	526
-30.00	0.00	0.51	1.35	1.44	1.62	1.67	1.35	0.92	0.97	0.90	1.02	0.78	0.56	0.17	0.15	0.01	0.01	0.00	0.04	0.00	13.46	1170
0.00	30.00	0.56	1.07	1.89	2.64	2.21	2.31	2.06	2.21	2.22	1.92	1.74	0.97	0.58	0.38	0.14	0.01	0.02	0.05	0.00	22.97	1996
30.00	60.00	0.05	0.27	1.02	1.83	2.16	3.33	2.32	2.62	2.82	2.52	2.39	1.88	0.77	0.32	0.06	0.06	0.02	0.00	0.00	24.44	2124
60.00	90.00	0.00	0.08	0.32	0.58	0.78	1.53	1.35	1.44	1.81	1.86	1.60	0.83	0.38	0.36	0.24	0.02	0.00	0.00	0.00	13.17	1145
90.00	120.00	0.01	0.02	0.12	0.30	0.47	0.52	0.60	0.66	0.86	0.63	0.47	0.40	0.18	0.22	0.13	0.02	0.00	0.00	0.00	5.62	488
120.00	150.00	0.00	0.04	0.13	0.18	0.40	0.35	0.38	0.39	0.39	0.27	0.13	0.18	0.12	0.05	0.00	0.02	0.00	0.00	0.00	3.02	262
150.00	180.00	0.00	0.04	0.08	0.17	0.24	0.28	0.30	0.27	0.17	0.28	0.09	0.09	0.10	0.14	0.02	0.02	0.00	0.00	0.00	2.29	199
Total Procentages [%]	-	1.19	3.43	6.18	9.30	10.02	11.66	9.99	10.20	10.36	9.43	7.79	5.26	2.47	1.77	0.67	0.20	0.05	0.08	0.00	100.00	-
Total Number of events	-	103	298	537	808	871	1013	868	886	900	819	677	457	214	154	58	17	4	7	0	-	8691

In Table 4-10 and Table 4-11 ice speed is listed versus the wind speed and current speed.

Table 4-10 Ice speed vs. wind speed direction based on hourly data 1985-1987 (January-April).

V_ice[m/s]/ Wind_speed[m/s]	Interval	0.00	0.10	0.20	0.30	0.40	0.50	0.60	0.70	Total [%]	Total number events
Interval	Interval	0.10	0.20	0.30	0.40	0.50	0.60	0.70	0.80	-	-
0.00	1.00	0.78	0.38	0.02	0.00	0.00	0.00	0.00	0.00	1.19	103
1.00	2.00	2.19	1.12	0.13	0.00	0.00	0.00	0.00	0.00	3.43	298
2.00	3.00	3.39	2.49	0.30	0.00	0.00	0.00	0.00	0.00	6.18	537
3.00	4.00	3.35	5.09	0.85	0.01	0.00	0.00	0.00	0.00	9.30	808
4.00	5.00	2.52	5.52	1.77	0.18	0.02	0.00	0.00	0.00	10.02	871
5.00	6.00	1.52	6.62	3.03	0.47	0.01	0.01	0.00	0.00	11.66	1013
6.00	7.00	1.44	4.17	3.42	0.92	0.02	0.02	0.00	0.00	9.99	868
7.00	8.00	1.06	3.03	4.56	1.38	0.17	0.00	0.00	0.00	10.20	886
8.00	9.00	0.66	2.50	4.36	2.41	0.39	0.05	0.00	0.00	10.36	900
9.00	10.00	0.31	1.52	3.65	3.21	0.66	0.07	0.01	0.00	9.42	819
10.00	11.00	0.08	0.60	2.57	3.19	1.16	0.16	0.04	0.00	7.79	677
11.00	12.00	0.01	0.40	1.21	1.82	1.51	0.27	0.05	0.00	5.26	457
12.00	13.00	0.00	0.13	0.66	0.64	0.74	0.28	0.02	0.00	2.46	214
13.00	14.00	0.00	0.09	0.47	0.56	0.38	0.18	0.08	0.00	1.77	154
14.00	15.00	0.00	0.01	0.21	0.22	0.07	0.10	0.05	0.01	0.67	58
15.00	16.00	0.00	0.00	0.07	0.05	0.02	0.01	0.05	0.00	0.20	17
16.00	17.00	0.00	0.00	0.00	0.00	0.00	0.02	0.02	0.00	0.05	4
17.00	18.00	0.00	0.00	0.00	0.00	0.00	0.01	0.04	0.04	0.08	7
18.00	19.00	0.00	0.00	0.00	0.00	0.00	0.00	0.00	0.00	0.00	0
Total Procentages [%]	-	17.31	33.65	27.26	15.06	5.16	1.19	0.35	0.05	100.00	-
Total Number of events	-	1504	2924	2369	1309	448	103	30	4	-	8691

Table 4-11 Ice speed vs. current speed direction based on hourly data 1985-1987 (January-April).

V_ice[m/s]/ Current speed[m/s]	Interval	0.00	0.10	0.20	0.30	0.40	0.50	0.60	0.70	Total [%]	Total number events
Interval	Interval	0.10	0.20	0.30	0.40	0.50	0.60	0.70	0.80	-	-
0.00	0.10	10.91	19.55	11.94	3.54	0.16	0.01	0.00	0.00	46.12	4008
0.10	0.20	5.55	11.54	11.25	8.42	2.09	0.13	0.01	0.00	39.00	3389
0.20	0.30	0.84	2.38	3.23	2.77	1.90	0.51	0.08	0.02	11.74	1020
0.30	0.40	0.01	0.17	0.79	0.32	0.87	0.43	0.12	0.01	2.73	237
Total Procentages [%]	-	17.31	33.65	27.22	15.06	5.03	1.07	0.21	0.04	99.57	-
Total Number of events	-	1504	2924	2366	1309	437	93	18	3	-	8654

In Table 4-12 the ice speed is listed versus the ice direction.

Table 4-12 Ice speed vs. ice direction based on hourly data 1985-1987 (January-April).

V_ice[m/s]/ theta_ice[Deg. N]	Interval	0.00	0.10	0.20	0.30	0.40	0.50	0.60	0.70	Total [%]	Total number events
Interval	Interval	0.10	0.20	0.30	0.40	0.50	0.60	0.70	0.80	-	-
345.00	15.00	1.38	2.61	2.00	0.87	0.38	0.15	0.04	0.00	7.43	646
15.00	45.00	1.62	2.97	1.90	1.27	0.58	0.13	0.07	0.04	8.56	744
45.00	75.00	1.75	2.93	1.97	0.52	0.14	0.00	0.00	0.00	7.31	635
75.00	105.00	1.31	3.42	2.13	0.55	0.01	0.00	0.00	0.00	7.42	645
105.00	135.00	1.38	2.78	1.54	1.32	0.46	0.05	0.00	0.00	7.54	655
135.00	165.00	1.19	1.78	1.36	1.01	1.08	0.50	0.21	0.01	7.14	620
165.00	195.00	1.21	2.35	1.63	0.96	0.39	0.22	0.04	0.00	6.79	590
195.00	225.00	1.46	2.45	1.55	0.71	0.20	0.05	0.00	0.00	6.42	558
225.00	255.00	1.50	2.51	1.38	1.08	0.04	0.00	0.00	0.00	6.50	565
255.00	285.00	1.32	3.06	2.84	1.15	0.15	0.02	0.00	0.00	8.55	743
285.00	315.00	1.36	3.46	5.01	2.85	0.56	0.00	0.00	0.00	13.24	1151
315.00	345.00	1.83	3.31	3.95	2.76	1.17	0.08	0.00	0.00	13.11	1139
Total Procentages [%]	-	17.31	33.64	27.26	15.06	5.16	1.19	0.35	0.05	100.00	-
Total Number of events	-	1504	2924	2369	1309	448	103	30	4	-	8691

In Table 4-13 and Table 4-14 the misalignment of wind – ice directions is listed.

Table 4-13 Wind speed vs. misalignment wind/ice directions based on hourly data 1985-1987 (January-April).

Wind_speed[m/s]/Miss_ aligment_wind[Deg. N]	Interval	0.00	1.00	2.00	3.00	4.00	5.00	6.00	7.00	8.00	9.00	10.00	11.00	12.00	13.00	14.00	15.00	16.00	17.00	18.00	Total [%]	Total number events
Interval	Interval	1.00	2.00	3.00	4.00	5.00	6.00	7.00	8.00	9.00	10.00	11.00	12.00	13.00	14.00	15.00	16.00	17.00	18.00	19.00	-	-
-180.00	-150.00	0.14	0.17	0.10	0.18	0.16	0.01	0.06	0.02	0.06	0.02	0.00	0.00	0.00	0.00	0.00	0.00	0.00	0.00	0.00	0.93	81
-150.00	-120.00	0.13	0.16	0.20	0.33	0.12	0.12	0.05	0.09	0.08	0.01	0.00	0.00	0.00	0.00	0.00	0.00	0.00	0.00	0.00	1.28	111
-120.00	-90.00	0.07	0.21	0.38	0.38	0.38	0.47	0.20	0.18	0.18	0.12	0.01	0.01	0.00	0.00	0.00	0.00	0.00	0.00	0.00	2.59	225
-90.00	-60.00	0.07	0.22	0.45	0.70	0.55	1.19	0.51	0.47	0.54	0.44	0.30	0.21	0.08	0.06	0.06	0.00	0.00	0.00	0.00	5.84	507
-60.00	-30.00	0.09	0.32	0.98	1.53	1.67	2.05	1.98	1.95	2.36	2.00	1.93	1.81	0.66	0.41	0.17	0.07	0.02	0.00	0.00	20.00	1738
-30.00	0.00	0.13	0.43	1.45	2.57	3.39	4.48	4.22	4.87	5.05	4.89	4.18	2.32	1.39	0.99	0.36	0.09	0.02	0.05	0.00	40.87	3552
0.00	30.00	0.06	0.63	1.09	2.00	2.59	2.43	2.20	2.07	1.80	1.80	1.36	0.87	0.33	0.31	0.08	0.04	0.00	0.04	0.00	19.69	1711
30.00	60.00	0.12	0.43	0.62	0.69	0.36	0.39	0.40	0.29	0.21	0.13	0.01	0.04	0.00	0.00	0.00	0.00	0.00	0.00	0.00	3.67	319
60.00	90.00	0.14	0.15	0.40	0.38	0.31	0.14	0.14	0.12	0.01	0.02	0.00	0.00	0.00	0.00	0.00	0.00	0.00	0.00	0.00	1.81	157
90.00	120.00	0.06	0.23	0.25	0.20	0.28	0.15	0.10	0.09	0.01	0.00	0.00	0.00	0.00	0.00	0.00	0.00	0.00	0.00	0.00	1.37	119
120.00	150.00	0.08	0.25	0.08	0.20	0.15	0.20	0.02	0.05	0.04	0.00	0.00	0.00	0.00	0.00	0.00	0.00	0.00	0.00	0.00	1.06	92
150.00	180.00	0.12	0.23	0.17	0.14	0.07	0.05	0.12	0.00	0.02	0.00	0.00	0.00	0.00	0.00	0.00	0.00	0.00	0.00	0.00	0.91	79
Total Procentages [%]	-	1.19	3.43	6.18	9.30	10.02	11.66	9.99	10.20	10.36	9.42	7.79	5.26	2.46	1.77	0.67	0.20	0.05	0.08	0.00	100.00	-
Total Number of events	-	103	298	537	808	871	1013	868	886	900	819	677	457	214	154	58	17	4	7	0	-	8691

Table 4-14 Ice speed vs. misalignment wind/ice directions based on hourly data 1985-1987 (January-April).

V_ice[m/s]/ Miss_aligment_wind[Deg. N]	Interval	0.00	0.10	0.20	0.30	0.40	0.50	0.60	0.70	Total [%]	Total number events
Interval	Interval	0.10	0.20	0.30	0.40	0.50	0.60	0.70	0.80	-	-
-180.00	-150.00	0.66	0.24	0.04	0.00	0.00	0.00	0.00	0.00	0.93	81
-150.00	-120.00	0.76	0.43	0.09	0.00	0.00	0.00	0.00	0.00	1.28	111
-120.00	-90.00	1.13	1.01	0.41	0.04	0.00	0.00	0.00	0.00	2.59	225
-90.00	-60.00	1.31	2.50	1.69	0.23	0.10	0.00	0.00	0.00	5.83	507
-60.00	-30.00	2.43	6.98	6.02	2.54	1.59	0.35	0.08	0.01	20.00	1738
-30.00	0.00	3.53	11.64	13.09	9.18	2.47	0.73	0.20	0.02	40.87	3552
0.00	30.00	2.76	7.32	5.45	2.99	0.98	0.10	0.07	0.01	19.69	1711
30.00	60.00	1.69	1.57	0.31	0.08	0.01	0.01	0.00	0.00	3.67	319
60.00	90.00	1.02	0.70	0.08	0.00	0.00	0.00	0.00	0.00	1.81	157
90.00	120.00	0.83	0.52	0.02	0.00	0.00	0.00	0.00	0.00	1.37	119
120.00	150.00	0.67	0.38	0.01	0.00	0.00	0.00	0.00	0.00	1.06	92
150.00	180.00	0.52	0.36	0.04	0.00	0.00	0.00	0.00	0.00	0.91	79
Total Procentages [%]	-	17.30	33.65	27.26	15.06	5.16	1.19	0.35	0.05	100.00	-
Total Number of events	-	1504	2924	2369	1309	448	103	30	4	-	8691

5 Climate and ice properties

Climate and ice properties relevant for estimating sea ice load are based on general available information for the southern part of the Kattegat and project specific data as described in section 1.3. Air properties can be found in Table 5-1. Water level information's can be found in Figure 5-1 and Figure 5-2.

5.1 Air properties

Table 5-1 Air properties (Based on data as described in section 1.3)

Parameter	Units	Mean	Extreme Min	Extreme Max
Air temperatures normal	(°C)	8.9	-13.5	26.3
Air temperatures extreme (turbine stopped)	(°C)	-	-20	45
Air density	(kg/m^3)	1.252	1.176	1.389
Air pressure	(hPa)	1013	955	1049
Relative humidity	(%)	81.0	35.5	99.8

5.2 Water levels and tidal range

The principal cause of water level fluctuation is meteorologically induced surge associated with surface wind forcing and response to atmospheric pressure fluctuations. Typical annual values of still water level fluctuation are around (+1.5 + |-0.85| = 2.35 m. ref. Figure 5-1 and Figure 5-2. The 100-year extreme positive surge elevation is estimated to: 1.75 m.

5.2.1 Water level distribution

The water level distribution is based on data as described in section 1.3.3. OBS: The input data represent the 4 winter months (Januar – April) for the years 1979-2019.

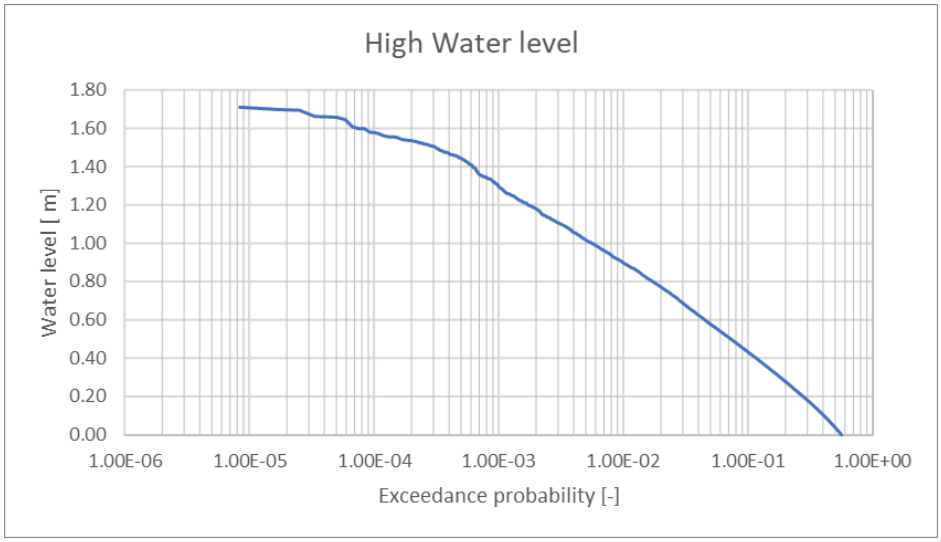

Figure 5-1 Exceedance probability (hourly) of high water level January to April, 1979-2019. Events: 118080. Probability 1h/1y: $1/(4*30*24) = 3.5*10^{-4}$

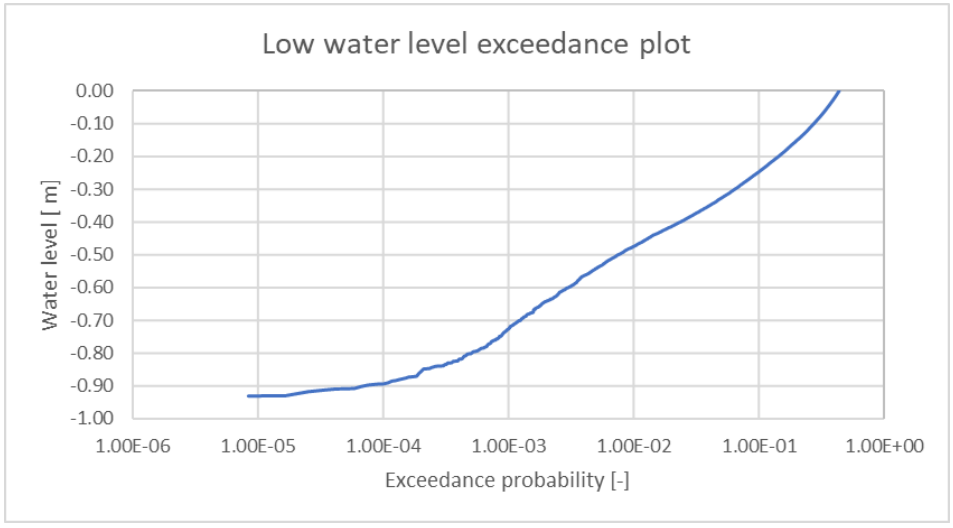

Figure 5-2 Exceedance probability (hourly) of low water level for January to Marts, (3 months) 1979-2019. Events: 118080. Probability 1h/1y: $1/(4*30*24) = 3.5*10^{-4}$

5.2.2 Sea level rise due to climate changes

Process-based (IPCC) global climate models project that the sea level rise in GMSL during the 21st century (i.e. in 2100, compared with 1986-2005) will likely (66 % confidence) be in the range of 0.29-0.59 m for a low emissions scenario (RCP2.6), 0.39-0.72 m for a medium emissions scenario (RCP4.5) and 0.61-

1.10 m for a high emissions scenario (RCP8.5). Minor land heave will happen in the area of Hesselø OWF which partly will compencate the water level rise.

In the lifetime (e.g. 40 years) of the Hesselø OWF, the yearly uniform increase in the water level with reference to Figure 5-3 is estimated to 2-3 mm/year. With an estimated uniform 3 mm/year water level increase the total water level increase is 0.12 m over 40 years.

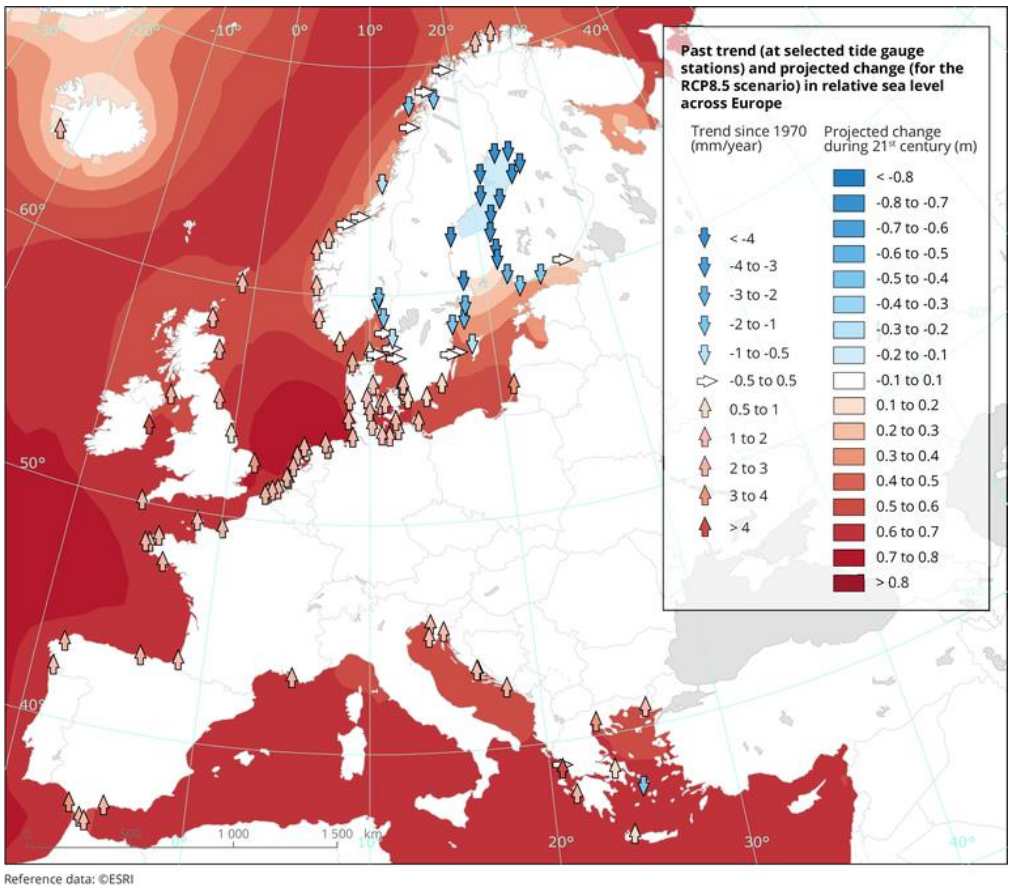

Figure 5-3 Sea level rise according RCP8.5 scenario (ESRI)

Note: The arrows show the trend in relative sea level at selected European tide gauge stations since 1970 (in mm/year) based on data from the Permanent Service for Mean Sea Level (PSMSL). The background colours show projections of European sea level change for 2081–2100 for RCP8.5 (in meters).

The water level rise for Denmark are estimated by DMI ref. [122] as shown in Figure 5-4.

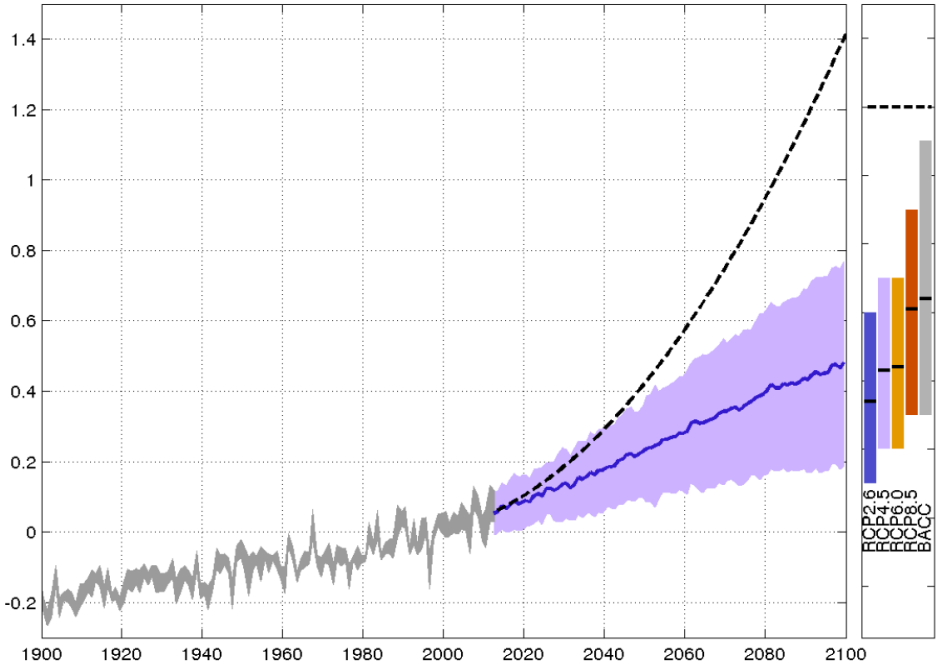

Figure 5-4 Average water level rise. Estimates according RCP are shown in the right site. Dashed line is the worst scenario estimate ref. DMI [122].

5.3 Temperature

Design water temperature: $-5°C < T_{sea,design} < 20°C$

Freezing point temperature of sea water (20 PSU): -0.9°C

5.4 Salinity

The seawater salinity in Kattegat varies from 3.0% in the north of Kattegat to about 1.5% in the south-western part of the Kattegat. For the present project salinity shall be taken as: 2%.

Figure 5-5 Salinity of the sea water in Kattegat with variations depening of the current direction (left: toward south and right: toward north). [125]

5.5 Ice brine volume

The ice brine volume v_b [ppt] of enclosed saline brine influences porosity and density of sea ice. Typical brine volumes are in the range of 20 to 100 ppt, depending on salinity, temperature, type and age of the ice. From salinity and ice temperature, v_b can be estimated by:

$$\nu_b = 41{,}64\, S_B^{0{,}88} \left|\vartheta_A\right|^{-0{,}67} \tag{5.1}$$

where:

S_B: Bulk salinity after completed ice growth [ppt].

ϑ_A: Ice temperature, averaged over the ice thickness [°C].

See section 1.3.2.4. of [106].

Note: This is an ice property that normally is used to determine the ice strength. In the present document this property is overruled by a generalized method to determine the ice strength.

5.6 Porosity

Naturally grown sea ice contains various inclusions and irregularities which lead to a porosity ϕ_B [ppt] of typically 3 to 20 ppt, approximately described by:

$$\phi_B = 19{,}37 + 36{,}18 \cdot S_B^{0{,}91} \cdot \left|\vartheta_A\right|^{-0{,}69} \tag{5.2}$$

Where S_B und ϑ_A are as defined under Section 5.5.

See section 1.3.2.5. of [106].

Note: This is an ice property that normally is used to determine the ice strength. In the present document this property is overruled by a generalized method to determine the ice strength.

5.7 Seawater and ice density

Seawater density variation:	1003-1013 kg/m³
Seawater typical density [106]:	1007 kg/m³

The sea ice density depends on salinity, temperature and the age of the ice. Typical values are in range of 912 kg/m³ to 925 kg/m³ [106]. For the Kattegat the value of 920 kg/m³ can be used as an average value [106].

5.8 Ice strength

Tensile strength, compressive (=crushing) strength and flexural (=bending) strength are basic properties of sea ice used in any analytical or empirical model. Approximation methods to calculate these values are given in ISO 19906 [103] or as found below according GL [106].

Three different ice crushing phenomena may occur, depending on the ice speed. Low ice speed below 0.04 m/s may lead to intermittent crushing.

Moderate ice speed in the range of 0.04 m/s to 0.1 m/s may lead to frequency lock-in. High ice speed of more than 0.1 m/s may lead to continuous brittle crushing. For more details refer to ISO 19906 [103].

5.8.1 Tensile strength

The tensile strength σ_t [MPa] of saline ice can be approximated from [106]:

$$\sigma_t = \left(1 - \sqrt{\frac{\nu_b}{\nu_0}}\right)^2 \cdot \sigma_0 + S \tag{5.3}$$

Where:

V_b: Brine volume [ppt] as given in Section 5.5

V_0: Reference volume between 100 and 142 ppt; for calculation purposes a value of 142 ppt should be used

σ_0: Reference strength 2.5 MPa

S : Security surcharge; S=0.4

Typical values are in range of 0.5 to 3 MPa.

Note: In the present document this property is overruled by a generalized method to determine the ice strength.

According the formulas of ISO 19906 [103] the tensile strength is about 10-20% lower than the bending strength. However due to the scatter of measured ice strength it is recommended using the same strength values for tensile and bending.

In connection to the Great Belt link project a review was carried out of the available ice load field measurement. This resulted in the data presented in Table 5-2. For a frost index of around 290 ref. Table 4-3 it is seen that the corresponding bending strength is 0.43 MPa and 0.47 MPa for a frost index around 350 ref. Figure 5-6.

The tensile strength can conservatively be assumed to be equal to the bending strength e.g. 0.43 MPa and 0.47 MPa for respectively the 1/50y and the 1/100y event.

5.8.2 Compressive/crushing strength

The compressive/crushing strength σ_c [MPa] of saline ice can be approximated from [106]:

$$\sigma_c = 2700 \cdot \dot{\varepsilon}^{1/3} \cdot \phi_B^{-1} \tag{5.4}$$

Where:

ε : Strain rate, typically $\varepsilon = 10^{-3}\ s^{-1}$, depending on the rate of interaction (ice drift velocity)

ϕ_B: Ice porosity as given in Section 5.6

Typical values for σ_c are in range of 0.5 and 12 MPa.

Note: In the present document this property is overruled by a generalized method to determine the ice strength.

For the South Baltic locations the ice crushing strength is recommended to be selected in accordance to section 6.1.1.

5.8.3 Flexural/bending strength

The flexural/bending strength σ_f [MPa] of saline ice can be approximated from [106]:

$$\sigma_f = 1.76 * e^{-5.88\sqrt{\frac{v_b}{1000}}} = 1.76 * e^{-0.19\sqrt{v_b}} \quad (5.5)$$

Where:

v_b: Brine volume [ppt] ref. Section 5.5

Typical values for σ_f are in range of 0.5 to 2 MPa. Actual design values are assessed below.

Ice bending strength

The bending strength is usually calculated on the basis of brine contents related to sea ice temperature and salinity – see above. But the variation of the ice temperature and salinity gives such large scatter that the procedure gives unreliable results. Therefore, a more robust estimate is suggested. This originates from the ice design basis applied for Danish Belt crossing projects as shown in Table 5-2. The results are reasonably consistent with the rough estimates which may be found from ice temperature/salinity estimates.

Table 5-2 Ice Design Basis applied for Great Belt and Øresund Links [114].

Return period (years)	5	10	50	100	500	700	1000	1320
K_{max} (-°C 24 hours)	170	245	410	480	665	700	721	744
σ_c (MPa) (no account to snow)	1.00	1.50	1.90	2.00	2.25	2.30	2.35	2.40
σ_f (MPa)	0.25	0.39	0.50	0.53	0.60	0.61	0.62	0.64
h (m)	0.33	0.42	0.57	0.63	0.75	0.77	0.78	0.80
h r_u	0.33	0.63	1.08	1.26	1.69	1.77	1.83	1.92
h^2 r_f	0.04	0.07	0.16	0.21	0.34	0.36	0.38	0.41

Where:

σ_c: the crushing strength of the ice

σ_f: the bending strength of the ice

h: thickness of the ice = 0.032 $(0.9\ K_{max} - 50)^{0.5}$

K_{max}: frost index = the sum of the 24-hour average temperature (in °C) during the frost period (<0°C).

Based on the design values as listed in Table 5-2 the following distribution of the bending strength vs. frost index can be found as shown in Figure 5-6.

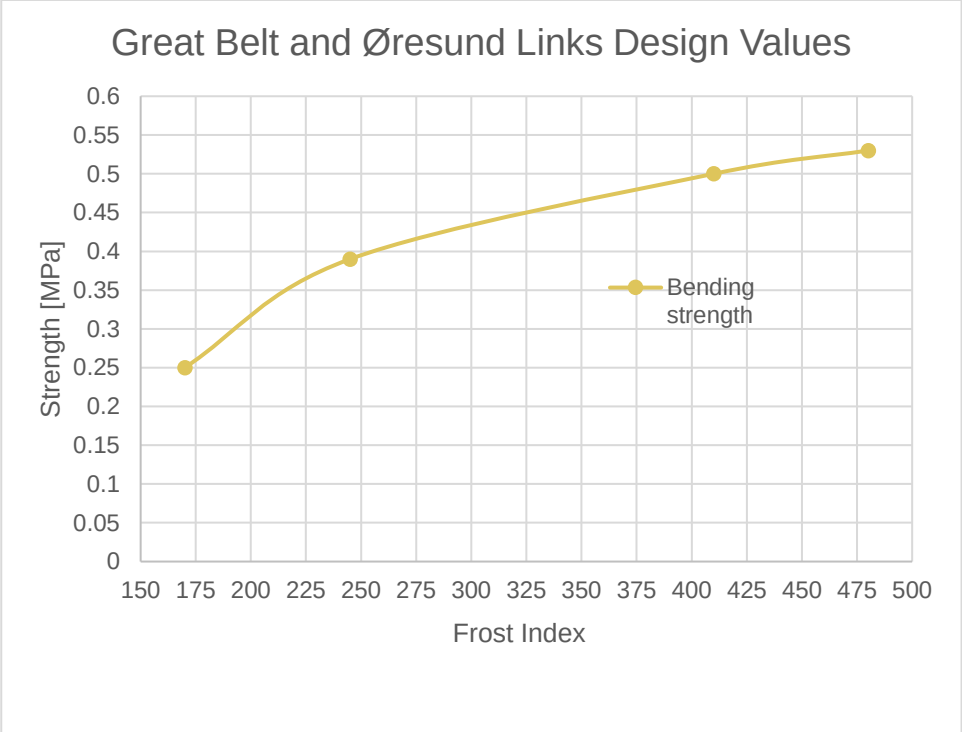

Figure 5-6 Bending strength vs. frost index (dots for Frost Index of 170, 245, 410 and 480) ref. Table 5-2.

For the Hesselø OWF project the frost indexes of 292 and 352 are estimated for the 1/50y and 1/100y return events ref. section 4.2 hence the bending strength of $\sigma_{f,50y}$ = 0.43 MPa and $\sigma_{f,100y}$ = 0.47 MPa can be applied ref. Figure 5-6. Due to limited documentation of the reduced bending strength for lower Frost indexes and smaller ice floe thickness the bending strength is generally set to minimum 0.30 MPa for all ice thickness estimated for Hesselø OWF (based on a requirement from the certifying agency in a previous project).

5.9 Poisson ratio

Poisson ratio of sea ice [115] and [103]: 0.33

Range: 0.3 – 0.35

5.10 Young's modulus

Effective elasticity ref. ISO 19906 A.8.2.8.9 [103]

$$E_f = 5.31 - 0.436{v_b}^{0.5} \quad (5.6)$$

E_f: is the effective elastic modulus

v_b: is the brine volume fraction

With an ice salinity of 2% and an ice temperature of -3 deg. the recommended effective elasticity modulus is:

2.7 GPa

Local range: 2 GPa – 4 GPa

5.11 Ice friction coefficient

The friction coefficient is usually described as static friction coefficient μ_s and dynamic friction coefficient μ_d. The dynamic friction coefficient has usually been considered to be a constant but newer investigations, Nakazawa et al (1993) [108] and Frederking & Barker (2002) [109] have shown that μ_d is strongly dependent upon the velocity between the structure and the ice. The velocity estimate shall include the eventual velocity of the structure due to structural deflection. The following estimate may be proposed:

$\mu_d = 2\ \mu_{d0}$, 1 m/s < V_{ice} ⇔ $\mu_d = \mu_{d0}\ (2 - \log V_{ice})$, 10^{-3} m/s < V_{ice} < 1 m/s

where μ_{d0} is a constant depending on the structure surface, see Table 5-3.

Table 5-3 Friction coefficients between ice and structures.

Surface of structure	Static friction coefficient μ_s	Dynamic friction factor μ_{d0}	Dynamic friction coefficient μ_d		
Ice velocity (m/s)	**-**	**-**	**0.01**	**0.1**	**1**
Concrete	0.3	0.05	0.20	0.15	0.1
New uncoated steel	0.3	0.03	0.12	0.09	0.06
Painted steel	0.25	0.02	0.08	0.06	0.04
Corroded steel	0.45	0.05	0.20	0.15	0.1
Ice-ice	<0.1	<0.1	0.1	<0.1	<0.1

6 Horizontal ice loading (Crushing)

Calculation of ice loads are not fully standardized. For this reason the main sections of the relevant standards, extensions and notes are included below.

ISO 19906 [103] A.8.2.4.3.2 includes a rational design method for calculation of horizontal ice loads from crushing ice based on field measurements now been implemented in IEC 61400-3 [102] D.4.4.

Ice crushing strength can be estimated based on measured and calibrated ice load data.

The global horizontal crushing ice load is calculated by:

$$F_G = p_G * w * h \quad (6.3)$$

p_G: is a value of the external global pressure (MPa),

w: is the width of the structure (m),

h: is the thickness of the ice sheet (m)

Data obtained from full-scale measurements in Cook Inlet, the Beaufort Sea, the Baltic Sea and Bohai Bay have been used to determine upper bound action values for scenarios where a first-year or multi-year sheet ice acts against a vertical structure. The data have also been used to analyse how the ice thickness and the width of the structure influence the global ice action. Based on these studies, the global ice pressure can be determined from equation (6.4):

The formula for p_G is according ISO 19906 [103]:

$$p_G = C_R \left[\left(\frac{h}{h_1} \right)^n \left(\frac{w}{h} \right)^m + f_{AR} \right] \quad (6.4)$$

where

p_G: is a value of the external global pressure (MPa),

w: is the width of the structure (m),

h: is the thickness of the ice sheet (m), h_1=1 m

m, n: n are the empirical exponents to take account of the size effect.
$m = -0.16$,
$n = -0.50 + h/5$ for $h < 1.0$ m and $n = -0.30$ for $h \geq 1.0$ m,

C_R: is the ice crushing strength coefficient, in MPa (in different ice regimes)

f_{AR}: is an empirical term for

$$f_{AR} = e^{\frac{-w}{3h}} \sqrt{1 + 5\frac{h}{w}} \quad (6.5)$$

If w/h > 5 the term f_{AR} can be disregarded.

Observations of ice interactions on relatively narrow lighthouse structures (structures width < ~2m, ice thickness <~1m) in the north Baltic Sea support the inclusion of the f_{AR} term (6.5) in the formula (6.4).

The ice crushing strength coefficient (C_R) is varying depending on the frost index. For the Beaufort Sea where the frost index is around 2000, the ice strength coefficient is typically around $C_{R\ 1/100y}$ = 2.8 MPa.

For a stiff structure in the North Baltic Sea (frost index = say 1000) $C_{R\ 1/100y}$ = 1.8 MPa in conditions where the ice speed was higher than 0.1 m/s and the maximum waterline displacements in the direction of ice action of the structure were about 0.4 % of the ice thickness.

There is a general experience that the ice load for ice floe speed lower than 0.1 m/s typically is twice the load for ice speed higher than 0.1 m/s.

According to ISO 19906 [103] One should combine a safe estimate of the (1/50-1/100y) ice thickness with C_R(1/y) and a 1/y ice thickness with a 1/100y C_R value. However for Hesselø OWF there is no ice thickness 1/y so this combination is not relevant.

The new version of IEC 61.400-3 [102] results in higher crushing forces for thinner ice than in the old version as it has to be assumed that C_R = minimum 0.66 MPa.

6.1.1 Modification of ice crushing strength

As the ice load models in ISO 19906 [103] are only representative for locations with heavy ice each year, the ISO 19906 [103] estimate has to be modified to include Kattegat, with only heavy ice around every 5 - 8 years. According ISO 19906 [103] the crushing strength is determined by the return period of ice occurrence. This has been described for areas with severe ice coverage but not for Kattegat. To cover the gap reference is made to Gravesen and Kärna (2009) [107]. The main conclusion yields C_R^{SB} = 1.0 MPa for South Baltic compared to C_R^{NB} = 1.3 MPa for the North Baltic for a 5 years return period. Based on similar frost indexes and ice coverage for the South Baltic Sea compared to Kattegat it is considered safe to use the conclusion of the reference [107] for Hesselø OWF. For a lower return period (1-2 years) Figure 6-1 show a CR value of 0.64 MPa. With the safety factors as used in [107] this lead to 0.64 * 1.2 * 1.11 = 0.85 MPa which is considered suitable for Hesselø OWF.

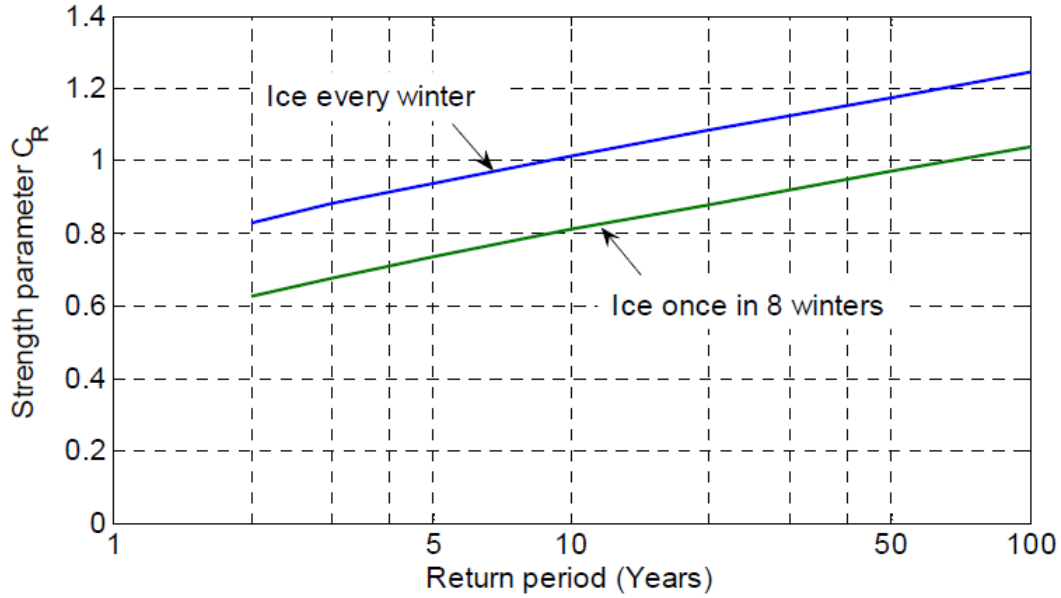

Figure 6-1 Two modes for ice strength parameter CR as function of the return period. [107] Figure 5

The evaluation of the ice crunching strength can be further supported by the measured Nordstrømgrund data as illustrated in Figure 6-2.

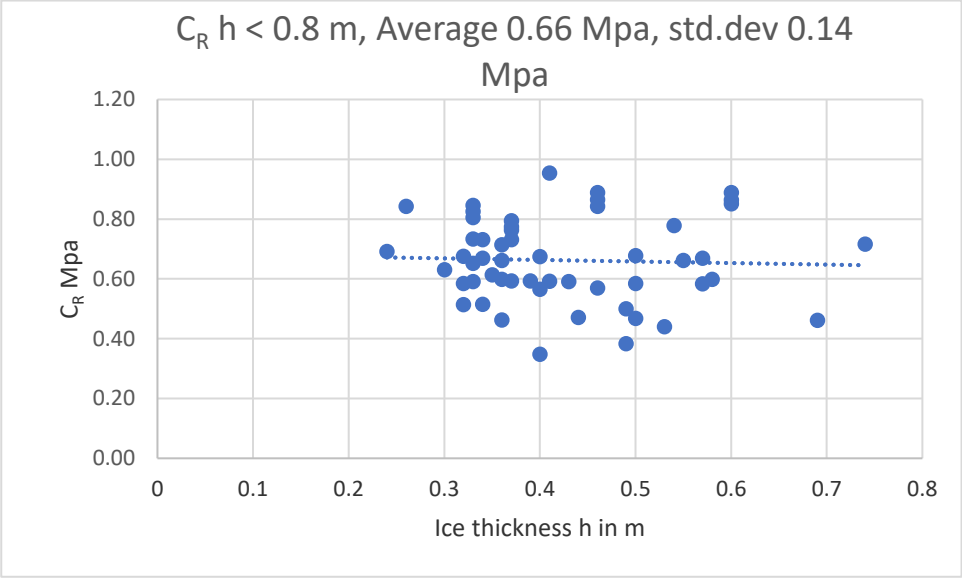

Figure 6-2 C_R values based on measured Nordstrømsgrund data on overall load for ice thickness h< 0.8 m [124].

By considering the Nordstrømsgrund data (Figure 6-2) and [124] creating the basis for ISO 19906 [103] it cannot be recommended to apply a C_R design value of less than 0.85 MPa for an extreme load and no less than 0.66 MPa for the average load.

According to ref. [107] both laboratory data and field data show that ice loads acting on a vertical structure will increase if the compliance of the structure increases. Accordingly, it can be concluded that the apparent ice strength will

increase if the waterline displacement u_w is higher than 0.5 % of the ice thickness [107]. A generalised empirical curve shown in Figure 6-3 is proposed for narrow monopile foundations that are a common option for offshore wind turbines. The compliance parameter γ_S shown in Figure 6-3 is used as a multiplication factor on the ice strength coefficient - C_R.

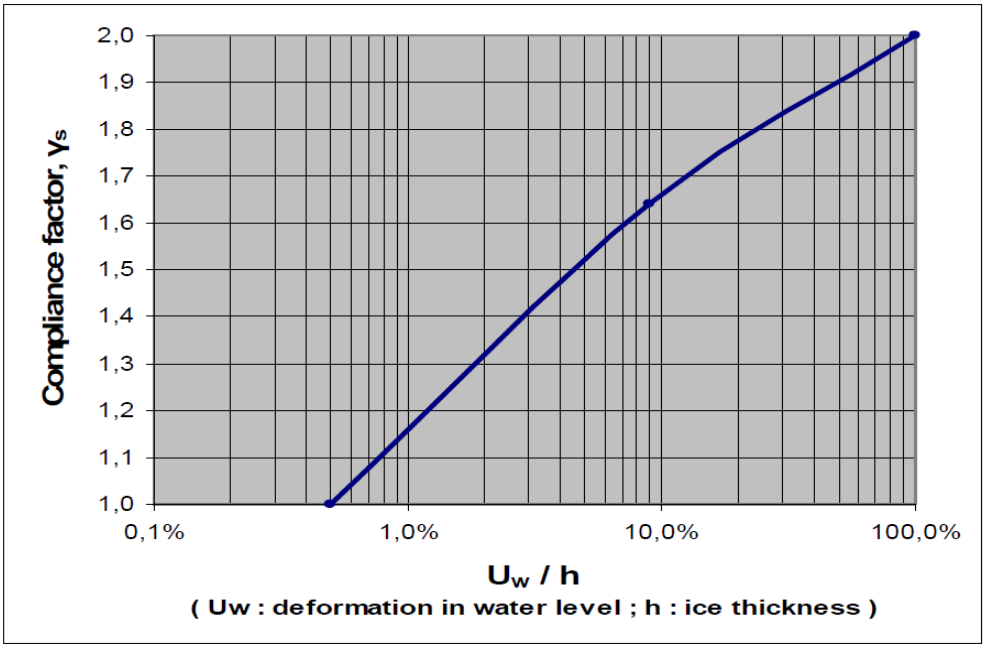

Figure 6-3 Compliance factor γ_s. versus relative deformation in water level for quasistatic ice load (Gravesen and Kärna (2009)) Ref. [107].

For the preliminary design assessment a crushing strength of 1 MPa shall be considered. If the ice crushing strength of 0.85 MPa is used for the one year return value for the final design it shall be verified that the final overall design parameters lead to a conservative design. Please observe that: The crushing strength shall be multiplied with the compliance factor or the load model shall include the crushing strength amplification related to the dimension of the structure and the water level variation.

7 Vertical ice loading according to IEC 61400-3

According IEC 61400-3 [102] D.4.5 the vertical load in case of fluctuating water level with a fast ice cover frozen to the support structure is limited either by the shear strength at adhesion to the support structure surface, V_τ , or by the bending strength if the ice is broken in a ring around the support structure, V_b . The lower of the two alternatives is decisive and should be used.

$$V_\tau = A\tau \tag{7.1}$$

where

τ is the adhesive shear strength, and

$A = \pi Dh$ is the contact surface for a circular vertical support structure.

The adhesive shear strength τ can be set to:

0.8 MPa for steel – freshwater ice,

0.3 MPa for steel – saline ice, or to

1 MPa for concrete – saline ice

$$V_b = 0.6A\sqrt{\sigma_b pg\Delta z} \tag{7.2}$$

where

A: is the contact surface;

σ_b: is the bending strength of ice, not less than 0.26 σ_c;

ρ: is the water density;

g: is the gravitational acceleration;

Δz: is the water level difference.

Note that ice can grow between braces in multi-legged structures.

8 Local ice pressures

According to IEC 61400-3 [102] Section D.4.4.4

The support structure should be designed for the following local ice pressure:

$$p_{c,local} = \sigma_c \, (1 + 5 \, h^2/A_{local})^{0.5} < 20 \text{ MPa} \qquad (8.1)$$

where

$p_{c,local}$	is the characteristic local ice pressure for use in design against moving ice
σ_c	is the characteristic crushing strength for local ice pressure. σ_c = 1.2 MPa is suggested.
h	is the characteristic thickness of the ice
A_{local}	is the local area considered

9 Dynamic ice loads

The wind turbine should be checked for dynamic effects from ice loading. When assessing whether dynamical effects can occur, and how often, it is often necessary to consider ice mobility, floe sizes, ice concentration, misalignment between ice drift- and wind-direction, as well as ice types. In particular, conclusions cannot be based on information on ice concentration alone.

It can be helpful to note that if the appropriate type of mobile ice is present at a site, frequency lock-in is almost always possible since the ice speeds required are usually small, e.g. of the order of 0.1 m/s. Although frequency lock-in is possible due to the factors above, it does not necessarily occur all the time: An assessment of this can be made based on the homogeneity of the ice. As a further guidance, frequency lock-in does normally not occur for ice concentrations below 7/10. All relevant ice speeds, in combination with durations and ice thicknesses, should be considered. Below some simplified equations are given for dynamic load simulation which can be used if statistical data, sufficiently advanced numerical models or measurements are not available.
The criterion for susceptibility to frequency lock-in for the ice acting on a single point is:

$$\xi_n \leq \frac{\phi_{nC}^2}{4\pi f_n M_n} \cdot h \cdot \theta \qquad (9.1)$$

where:

f_n	is the *n*'th eigenfrequency [Hz],
M_n	is the modal mass of the *n*'th eigenmode in [kg],
ξ_n	is the damping of the *n*'th eigenmode as a fraction of critical damping [s],
ϕ_{nC}	is the magnitude of the *n*'th eigenmode at the ice action point,
h	is the ice thickness [m], and
θ	is a coefficient with the suggested value of $40 \cdot 10^6$ kg/m·s.

Thus, the design procedure for analyzing frequency lock-in consists of the following steps:

a) Solve the eigenvalues and modes of vibration.
b) Identify the modes that could be susceptible to frequency lock-in using the criterion above: i.e. if a mode's damping is smaller than or comparable to the right hand side of equation (9.1), it could be susceptible to frequency lock-in.
c) Calculate the dynamic response.

Simplifying forcing functions
The simplified forcing function from Figure 9-1 can be used for determination of response of the vertical structure under frequency lock-in vibrations. The frequency f = 1/T, of the forcing function corresponds to the frequency of one of the susceptible natural modes with a natural frequency below 10 Hz, as derived from equation (9.1). The maximum force Hmax, as well as the amplitude ΔH =

Hmax − Hmin, can be assumed constant. The peak values can be determined according to equation (6.3). The forcing function should be long enough to assure a steady-state response of the structure. The amplitude ΔH depends on the vibrational modes of the structure and on the ice velocity. It can be expressed as a fraction q, of the maximum force Hmax. The amplitude ΔH should be scaled so that the velocity response at the waterline is 1.4 times the highest ice velocity. This should assure conservative results in terms of the structural response.

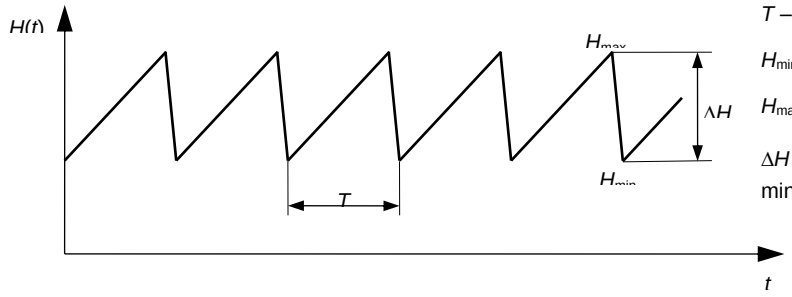

T – period of ice action

H_{min} – minimum value of ice action

H_{max} – maximum value of ice action

ΔH – difference between maximum and minimum values of ice action

Figure 9-1 Ice load history for frequency lock-in conditions.

A cone at the waterline can reduce the magnitude of ice-induced vibrations relative to the analogous vertical structure. However, structures with narrow cones at the waterline can still experience ice-induced vibrations. The vibrations are enhanced when stable ice rubble does not form on the front face of the cone. The time history for this kind of ice action is presented in Figure 9-2. The dynamic response of the structure excited by this random forcing function is less than due to frequency lock-in on a similar vertical structure.

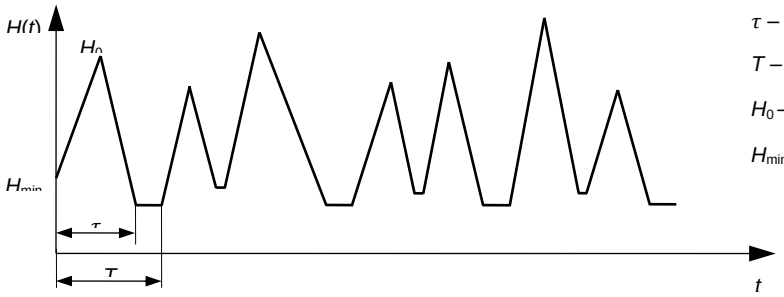

τ – duration of loading/unloading cycle

T – period of ice action

H_0 – peak value of ice action

H_{min} – minimum value of ice action

Figure 9-2 Time history of horizontal force component of ice load acting on a conical structure.

The time-varying action, H(t), is a function of several parameters, including the width of the structure, slope angle and the frictional actions involved.

The dynamic behaviour of ice introduced vibrations are further described in the guidelines from ISO 19906 [103] section A.8.2.6.1.1, A.8.2.6.1.2 and A.8.2.6.1.3, that are included in the following.

A.8.2.6 Dynamic ice actions

A.8.2.6.1 Dynamic actions on vertical and near-vertical structures

A.8.2.6.1.1 General

Ice-induced vibration is observed for practically all vertical and near-vertical fixed structures exposed to moving ice conditions, such as production platforms in Cook Inlet, the Bohai Sea and the Sea of Okhotsk and lighthouses and light piers in the Baltic Sea. Severity of observed ice-induced vibration varies significantly depending on structural properties and ice conditions.

Ice-induced vibration is observed when the ice fails predominantly by crushing. Figure A.8-30 illustrates the three primary modes of interaction in terms of the ice action, $F(t)$, and the corresponding structural displacement at the ice action point, $u(t)$. These loading traces are typical for vertical and near-vertical piles or multi-legged structures. The dynamic ice-structure interaction process is influenced significantly, but not exclusively, by the ice velocity and the waterline displacement of the structure. As a result, the three modes are not necessarily observed for all structures. In general, all three dynamic ice-structure interaction modes are observed for narrow vertical structures. For wide structures, intermittent crushing has been observed in severe ice conditions[186]. The processes involved in these three modes of interaction are described in A.8.2.6.1.2.

The structural response in the three primary modes of interaction is important primarily for FLS design. The challenge for FLS design is to determine the combinations of ice drift velocities and ice properties for which each of the three modes can be expected to develop. Guidance for determining velocity ranges associated with frequency lock-in can be found in References [187], [188] and [189]. One aspect of this process is the potential decrease in the load borne by the ice as the ice velocity relative to the structure increases[188][189].

Frequency lock-in can cause resonant loading and can contribute significantly to fatigue accumulation in structures. This dynamic loading state can cause low-cycle fatigue in steel structures and can also cause liquefaction in the soil foundation. Vibrations can also affect topsides structures, such as flare booms, see 15.1.1.3. The vulnerability of structures to frequency lock-in is addressed in A.8.2.6.1.4.

Once the expected modes of interaction are identified for a structure, the structural response can be determined:

— based on ice action data from a similar structure in similar ice conditions;

— using prescribed force-time histories applied to finite-element or other types of structural dynamics models;

— using numerically-generated loading based on a knowledge of ice mechanics applied to finite-element or other types of structural dynamics models.

In the case of intermittent crushing, the ice action peaks can also be important for ULS design.

When ice action data from other structures are applied, it is emphasized that the dynamic interaction problem is strongly non-linear which puts stringent requirements on the similarity. With numerically-generated loading it is emphasized that different theories regarding the development of ice-induced vibration can result in different predictions. Prescribed force-time histories are given in A.8.2.6.1.3 for intermittent crushing and in A.8.2.6.1.5 for frequency lock-in.

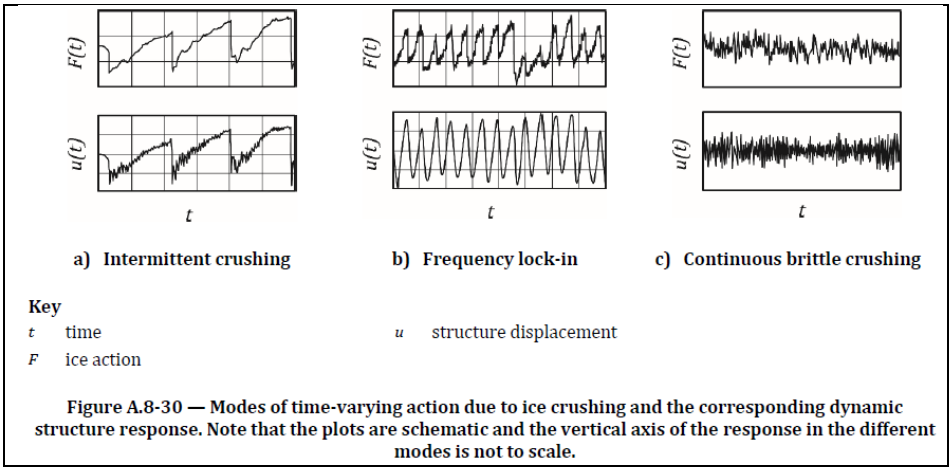

Figure A.8-30 — Modes of time-varying action due to ice crushing and the corresponding dynamic structure response. Note that the plots are schematic and the vertical axis of the response in the different modes is not to scale.

Figure 9-3 ISO 19906 [103] Section A.8.2.6.1.1 Dynamic ice actions

A.8.2.6.1.2 Time-varying interaction processes

Intermittent ice crushing, depicted in Figure A.8-30 a), can arise if a compliant structure is exposed to actions from slowly moving ice. The interaction involves load build-up and unloading phases.

During the loading phase, the ice action increases and ice edge contact increases due to local crushing and ductile deformations. The velocity of the structure at the waterline is approximately the ice velocity. Elastic energy accumulates in the structure until local brittle ice failure occurs at the edge of the contact area, which spreads quickly to the entire loaded contact area. During the subsequent ice crushing phase, the structure springs back as the elastic energy of the structure is dissipated in ice crushing and converted into kinetic energy. The responses for the dominant structural modes tend to decay before the next cycle starts.

The structure displacement and ice action time histories at the waterline typically display a sawtooth pattern, growing linearly prior to a rapid unloading phase. A double-stroke waveform has also been observed in full-scale data[190], with the translational and tilting modes of the superstructure both contributing to the process.

Frequency lock-in, depicted in Figure A.8-30 b), can occur at intermediate ice speeds, with typical speeds for Baltic Sea structures ranging from 0,04 m/s to 0,1 m/s. In this case, the ice failure frequency in crushing adapts to one of the lowest natural frequencies of the structure. Particularly for circumstances with low structural and foundation damping, structural response can be amplified significantly due to resonant behaviour. The period between subsequent sudden ice crushing failures and the amplification depends on the ice properties, the ice velocity and the dynamic properties of the structure. Similar to intermittent crushing, frequency lock-in exhibits alternating phases of ductile loading and brittle unloading.

For frequency lock-in, the motion of the structure is close to sinusoidal while the time history of the ice action depends on the characteristics of both the ice and the structure. Based on field experience, structures with a lowest natural frequency in the range of 0,4 Hz to 10 Hz have experienced frequency lock-in when the total structural damping (as a fraction of critical) has been low.

Continuous brittle crushing, Fig. A.8-30 c) shows typical records of the ice action and the structural displacement response at ice velocities well above the maximum velocity for which frequency lock-in occurs. In this case, both the ice action and the response of the structure are random. The response of the structure can be calculated in the frequency domain using the power spectral density for the random ice action.

Figure 9-4 ISO 19906 [103] Section A.8.2.6.1.2 Time-varying interaction process

A.8.2.6.1.3 Dynamic response to intermittent crushing

Figure A.8-31 shows idealized time histories of ice actions that can arise due to intermittent crushing. The ice action build-up and failure cycle period, T, of the ice action is much longer than the longest natural period of the structure. The time history shown in Figure A.8-31 a) can also arise from an ice spalling failure mode where the period, T, of the ice action is longer than the duration of the loading/unloading cycle.

General-purpose FE software can be used to calculate the response of the structure due to these assumed repeating ice actions. The peak action, F_{max}, can be determined by the method described in A.8.2.4.3 as the static global ice action, F_G. For an FLS analysis, the period, T, can be assumed to decrease linearly with increasing ice velocity until a velocity is reached at which frequency lock-in is expected to develop. The number of load cycles can be estimated by dividing the ice movement distance at each ice thickness by the static deflection of the structure for the ice thickness in question.

The dynamic analysis is focused on effects of the decaying oscillations of the structure following unloading. As a result, it is often sufficient to determine the response to a single loading cycle.

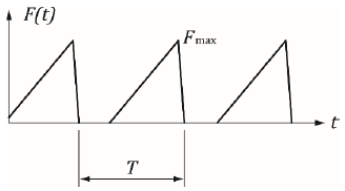

a) Period of ice action greater than duration of loading/unloading cycle

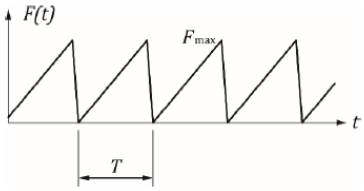

b) Period of ice action equal to duration of loading/unloading cycle

Key

t	time	F_{max}	maximum value of ice action
F	ice action	T	period of ice action

NOTE Both F_{max} and T can vary randomly

Figure A.8-31 — Idealized time histories of the ice action due to intermittent crushing

Figure 9-5 ISO 19906 [103] Section A.8.2.6.1.3 Dynamic response to intermittent crushing.

Loads from shock impact of a large ice floe should be checked with a transient load approach as suggested below.

$$H(t) = kUt \quad \text{for} \quad t \le \frac{H_d}{kU}$$

$$H(t) = \begin{cases} 0 \\ \text{or} \\ H_d \end{cases} \quad \text{for} \quad t > \frac{H_d}{kU} \qquad (9.2)$$

where

U is the impact velocity,

t is the time,
k is the stiffness of the structure at the waterline.

Recommendations for detailed design:

Above formulas represents a simplified safe methodology to assess dynamic ice loads.

For Baltic 2 (Kriegers Flak D) a more advanced methodology was applied:

For cone structures ice load time series were produced based on ice model tests time series from a research project, see Gravesen et al (2003) [114]. It was realized that the corresponding ice model tests results for vertical structures were not reliable probably due to a to larges model ice flexibility.

For vertical structures a model calibrated based on ice field tests is required.

Kärna (2008) [116] developed an integrated stochastic model of ice load and turbine dynamics. The results from this model been applied for vertical structures in Baltic 2 are illustrated in Kärna et al (2010) [117] and in Gravesen, Helkjaer and Kärna (2011) [118] The key assumption is a stochastic ice crushing load been sketched in Figure 9-6 below:

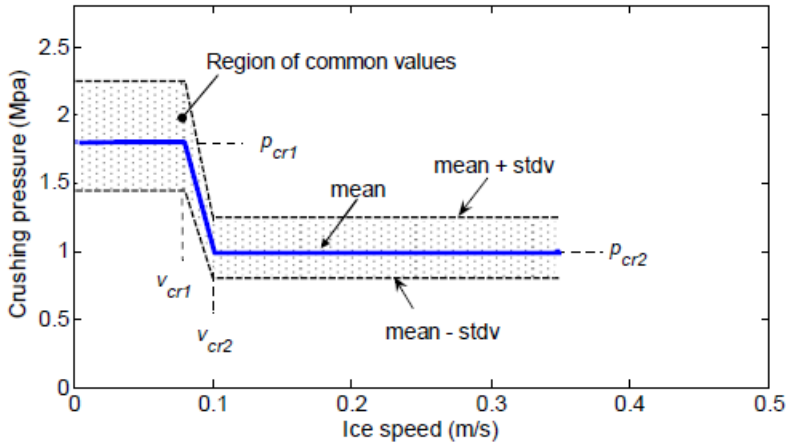

Figure 9-6 Mean value of the full-thickness ice pressure as a function of relative ice speed (ice speed relative to foundation speed)[116]

For Kriegers Flak DK a model developed by Hayo Hendrikse was used for monopiles without cones, see Willems and Hendrikse (2019) [120].

But in addition to the required more advanced modelling of ice crushing, it is important to understand that the ice field measurements are showing relative few periods with lock-in between the ice load and the structure vibrations. So there exist in practice not the stationary conditions assumed in the simplified models proposed in the standards. This aspect is important for the design because it means that ice fatigue loads are overestimated if the simplified models are been used for detailed design.

It is proposed that both the extreme ice loads as well as the fatigue ice loads are been estimated by a dynamic ice load simulation including the structural and damping conditions of the structure loaded by an advanced ice load like in the models from Kärna and Hendrikse. Account to lack of stationary lock-in should be included.

Reference is also made to the comments in Annex D. Here it is discussed when the wind turbine is idling (mainly due to U_nacelle less than 4 m/s, but account should also be given to other events without power production or with a high misalignment between wind direction and ice drift direction). This is because the 1 mode damping then usually is assumed to be say 2% instead of say 7 % for 1 mode oscillations when the wind turbine is in operation (due to aerodynamic damping).

The conditions are further complicated by that the maximum ice forces from ice floes of importance for mainly fatigue occurs for Vice < 0.1 m/s. But with that low incident velocity at least vertical structure has a that large resistance so the ice floes are been stopped after a limited penetration and few force oscillations. This occurs even though a certain amount of ice rubble behind the design ice floe can give a limited contribution to increased penetration and more oscillation on the ice force. Rough estimates of potential scenarios are mentioned in Section 4.5.

10 Ice Ridges

Ice ridges generated by nearshore effect or ice packing are expected to occure in ice winters. It is, further found relevant to evaluate if risk ice ridge generation by the blocking effect from the wind turbine foundations in the wind farm and eventual neighboring wind farms.

In general, ice engineering is based on few field measurements typically made in regions with severe sea ice. In the best case the standards include estimates of characteristic values, the uncertainties to these and the actual probability are not defined. For the Kattegat region, the sea ice occurrence is moderate, and the ice parameters shall be selected based on these less consistent design parameters. For ice ridge design this includes selection of: basic ice thickness and assumed thickness of consolidated layer, assumed ice floe maximum size, etc.

The selected characteristic parameters for the ridge design are found in accordance with recommendations in ISO 19906 [103].

The estimated ice ridge properties are based on ice analyzis for wind farms located in the south-western part of the Baltic Sea ref. [123]. The ice conditions in this area is considered similar to the area at Hesselø OWF.

Hesselø OWF will in the future be surrounded by many other offshore wind farms. The Hesselø OWF wind farm is primarily exposed to ice ridge creation with ice drifting from southly and northly directions.

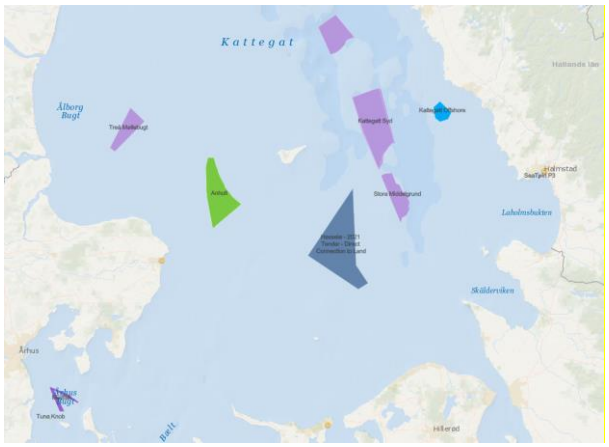

Figure 10-1 Planned offshore windfarms in Kattegat.

It is expected that the most actual planned installations of wind farms are:

Wind farm	Building year	Size
Anholt	2013	0.4 GW
Hesselø OWF	2026	1.5 GW
Store Middelgrund	2026	0.86 GW
Kattegat syd	2027	1.2 GW

Table 10-1 Building year and size of neighbouring wind farms

It can be assumed that a substantial number or foundations will add to generation of ice ridges no matter of the direction of the ice movement in the Hesslø OWF. When neighboring windfarms are build the blocking effects from a large number of additional foundations shall be included.

10.1 Ice ridge generation pressure

The ice ridge generation pressure can be derived from ISO 19906 [103] section A.8.2.4.6 which include an equation (A.8-65) for ice ridge generation pressure. It shall be commented that the ice ridge generation method of ISO 19906 [103] is based on ice thickness of 1m and above. For the Hesselø OWF projects the ice thickness is less 0.15m – 0.35m and it is not verified that the method can be used directly for the actual case.

A general expression for the ridge-building action is given by Formula (A.8-65):

$$p_D = R\,h^{1,25} D^{-0,54} \qquad \text{(A.8-65)}$$

where

- p_D is the ridge-building action per unit width, expressed in meganewtons per metre;
- h is the thickness of the ice sheet acting on the thicker ice feature, expressed in metres;
- D is the width of the thicker ice feature, expressed in metres;
- R is a coefficient, see Figure A.8-21.

Figure 10-2 Ridge building equation ref. ISO 19906 [103]

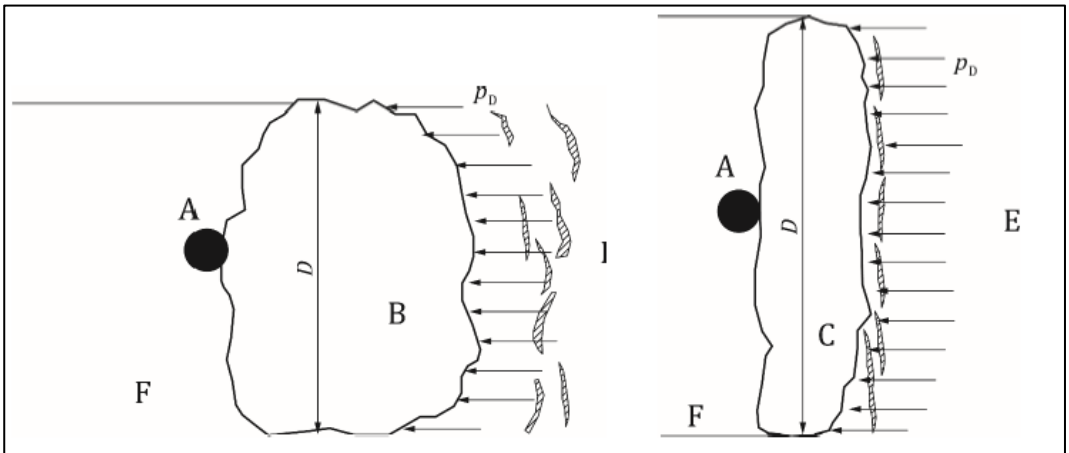

a) Ridge-building action for thick floe

b) Ridge-building action for consolidated ridge

Key

A	structure	E	surrounding ice sheet
B	thick ice floe	F	open water in wake of structure and ice feature
C	thick consolidated ice ridge	D	width of the ice feature, expressed in metres
		p_D	line action imposed on the width of the ice feature

Figure A.8-20 — Ridge-building action behind thick floe or ridge

Figure 10-3 Ridge building action illustration ref. ISO 19906 [103]

10.2 Design loads for ice ridge

The ice ridge loads can be calculated according to ISO 19906 [103] section A.8.2.4.5.1 equation A.8-49.

An accurate, theoretical determination of the actions caused by ice ridges is difficult. An upper bound estimation of the horizontal action caused by a FY ridge, F_R, can be obtained as given by Formula (A.8-49):

$$F_R = F_c + F_k \quad \text{(A.8-49)}$$

where

F_c is the action component due to the consolidated part of the ridge;

F_k is the keel action component.

Since the volume of the sail is small compared to that of the keel, the effects of the ridge sail can be neglected in the case of FY ridges. The action component, F_c, can be determined, as an estimate, using instructions given in A.8.2.4.3 for parameters of the consolidated layer of an ice ridge, or A.8.2.4.4 for sloping structures by substituting h_c for h.

Figure 10-4 Ridge loads ref. ISO 19906 [103]

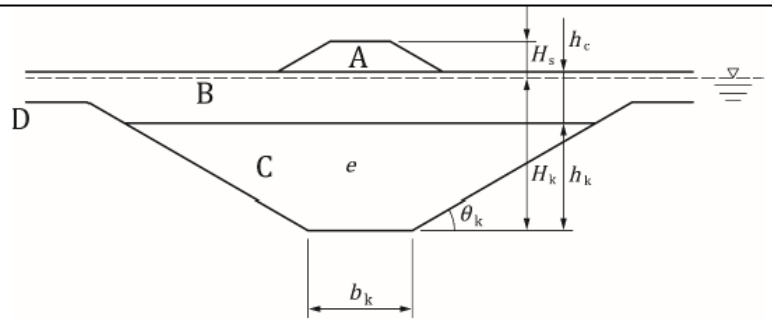

Key

A	ridge sail	h_c	consolidated layer thickness
B	ridge consolidated layer	h_k	vertical distance between the base of the consolidated layer and the base of the keel
C	ridge keel		
D	level ice	b_k	width of the base of the keel
H_s	sail height	e	keel porosity
H_k	keel depth	θ_k	keel angle from horizontal

Figure A.8-16 — Idealized geometry of a first-year ridge

Figure 10-5 I*dealized geometry of a first-year ice ridge ref. ISO 19906 [103]*

Several models are available for the determination of the unconsolidated keel action component F_k. Passive failure models are generally used to determine the unconsolidated keel action component acting on vertical or inclined structures. Measurements indicate that the keel cohesion often varies from zero at the base of the keel to a maximum immediately beneath the consolidated layer. Under such conditions, the keel action can be determined for vertical structures (see Reference [148]), with suitable modification (see Reference [149]) as given by Formulae (A.8-50) and (A.8-51):

$$F_k = \mu_\phi h_k w \left(\frac{h_k \mu_\phi \gamma_e}{2} + 2c \right) \left(1 + \frac{h_k}{6w} \right) \quad \text{(A.8-50)}$$

$$\mu_\phi = \tan\left(45° + \frac{\phi}{2} \right) \quad \text{(A.8-51)}$$

where

- μ_ϕ is the passive pressure coefficient;
- ϕ is the angle of internal friction;
- c is the apparent keel cohesion (an average value over the keel volume should be used);
- w is the width of the structure;
- γ_e is the effective buoyancy, in units consistent with c.

The effective buoyancy is given by Formula (A.8-52):

$$\gamma_e = (1-e)(\rho_w - \rho_i) g \quad \text{(A.8-52)}$$

where

- e is the keel porosity;
- ρ_w is the water density;
- ρ_i is the ice density.

Guidance for the specification of ridge keel parameters is provided in A.8.2.8.8.

Figure 10-6 *Ridge keel load equation ref. ISO 19906 [103]*

Ice ridge parameter guidelines are described in ISO 19906 [103] as shown in Figure 10-7.

The sail height and the level-ice thickness are often used as key parameters to define other geometrical shape parameters. For the ridge profile shown in Figure A.8-16, typical relationships are given as $h_c = 1{,}6h$, $H_k = 4{,}5H_s$ and $\theta_k = 26°$. The width parameter can vary from $b_k = 0$ to $b_k = 5H_s$. The porosity of the ridge keel depends on the age of the ice ridge and varies in different sea areas. Some key indices of ridge shape are outlined in Reference [147].

The thickness parameters h_c and H_k depend on geographical location. Thicker consolidated layers and keels develop in highly dynamic sea areas due to the rafting process. Therefore, it is suggested that field data be used to specify statistical characteristics of the consolidated layer. Existing field data suggest that the parameters h_c and H_k are not correlated with each other. In the absence of field data, it can be assumed in a deterministic analysis that h_c is 2,0 times the thickness of an ice sheet that has grown in open water under the same conditions as the ice ridge.

The thickness h_c of the consolidated layer of an ice ridge is locally variable in the vicinity of the structure during an ice action. This can be considered if field data are available to create a probability distribution for the consolidated layer thickness. Using this probability distribution, an average value of the consolidated layer thickness can be determined for each event. The average value can be determined by considering the thickness variability in an area of $A = w^2$, where w is the width of the structure.

Figure 10-7 Ice ridge parameter guidelines ref. ISO 19906 [103]

Various arbitrary methods to assess the thickness of the consolidated ice layer are described in standards and papers. In revision 00 of this report the ice ridge parameters were suggested in line with the ice ridge assessment prepared by Toumo Kärnä for the Arkona OWF project in year 2012 where a consolidated layer of 45cm and a parent ice thickness of 10cm-15cm is suggested. According the Kriegers Flak ice ridge assessment [123] a consolidated ice thickness of 43 -67 cm is suggested and are formed of ice blocks of 20cm in thickness. Both analysis of the ice ridge conditions for the South Baltic Sea (Arkona and Kriegers Falk) are based on the same data set.

Both the Arkona and Kriegers Flak ice ridge assessments are based on data from much severe ice locations (North Baltic Sea, Beaufort sea and Sea of Okhotsk). Further ice ridge measurements have not been made for OWFs where the ice is blocked by several structures located in a random structure seen from the ice. We consider the methods describe in ISO 19906 [103] being very conservative with respect to ice ridge generation in Kattegat. But due to lack of analysis of ice ridge generation for Kattegat it is suggested to include the ice ridge parameters in line with ISO 19906.

Consolidated layer thickness: hc = 0.35 * 1.6 = 0.56 m

Parent ice floe thickness: hp = 0.2 m

Sail Height: hs = 4.2 * sqrt(0.2) = 1.88 m

Keel depth: hk = 4.5 * 1.88 = 8.45 m

The ice keel porosity has been measured to reduce from 0.45 to 0.29 in a month for a newly generated ice keel. A design value of 0.35 ref. [111] is suggested for a ten to fifteen days old ridge.

The internal friction and keel cohesion are selected based on the investigations as listed in ref. [111] “Table 4 Summary of Strength Properties of Ice Rubble” and discussions in ref. [111] for moderate sea ice conditions as considered for the Hesselø OWF location.

Suggested parameters for the ice ridge loads for 1/50y and 1/100y case:

- Thickness of consolidated layer (1/50y): h_c = 0.56 m
- Thickness of consolidated layer (1/100y): h_c = 0.62 m
- Depth of the ridge keel: H_k = 8.45 m
- Keel porosity: e = 0.35

- Internal friction of the keel: $\varphi = 30^0$
- Keel cohesion: $c = 3$ kPa

Due to the relative short period with critical ice conditions we estimate that the strength of the consolidated layer is corresponding to the generating ice sheet layer and not the assumed thickness of the consolidated layer.

It is proposed to assume that the ice crushing strength in the consolidated layer is been calculated based on $C_R = 0.66$ MPa and an ice thickness of 3 sub-layers of 0.15 m corresponding to the likely value of the original ice sheets creating the consolidated layer.

Please be aware that for a down-bending cone the forces from breaking the consolidated layer is increased due to the rubbles in the ridge so this force component is approximately equal to the force component from an up-bending cone, see Croasdale et al 2019 [113].

The overall analysis shows in general (Annex B and Annex C) that all foundations in Hesselø OWF has a risk of been exposed to ice ridges, so ice ridge is a standard design case.

In the case that Hesselø OWF foundations are constructed with cones the risk of ice ridge generation is reduced. Surrounding wind farm with foundations constructed without cones will increase the risk of ice ridge generation.

11 Icing (Marine and atmospheric)

According to ISO 19901-1, ice accretion (or icing) refers to the accumulation of ice or snow on a structure. Icing can be categorised into two types: the atmospheric icing and the marine icing. Atmospheric icing includes freezing rain, supercooled fog and snow, while marine icing mainly occurs by freezing sea spray from breaking waves and/or strong winds blowing over the sea surface. Atmospheric icing occurs when rain, fog or snow freezes upon the contact with a surface.

Required conditions for atmospheric icing are low air temperatures between -20°C and 0°C combined with low wind speeds (less than 10m/s).

Marine icing occurs when sea spray from breaking waves or strong wind blowing over the sea surface freezes upon the contact with a surface. Required conditions for marine icing are wind speed greater than 10m/s, air temperatures less than the freezing point of seawater, i.e. -0.9°C and sea surface temperature smaller than 8°C.

The combination of conditions necessary for atmospheric icing occur rarely in the area see Figure 11-1. It is evaluate the nearby onshore conditions for atmospheric icing can be extended to Hesselø OWF. Hence the risk of atmospheric icing is 2-7day/year

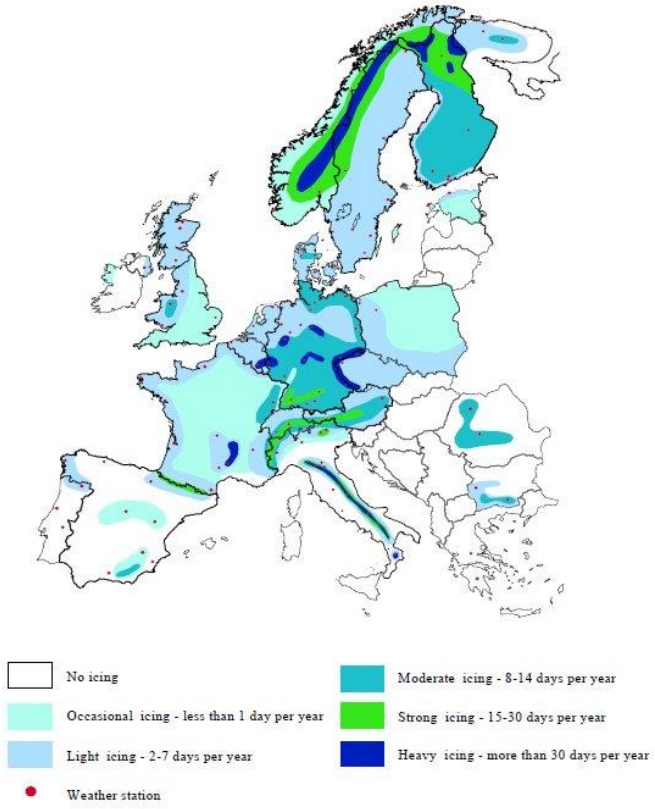

Figure 11-1 Atmospheric icing map of Europe

Table 11-1 Type of snow or ice ref. DNVGL-ST-0437 [101]

Type of snow or ice	Area	Thickness and density
Marine icing Ice from freezing sea spray.	At sea level to highest wave elevation: From highest wave elevation: Linearly reduced up to +60m MSL:	100 mm 100 mm 0 mm Density: 850 kg/m^3
Atmospheric icing	In the full height of the structure from the water surface to the top of the WTG tower, nacelle and blades.	Thickness: 30mm, Density: 700 kg/m^3

The recommended praxis DNVGL-RP-0175 [115] can be used for designing issues related to icing. However this recommendation is not fully aligned with the load standard DNGL-ST-0437 [101] and it is recommended following [101] were discrepancies are found.

For atmospheric icing on WTG blades it is recommended to follow DNGL-ST-0437 [101] ref. Figure 11-2.

With the rotor rotating under in-cloud icing conditions, the cases "ice formation on all rotor blades" and "ice formation on all rotor blades except one" shall be investigated. The mass distribution (mass/unit length) shall be assumed at the leading edge. It increases linearly from zero in the rotor axis to the value μ_E at half the radius, and then remains constant up to the outermost radius. The value μ_E is calculated as follows:

$$\mu_E = \rho_E \cdot k \cdot c_{\min}(c_{\max} + c_{\min}) \quad (2.39)$$

where:

μ_E	=	mass distribution on the leading edge of the rotor blade at half the rotor radius [kg/m]
ρ_E	=	density of the ice (900 kg/m^3)
k	=	0,00675 + 0,3 exp(–0,32 R/R_1)
R	=	rotor radius
R_1	=	1 m
$c_{\max}$	=	maximum chord length
$c_{\min}$	=	chord length at the blade tip, linearly extrapolated from the blade contour

Figure 11-2 Atmospheric icing for WTG blades ref. DNVGL-ST-0437 [101]

12 Design load cases acc. IEC 61400-3

Ice loads shall be evaluated for different ice load situations according IEC 61400-3 [102] Table 3 as copied in Table 12-1 below. Identical listing of design loads for ice conditions can be found in DNVGL-ST-0437 [101]. The recommendation DNVGL-RP-0175 [115] provide additional recommendations to consider for the ice loads assumptions. To perform the load analysis, wind turbine loads shall be combined with the ice loads on the support structure as specified in Table 12-1 and Table 12-2. In this report the ice load input is provided to enable the foundation designer to perform the required analysis of the combined model.

Table 12-1 Ice design load cases (DLC) according to IEC 61400-3 [102] (Table 3)

Table 3 – Design load cases for sea/lake ice

Design situation	DLC	Ice condition	Wind condition	Water level	Type of analysis	Partial safety factor
Power production	D1	Horizontal load from temperature fluctuations	NTM $V_{hub} = V_r \pm 2$ m/s and V_{out} Wind speed resulting in maximum thrust	NWLR	U	N
	D2	Horizontal load from water level fluctuations or arch effects	NTM $V_{hub} = V_r \pm 2$ m/s and V_{out} Wind speed resulting in maximum thrust	NWLR	U	N
	D3	Horizontal load from moving ice at relevant velocities $h = h_{50}$ or largest value of moving ice.	NTM $V_{in} < V_{hub} < V_{out}$	NWLR	U	N
	D4	Horizontal load from moving ice at relevant velocities *Use values of h corresponding to expected history of moving ice occurring.*	NTM $V_{in} < V_{hub} < V_{out}$	NWLR	F	*
	D5	Vertical force from fast ice covers due to water level fluctuations	No wind load applied	NWLR	U	N
Parked	D6	Pressure from hummocked ice and ice ridges	EWM Turbulent wind model $V_{hub} = V_1$	NWLR	U	N
	D7	Horizontal load from moving ice at relevant velocities *Use values of h corresponding to expected history of moving ice occurring.*	NTM $V_{hub} < 0,7\ V_{ref}$	NWLR	F	*
	D8	Horizontal load from moving ice at relevant velocities $h = h_{50}$ or largest value of moving ice.	EWM Turbulent wind model $V_{hub} = V_1$	NWLR	U	N

To be added: D9 Power production. Pressure from hummocked ice and ice ridges. Most situation where pressure from hummocked ice and ice ridges may occur is corresponding to Power production.

In the following, an initial assessments of the design load cases (DLC's) are made though without knowledge about the wind turbine to be mounted on the foundation. Any of the DLC's [102] can be design driving; however, DLC D1 and DLC D5 are likely not design driving due to the moderate water level and temperature variations.

For the Ultimate Limit State (ULS) DLC the ice load input in Table 0-1 is provided for calculation of DLC D2, D3, D5 and D6.

DLC D3 is most likely dominant relative to DLC D6 due to the higher shear loads from a running turbine.

Loads from passing or service vessels shall be taken into consideration.

Dynamic ice load analysis ref. section 9 shall be carried out to check the load response. It is required to carry out dynamic analyses including an integrated dynamic model for DLC D3, D4, D6 and D7 based upon the load matrix. This calculation shall preferably be carried out by the WTG supplier to integrate the sea ice dynamic with the WTG dynamic model.

For a monopile structure without ice cone it is recommended to carried out model simulation analysis with dynamic ice crushing for all important frequencies of ice and structure interaction and the associated damping estimates. It is needed carefully to evaluate how to treat the non-linearities and associated plastic deformation in the soil support, in case this leads to changed stiffness of the structure during the load simulation.

Table 12-2 Additional load case for icing during operation acc. DNVGL-RP-0175 [115].

Table 3-1 Definition of icing design load cases

DLC	*Wind Conditions*	*Icing conditions*	*Load evaluation*	*Partial safety factor for loads*
13.1 Power production under icing conditions	NTM* vin < vhub < vout	Icing modelling according to ice class	F (fatigue) U (ultimate)	N*
*defined according to DNVGL-ST-0437, IEC 61400-1, IEC 61400-2 and IEC 61400-3-1				

13 References

13.1 Project specific documents

[1]. Ice observation reports for the Danish waters from year 1861 to year 2019. SOK, Last one for the winter 2018-2019, ISSN 0106-5076

[2]. Climatological Ice Atlas for the Kattegat, Kattegat, Skagerrak and Lake Vänern (1963-1979), SMHI, Swedish Meteorological and Hydrological Institute 1982.

13.2 Normative and general references

[101]. DNVGL-ST-0437, Loads and site conditions for wind turbines, DNV-GL, November 2016.

[102]. IEC International Standard, IEC 61400-3, Wind Turbines – Part 3: Design Requirements for offshore wind turbines, IEC. 2019.

[103]. ISO 19906:2019 Petroleum and natural gas industries - Arctic offshore structures. 2019.

[104]. Extreme ice properties. Journ. Cold Reg. Engng. Vol 5 No 2, Christensen, F.T. and Skourup, J. ASCE. 1991.

[105]. Determination of extreme ice forces. Lecture notes. Thunbo Christensen, F. and Gravesen, H. MEK. DTU. 2003.

[106]. Offshore Installations, IV Part 6, Chapter 7, Oil and Gas, Guidelines for the Construction of Fixed Offshore Installations in Ice Infested Waters, Germanisher Lloyd. GL Edition 2005.

[107]. POAC 09, Ice Loads for Offshore Wind Turbines in Southern Kattegat. June 2009, Paper by: Helge Gravesen and Tuomo Kärnä.

[108]. POAC 1993, Factors influencing the coefficient of friction between sea ice and various materials. Nakazawa et al. 1993.

[109]. PERD/CHC Report 3-49, HYD-TR-067, Friction of Sea Ice on Various Construction Materials. Frederking, R. and Barker, A. Ottawa, Canada. 2001.

[110]. ISO 19906 Ice crushing load design extension for narrow structures. Määttänen and Kärna. 2011.

[111]. An overview of first-year sea ice ridges, HYD-TR-047, PERD/CHC Report 5-112, August 2000.

[112]. Ice ridge-structure interaction, Part I: Geometry and failure modes of fist-year ice ridges, Norwegian University of Science and Technology,

[113]. POAC 2019, Ice load signatures for ridge action on wind turbines with conical collars, Croasdale, K, Thijssen, J. and Allyn, N, Delft. The Netherlands. 2019.

[114]. POAC 2003, Ice forces to wind turbine foundations in Denmark. Gravesen, H., Pedersen, B., Sørensen, S.L., and Vølund. P. Trondheim, Norway. Paper No. 187 (2003)

[115]. DNVGL-RP-0175. Recommended Practice. Icing of wind turbines, December 2017

[116]. Kärnä, T. (2008): Ice-induced vibrations of slender structures. In: Fransson, L. (ed.). Ice Mechanics and Shipping in Ice-infested waters. Luleå University of Technology. (2008)

[117]. Kärna. T., Gravesen, H., Fransson, L., and Løset, S. (2010): Simulation of multi-modal vibrations due to ice actions. 20th IAHR Intern. Symp. On Ice. Lahti, Fin-land. June 14-18th, 2010.

[118]. Gravesen, H. Helkjær. A. and Kärna. T. (2011): Improved practical ice load design methods for wind foundations. European Offshore Wind (EOW'11). PO 342. Amsterdam
[119]. Nord, T. et al (incl. Hendrikse H.) (2018): Ice induced vibrations in the Nordstrømsgrund Lighthouse. Cold Region Technology 155/2018, pp 237-251.
[120]. Willems, T., Hendrikse, H. (2019): Coupled simulation of ice structure interaction for offshore wind turbines in BHawc using Vanilla. Poac 2019. The Netherland.
[121]. Owen, C.C., and Hendrikse, H. (2019): A study of the transition ice speed from intermittent crushing to frequency lock-in vibrations based om model-scale experiments. POAC 2019, Delft. The Netherlands.
[122]. DMI. Future climate changes in Denmark (Danish language). Report no. 6 (2014).
[123]. Estimating extreme level ice and ridge thickness for offshore wind turbine design: Case study Kriegers Flak. Doc.:10.1002/we.2690, 19/2 2021, Wiley
[124]. POAC11-064, Data for crushing formula, T. Kärnä, D.M. Masterson, July 2011
[125]. Hav- og Fiskeribiologi, Siz Madsen, Fiskericirklen, ISBN 87-90749-08-1, 2008

Annex A Recorded ice data, Area 17

Location of areas in the Kattegat where ice thickness distribution is detailed recorded ref. the Swedish Ice Atlas [2]. Comparison with area 17 is made since this is the nearest location with detailed recorded ice conditions.

Ice thickness distribution areas
Områden för vilka istjockleksfördelningen beräknats
Jään paksuuden jakautumia vastaavat alueet

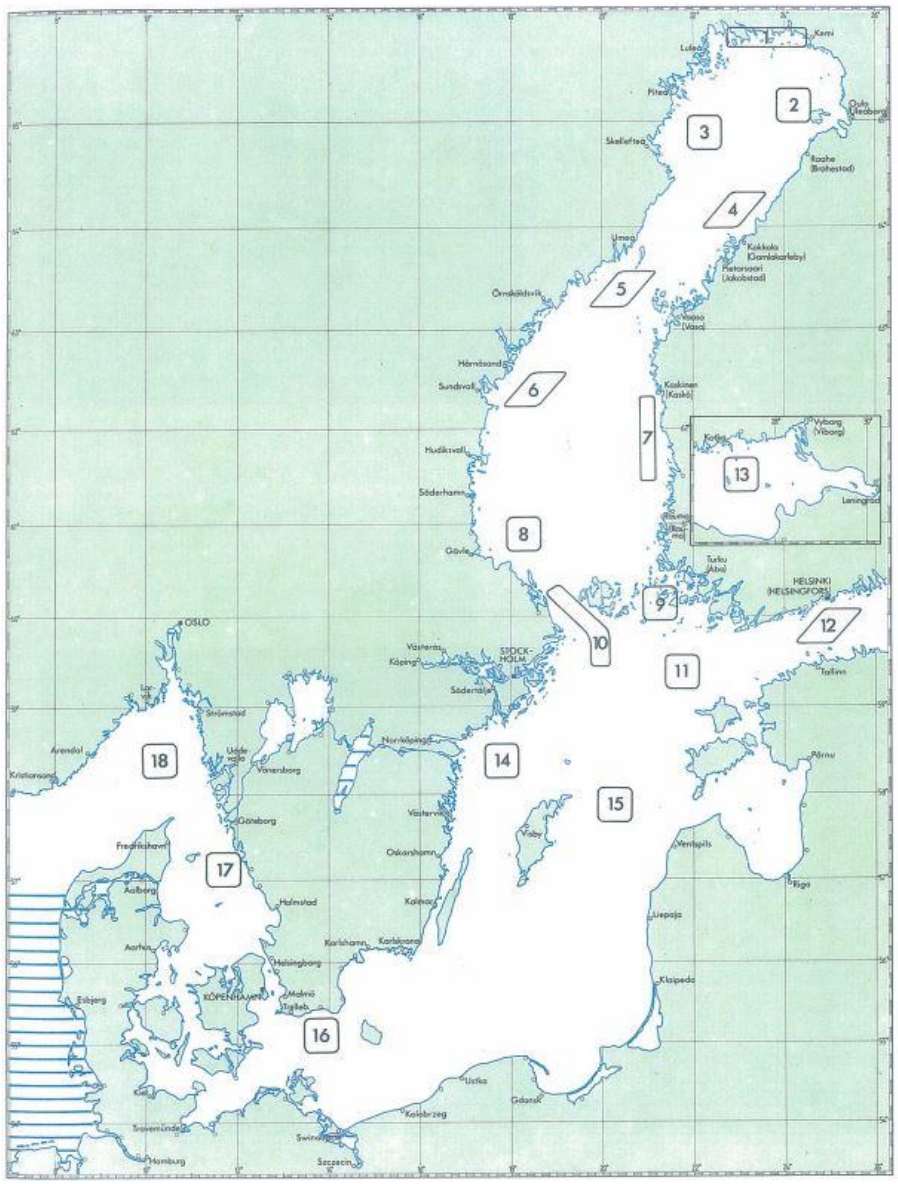

Area 17

Day	1	11	21	1	11	21	1	11	21	1	11	21	1	11	21	1	11	21	1	11	21	1
Month	11	11	11	12	12	12	1	1	1	2	2	2	3	3	3	4	4	4	5	5	5	6
Ice frequency	0	0	0	0	0	0	2	6	15	17	23	26	19	8	5	2	0	0	0	0	0	0
Thickness																						
1 – 2 cm	0	0	0	0	0	0	0	0	0	0	0	5	7	0	0	0	0	0	0	0	0	0
3 – 6 cm	0	0	0	0	0	0	0	0	100	47	45	5	27	60	100	0	0	0	0	0	0	0
7 – 12 cm	0	0	0	0	0	0	0	0	0	40	34	64	47	20	0	0	0	0	0	0	0	0
13 – 20 cm	0	0	0	0	0	0	0	0	0	13	21	23	20	0	0	0	0	0	0	0	0	0
21 – 30 cm	0	0	0	0	0	0	0	0	0	0	0	5	0	20	0	0	0	0	0	0	0	0
31 – 42 cm	0	0	0	0	0	0	0	0	0	0	0	0	0	0	0	0	0	0	0	0	0	0
43 – 56 cm	0	0	0	0	0	0	0	0	0	0	0	0	0	0	0	0	0	0	0	0	0	0
57 – 72 cm	0	0	0	0	0	0	0	0	0	0	0	0	0	0	0	0	0	0	0	0	0	0
> 73 cm	0	0	0	0	0	0	0	0	0	0	0	0	0	0	0	0	0	0	0	0	0	0
Mean thickness	0	0	0	0	0	0	0	0	4	8	8	11	9	9	4	0	0	0	0	0	0	0
Number of ice years	0	0	0	0	0	0	0	0	2	2	3	4	2	3	1	0	0	0	0	0	0	0
Number of data	0	0	0	0	0	0	0	0	10	15	29	22	15	5	1	0	0	0	0	0	0	0

Annex B Ice drift directions

In order to understand the ice floe generation and drift direction the scenario for the ice winters 1985, 1986 and 1987 are analysed.

B.1 Ice generation and drift pattern.

The ice generation and drift pattern of ice floes during the most critical part of the ice winters 1985, 1986 and 1987 are analyzed.

The ice generation factors are simplified by using the (4.4) formulae in section 4.2 on a daily basis that quantify the ice growth based on only the temperature and number of frost days. The same method is used for generation of Figure 4-4 and Figure 4-5 in section 4.2.

In Figure 13-1, Figure 13-2 and Figure 13-3 the ice growth and temperatures during the ice winters 1985, 1986 and 1987 are show.

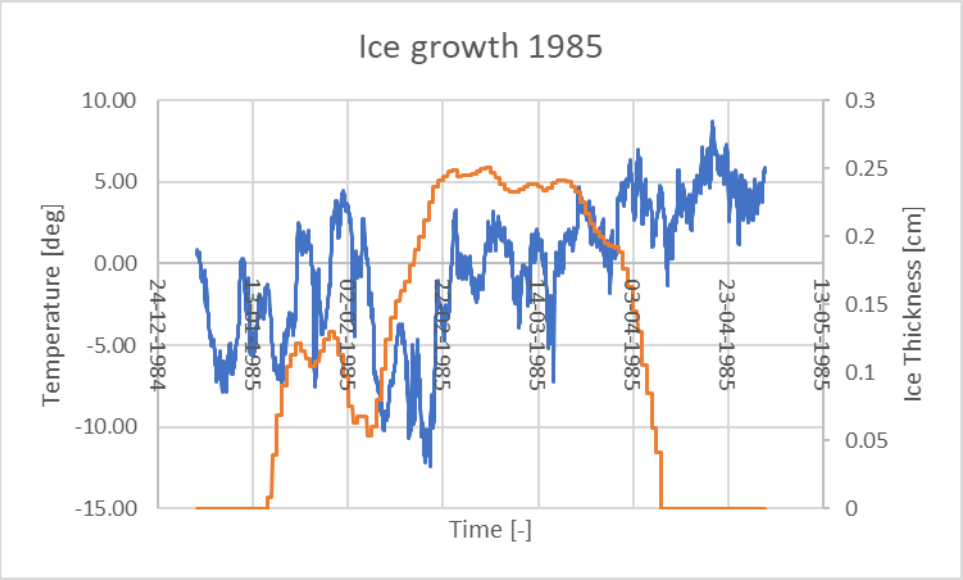

Figure 13-1 Ice growth and temperature during the winter 1985.

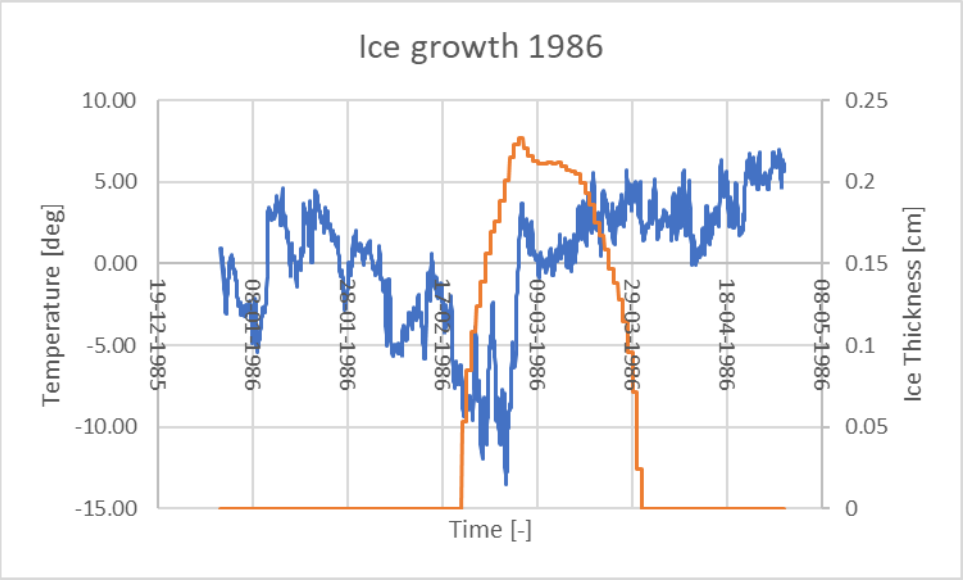

Figure 13-2 Ice growth and temperature during the winter 1986.

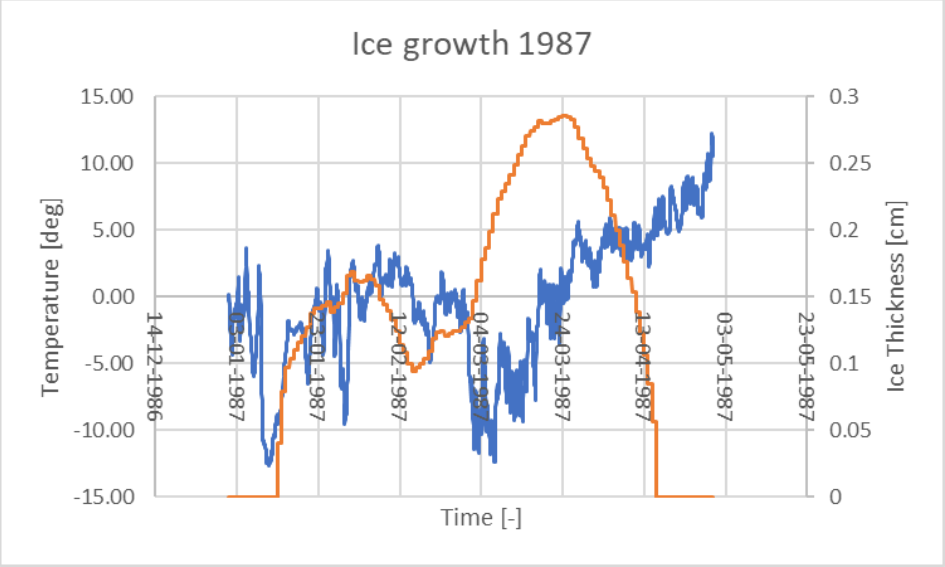

Figure 13-3 Ice growth and temperature during the winter 1987.

The assumed ice floe movements in the next plots (Figure 13-4, Figure 13-5 and Figure 13-6) are based on the hourly current and wind speed and direction. The wind is considered to drive the ice floe with a factor of 0.025 * U_{wind} as described in section 4.5.

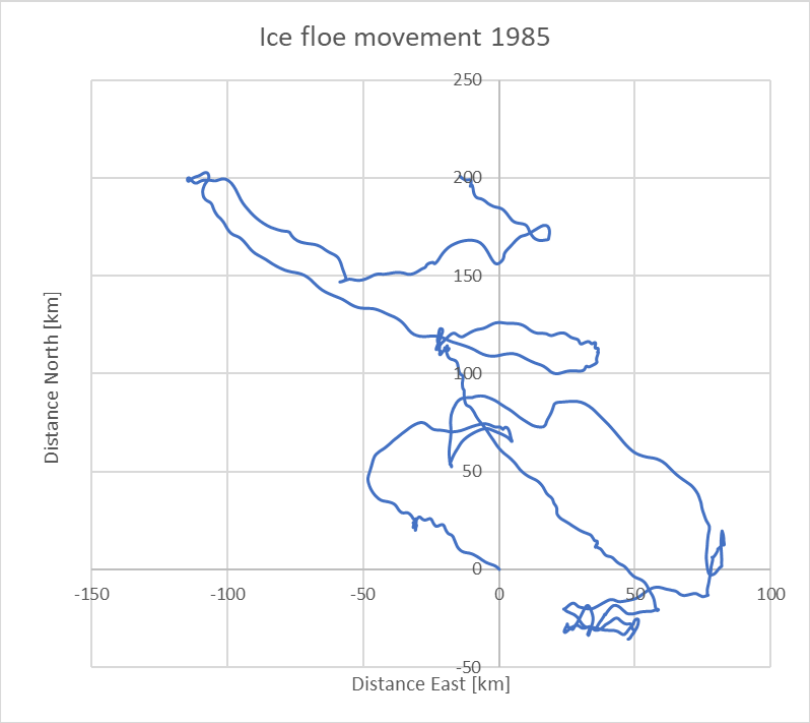

Figure 13-4 Ice floe movement during the winter 1985. Arbitrary starting point in (0,0).

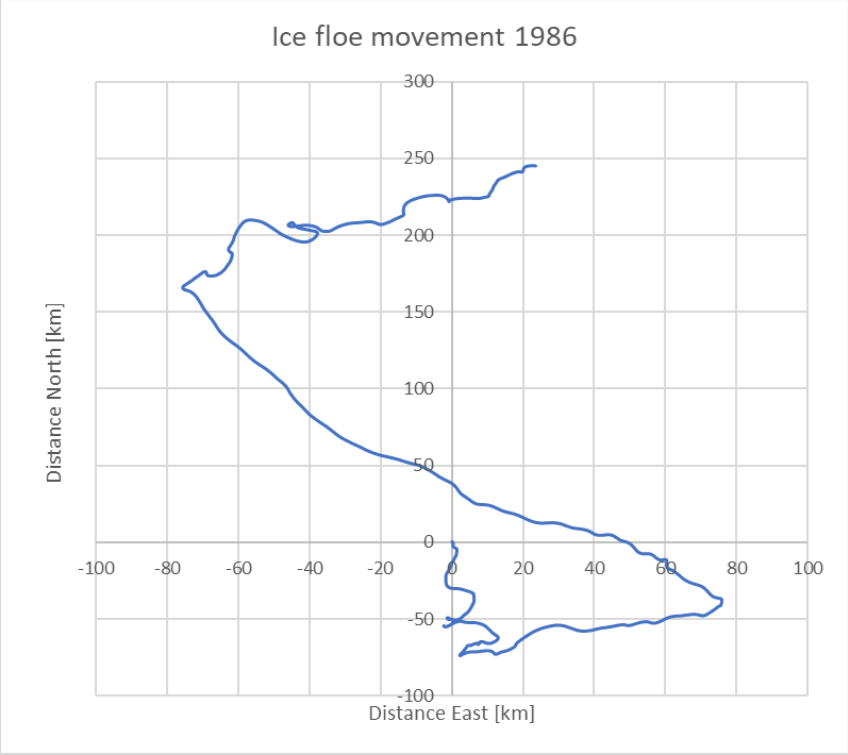

Figure 13-5 Ice floe movement during the winter 1986. Arbitrary starting point in (0,0).

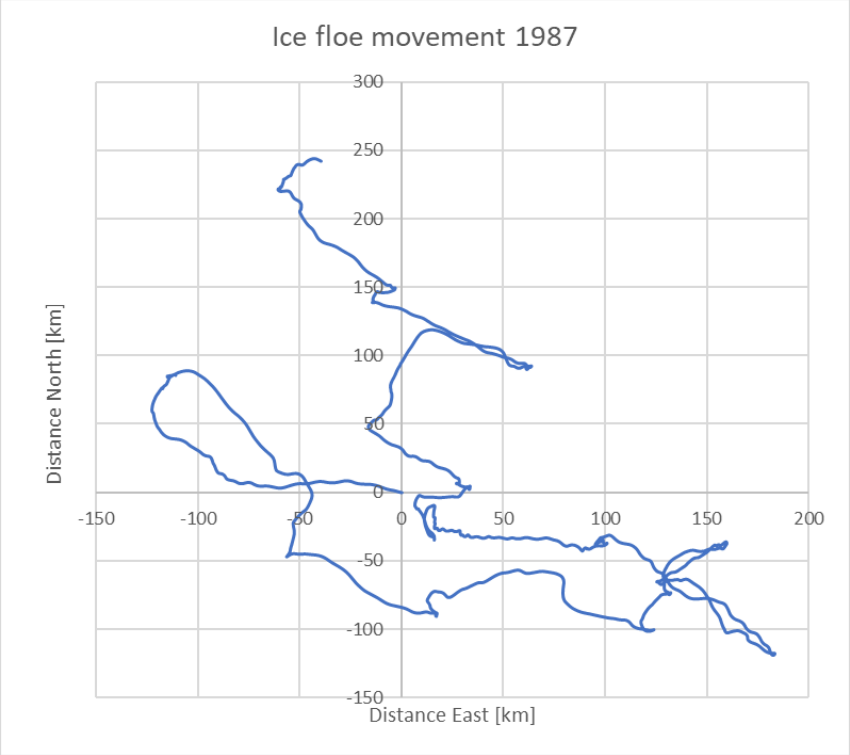

Figure 13-6 Ice floe movement during the winter 1987. Arbitrary starting point in (0,0).

From the simulations of ice floe drift traces it can be seen that the drift directions include several directions and that the floe may return back to the origin after some movement. This confirms that in general the Hesselø OWF wind farms have to be analyzed for ice ridge generation for any direction.

The wind will push the ice floe but also create waves on the edges of the ice floe that will break the ice. Ice floes that hit foundations on the side of the ice floe will tend to turn the ice floe instead of stopping it. Due to high number of affecting factors the ice ridge generation by the wind turbine foundations is considered to be quite likely. Especially will repeated movements of ice floes through the wind farm add to the ice ridge generation.

Annex C Ice ridge case study

C.1 Ice ridge generation in a wind farm.

The blocking effect is related to the shape of the foundation and the number of foundations that add to the blocking effect and thereby the ice ridge generation. A foundation with an ice cone will break the ice and is not considered to create ice ridges.

A foundation without an ice cone will have a considerably higher blocking effect and is in special situations considered to generate ice ridges. In this annex examples of typical relevant wind turbine foundations are considered to evaluate the blocking effect. In both cases the total blocking effect is a summation of the blocking effect by the individual foundations in the direction of the ice floe.

The ice floe movement is primarily generated by the wind acting on the ice floe.

C.2 Ice blocking effect for Hesselø OWF

Ice floe drift from all directions can create the ice ridge building pressure as there are minimum number of rows are above 3 in all directions.

It can also be assumed that the distance to shore has a sufficient length so ice ridge exposure is possible for all incident ice drift directions.

Neighboring wind farm foundations will as well have influence on ice blocking and ice ridge generation. There is a risk that ice ridges can be released from a neighboring wind farm depending on the wind and current direction.

But there exists no way of analyzing if and when the ridges are been released. It is generally assumed that the ridges most frequently are generated in periods with heavy frost and are frozen together with the ice sheet in the wind farms. The most likely release occurs with milder weather potentially associated with waves and different wind patterns.

C.3 Foundations with cones

The basis for calculating the ice ridge generating pressure is described in section 10.1.

The resistance for relevant foundations (dia. 9m) with cones is typically 0.02 MN on foundation for an ice sheet of 10 cm and typically 0.042 MN for an ice sheet of 15 cm.

So, for structures with cones the ice scenario will be that the ice sheets will be pressed trough the wind farm without generating a ridge. It is further considered statistically unlikely that there are sufficient number of repeated passing of the ice sheets so the broken pieces from the cone effect can create an ice ridge.

In the case that Hesselø OWF are constructed with cones and the surrounding wind farms are with vertical structures without cones it cannot be excluded that ice ridges been created from wind farms without cones can move over to Hesselø OWF. It is deemed that the risk for ice ridges generated in other wind farm is moving to Hesselø OWF is much lesser than if Hesselø OWF are constructed without cones.

C.4 Monopiles and jackets without cones

The resistance for relevant foundations without ice cones is typically 0.9 MN for a monopile with diameter of 9 m and an ice sheet of 10 cm and typically 1.1 MN for an ice sheet of 15 cm. A jacket will have ice forces of the same order of magnitude.

This means that typically 11 foundations (range 4 to 18) are required to create the ridge generation pressure for ice thickness of 10 cm and typically 15 foundations (range 5 to 25) for an ice thickness of 15 cm. With assumed 1,5 turbines per 1500 m a wind farm with say 10 rows of foundations (range 3 to 15) can generate the ridge building pressure.

C.5 Summation of ice ridge blocking effects

The ice ridge blocking effects analysis can be summarized in Table 13-1.

Examples of ridge blocking			**Case 1**	**Case 2**
Flow size (load length)	D	m	1500	1500
Ridge generation factor	R_{min}		2	2
Ref. ISO 19906 Figure A.8-21	R_{ave}		6	6
	R_{max}		10	10
Ice thickness	h	m	0.1	0.15
Ridge generating load acc. ISO 19906 formulae (A.8-65)				
Load minimum for R_{min}	F_{min}	MN	3.3	5.4
Load average for R_{ave}	F_{ave}	MN	9.8	16.2
Load maximum for R_{max}	F_{max}	MN	16.3	27.0
Blocking effect for structures with cones	**Cone**			
Blocking load per foundation	F_{cone}	MN	0.02	0.042
Number of foundations, Minimum	N_{min}		163	128
Number of foundations, Average	N_{ave}		488	385
Number of foundations, Maximum	N_{max}		813	642
Blocking effect for straight structures	**Vertical**			
Blocking load per foundation	F_{vert}	MN	0.9	1.1
Number of foundations, Minimum	N_{min}		4	5
Number of foundations, Average	N_{ave}		11	15
Number of foundations, Maximum	N_{max}		18	25

Table 13-1 Numbers of foundations to create forces sufficient to ice ridges generation.

It is concluded that Hesselø OWF has to be designed for ice ridges if constructed without cones.

Order of magnitude for Ice ridge on structure with basic diameter of 9 m:

Ice ridge keel force:	1.8 MN
Cone down-bending: by a 2 factor	0.3 MN rubble increases the load
Cone up-bending:	0.6 MN
Vertical structure consolidated layer:	2.3 MN
Total load up- or downbending cone	2.4 MN
Total load vertical structure:	4.1 MN

Annex D Discussion of dynamic ice loading scenarios

The dynamic design ice condition shall be found for:

- Idling with low damping of first system mode (This can occur due to wind velocity at nacelle less than 4 m/s, general error incl. errors at transformer stations, icing at rotor or other reasons for no production)
- power production with higher damping of first system mode
- power production with low damping of first system mode due to large misalignment

The incident kinetic energy even from larger ice floe (of km size) is very small for low Vice so only a limited load circles occur before the ice floe are stopped. Weak wind and current means also that it is unrealistic to assume that the required additional shear stress to an ice rubble field behind the ice floes can maintain the velocity. So at least at smaller ice velocities the ice floes are been stopped within few metres penetration. During this transition until the ice floes are stopped, very different ice velocities will cause a limited number of load circles with incident ice velocities between 0 and 0.1 m/s, where the ice force is maximum.

The different scenarios have to be selected interactive with the detailed dynamic ice loading carried out interactive with the turbine model (idling or production) so the final scenarios have to await the results from the detailed modelling. Below is given some rough estimates.

Incidence of ice floes:

There does not exist information on extend of ice rubble behind incident ice floes. A rough estimate could be that for fatigue load one assumes:

- for 70 % of the cases a 500 m ice floe with maximum 5 km open to close pack ice exposed to the shear force corresponding to the ice velocity considered (tau (pa) = 3 $Vice^2$, vice in m/s) (no kinetic energy contribution is assumed for the pack ice)
- For 20 % of the cases a 500 m floe with 5 km area of ice floes in close contact + shear force
- For 10 % of the cases a 500 m floe with 10 km area of ice floes in close contact + shear force

For ULS a rough estimate could be a 2 km ice floe with 5 km ice rubble behind.

Incidence of ice ridges:

Apply the estimate of the ice ridge geometry only for ULS and only as a equivalent static load as the rubble in the ridge will create that large damping so there will not be coincidence of maximum ice ridge load and high dynamic ice loads from failure of the consolidated layer.

Assume a 5 km zone of ice sheet with a thickness of typical 15 cm behind the ridge. Include shear stress corresponding to the Vice. Calculate which incidence ice velocities (Vice) will make it possible for the ice ridge to penetrate so maximum ice ridge forces is obtained. In case the maximum ridge force can only be obtained for rare combinations of high ice velocities, the risk could be less than 1/50 y so the ice ridge design should be carried out without a partial coefficient or with reduced partial coefficients.

Owen, C.C., and Hendrikse, H. has made a study of the transition ice speed from intermittent crushing to frequency lock-in vibrations based om model-scale experiments. [121]. From there following four figures are included to illustrate the shift in intermittent crushing, frequency lock-in and continuous brittle crushing during ice floe movements.

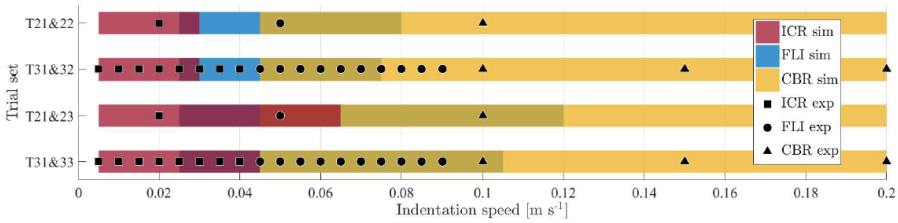

Figure 3. Comparison of the simulated (sim) ranges and experimental (exp) observations of intermittent crushing (ICR), frequency lock-in (FLI), and continuous brittle crushing (CBR) regimes of ice-induced vibrations with mean load adjustments for the relevant trial sets. The simulated ranges indicate the indentation speeds during which the different regimes of ice-induced vibrations develop for the range of ice conditions.

Figure 13-7 Comparison of simulated and experimental observations. [121] Figure 3.

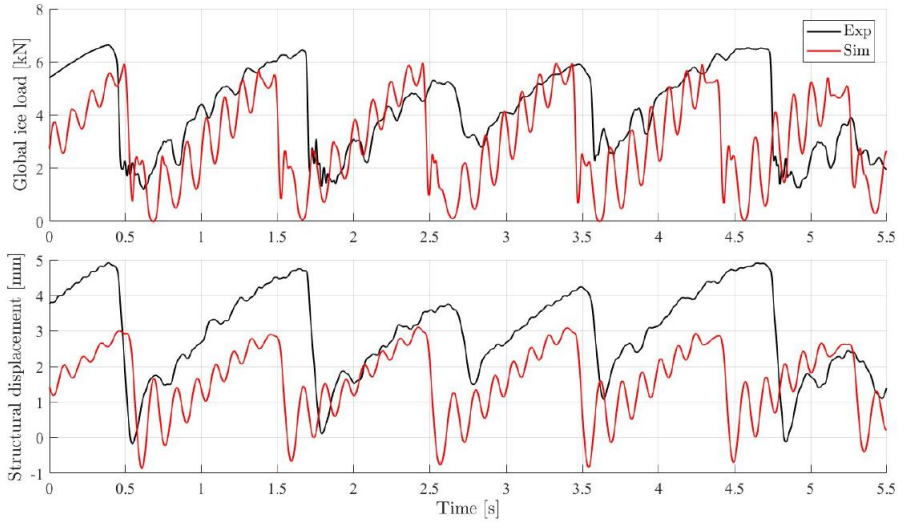

Figure 4. Comparison of global ice load and structural displacement time histories in the intermittent crushing regime from experimental (Exp) results and simulated (Sim) results with maximum ice conditions (trial T32) at an indentation speed of 0.010 m s^{-1}.

Figure 13-8 Comparison of global ice load and structural displacement. [121] Figure 4.

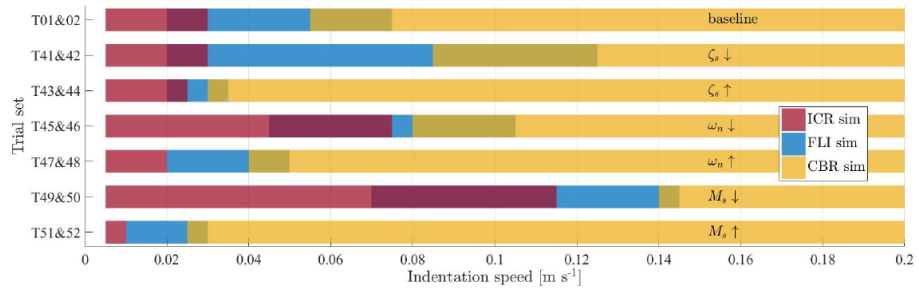

Figure 6. Results on the effect of change of structural properties on the transition speeds between the ice-induced vibrations regimes for the baseline trial set of T01 and T02.

Figure 13-9 Results on effect of change in structural properties [121] Figure 6.

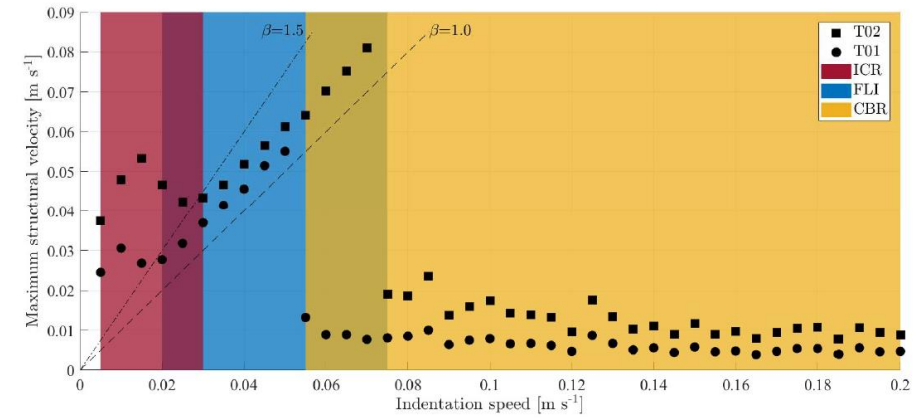

Figure 8. Example case (trial set of T01 and T02) of the difference in transition from intermittent crushing (ICR) to frequency lock-in (FLI) and from frequency lock-in to continuous brittle crushing (CBR) vibrations based on change in maximum structural velocit as a function of indentation speed.

Figure 13-10 Example case (trial T01 and T02) [121] Figure 8.

Above figures (Figure 13-7, Figure 13-8, Figure 13-9 and Figure 13-10) illustrates that the structural conditions may limit the frequency lock-in to quite a narrow ice floe range or in certain cases it does not occur.

The conditions are further complicated for the actual OWF:

- There is rarely ice concentrations above 0.8 even at the reference area 17 and intermittent crushing require heavy ice conditions, where an ice concentration of less than 0.8 maybe will make intermittent crushing to a very rare event.
- Even if there is a potential for intermittent crushing and frequency lock-in the kinetic energy in the incoming ice floes is that low so ice penetration stops after 1-2 dynamic events. Even if a certain 1-few km ice belt is behind the incoming ice floes, the penetration will stop after a few force oscillations. For larger incoming velocities there is a risk that a few load cycles in the frequency lock-in range can occur when the floe velocity id de-accelerated and hit the 0.06-0.12 m/s range.